

UNIVERSITÀ DEGLI STUDI DI GENOVA

Doctoral Program in Bioengineering and Robotics

DOCTORAL THESIS

**Co-adaptive Control Strategies in
Assistive Brain-Machine Interfaces**

Author:
Lucia SCHIATTI

Supervisors:
Leonardo S. MATTOS, Ph.D.
Prof. Darwin Caldwell

Reviewers:
Prof. Aldo Faisal
Claudio Pacchierotti, Ph.D.

Department of Informatics, Bioengineering,
Robotics and Systems Engineering
and
Biomedical Robotics Lab
Department of Advanced Robotics
ISTITUTO ITALIANO DI TECNOLOGIA

2018 - XXX Cycle

UNIVERSITÀ DEGLI STUDI DI GENOVA

Abstract

Co-adaptive Control Strategies in Assistive Brain-Machine Interfaces

by Lucia SCHIATTI

A large number of people with severe motor disabilities cannot access any of the available control inputs of current assistive products, which typically rely on residual motor functions. These patients are therefore unable to fully benefit from existent assistive technologies, including communication interfaces and assistive robotics. In this context, electroencephalography-based Brain-Machine Interfaces (BMIs) offer a potential non-invasive solution to exploit a non-muscular channel for communication and control of assistive robotic devices, such as a wheelchair, a telepresence robot, or a neuroprosthesis. Still, non-invasive BMIs currently suffer from limitations, such as lack of precision, robustness and comfort, which prevent their practical implementation in assistive technologies.

The goal of this PhD research is to produce scientific and technical developments to advance the state of the art of assistive interfaces and service robotics based on BMI paradigms. Two main research paths to the design of effective control strategies were considered in this project. The first one is the design of *hybrid systems*, based on the combination of the BMI together with gaze control, which is a long-lasting motor function in many paralyzed patients. Such approach allows to increase the degrees of freedom available for the control. The second approach consists in the inclusion of *adaptive techniques* into the BMI design. This allows to transform robotic tools and devices into active assistants able to co-evolve with the user, and learn new rules of behavior to solve tasks, rather than passively executing external commands.

Following these strategies, the contributions of this work can be categorized based on the typology of mental signal exploited for the control. These include: 1) the use of active signals for the development and implementation of hybrid eye-tracking and BMI control policies, for both communication and control of robotic systems; 2) the exploitation of passive mental processes to increase the adaptability of an autonomous controller to the user's intention and psychophysiological state, in a reinforcement learning framework; 3) the integration of brain active and passive control signals, to achieve adaptation within the BMI architecture at the level of feature extraction and classification.

Acknowledgements

While approaching the end of this intense and enriching experience, I would like, first of all, to thank my supervisor Leonardo De Mattos. I thank him for giving me the opportunity to work on a challenging and motivating doctorate project at the Biomedical Robotics Lab, and for encouraging in these three years the freedom of my research interests, while giving me a guide that kept me solid and pragmatic in the results.

I thank Prof. Darwin Caldwell, for giving me the opportunity to carry on my job at the Department of Advanced Robotics.

I cannot miss to thank my team colleagues in the TEEP-SLA project, Giacinto Barresi, Jacopo Tessadori, Louis King, Fanny Larradet, Alexey Petrushin, for their collaboration, advices, and constructive discussions.

I also thank colleagues from the administrative office, who helped me dealing with all practical issues, Silvia Ivaldi, Simona Ventriglia, and in particular Valentina Rosso, for her friendship beyond the work.

A special thanks to my companions of adventure and misadventure of the XXX doctoral cycle, Alperen Acemoglu, Matteo Rossi, Zhuoqi Cheng, Lorenzo Saccares, Stefano Toxiri, Sara Moccia, and to the old and new friends in the open space at the 4th floor (and beyond), who helped me a lot in my learning process on how to do research, and made my stay in Genova very enjoyable, especially Veronica Penza, Jesus Ortiz, Olmo Moreno, Jorge Fernandez, João Bimbo, Claudio Pacchierotti, Andrea Ciullo, André Geraldes, Ioannis Sarakoglou and Nikhil Deshpande.

I thank my flat mates and colleagues Samuele Martelli, Sep Driessen, and Marco Contardi (even if he is not an engineer) for the inspiring discussions on the future and for sharing with me their vision and experiences.

Finally, I thank my family, because it is thanks to them that I had the degree requirements to access this doctoral course, and for being always present.

Contents

Abstract	iii
Acknowledgements	v
I State of the Art and Contribution	1
1 Assistive Technologies based on the BCI paradigm	3
1.1 Background	3
1.1.1 Assistive Technologies for Paralyzed People	3
1.1.2 Brain-Machine and Brain-Computer Interfaces	6
System Architecture	7
BCI Classification	7
Neuroimaging Methods	9
Mental Control Signal	9
1.1.3 Applications for Paralyzed People	11
1.2 Current challenges	12
1.3 Towards Intelligent Assistive BCIs	13
1.3.1 Hybrid approach	13
1.3.2 Adaptation	14
2 Contribution and Objectives	17
II Active Control Signals: Hybrid ET-BCI Approach	21
3 Focus Sensitive Dwell time in Eye-BCIs	23
3.1 Introduction	23
3.1.1 Background: EyeBCI Paradigms	24
3.1.2 Introducing a Focus-Sensitive Dwell Time in EyeBCI	24
3.2 Methods	25
3.2.1 Setup	25
3.2.2 Task	27
3.2.3 Experimental Conditions	27
3.2.4 Experimental Procedure	27
3.2.5 Measures	28
Objective Measures of Performance	28
Subjective Measures of User Experience	28
3.3 Results and Discussion	28
3.4 Conclusions	31

4	Soft Brain-Machine Interfaces for Assistive Robotics	33
4.1	Introduction	33
4.2	Methods	35
4.2.1	Web cameras	36
4.2.2	Eye-Tracker	36
4.2.3	Brain-Computer Interface	37
4.2.4	Graphical User Interface (GUI)	38
4.2.5	Actuated System	39
4.3	System evaluation	39
4.3.1	Tasks	41
4.4	Results and Discussion	41
4.5	Conclusions	43
III	Passive Control Signals: Machine Adaptation to User	45
5	The Effect of Tactile Feedback on ErrP Single-Trial Detection	47
5.1	Introduction	47
5.2	Methods	49
5.2.1	Experimental protocol	49
5.2.2	EEG signal processing	50
	Error related potentials	50
	Classification	51
5.3	Results and Discussion	52
5.3.1	Error related potentials	52
5.3.2	Classification	53
5.4	Conclusions	55
6	EEG-based Reward Signal for Robot Learning	57
6.1	Introduction	57
6.2	Methods	59
6.2.1	Experimental Protocol	59
6.2.2	Experimental Setup	61
6.2.3	Algorithms	61
	EEG Analysis	61
	Robot Learning	63
6.3	Simulation Study	65
6.4	Results and Discussion	67
6.4.1	EEG Analysis	67
	ErrP Detection	67
	ErrP Classification	68
6.4.2	Robot Learning	69
	Route Learning	69
	Target Learning	70
6.5	Conclusions	70
IV	Active and Passive Control Signals: Co-adaptive Systems	71
7	Mutual Information-based Feature Selection for Motor Imagery	73
7.1	Introduction	73
7.2	Methods	74

7.2.1	Dataset	74
7.2.2	Pre-processing	75
7.2.3	Feature Selection and Classification	75
7.3	Results and Discussion	76
7.4	Conclusions	80
8	Tactile Feedback in Error-based Adaptive Classification of Motor Imagery	81
8.1	Introduction	81
8.2	Methods	83
8.2.1	Adaptive classification	83
8.2.2	Experimental protocol	84
8.2.3	Experimental setup	85
8.2.4	ErrP classification	86
8.2.5	Motor imagery task classification	87
8.3	Results and Discussion	88
	ErrP classification	88
8.3.1	Motor imagery task classification	88
	Static classification	88
8.3.2	Adaptive classification	89
8.4	Conclusions	91
	Conclusions	93
	Bibliography	97

List of Figures

1.1	Access solution scheme, adapted from Doble et al., 2003.	4
1.2	Categorization of access technologies based on the source used to generate the User Interface (UI) control signal expressing a functional intent. Adapted from Doble et al., 2003	5
1.3	Components of a Brain-Computer Interface system (Wolpaw et al., 2002).	7
1.4	BCI classification according to (Ramadan et al., 2017).	8
1.5	Active and Passive BCI classification based on EEG activity exploited to generate mental control signal (adapted from Ramadan et al., 2017). Among evoked activity, the most used paradigms include Steady-State Evoked Potentials (SSEPs), P300, Error Potentials (ErrPs). Among spontaneous activity, modulation of sensorimotor rhythms, Slow Cortical Potentials (SCPs) and non-motor cognitive tasks are the main control strategies.	9
2.1	Co-adaptive assistive BMI.	18
2.2	Contributions and thesis structure.	19
3.1	(a) Experimental setup, (b) on-screen keyboard and (c) states of a key.	25
3.2	Performance indices - means (across users in each trial, representing a condition) with upper standard deviation bars.	28
3.3	Scores - means with upper standard deviation bars, across subjects - of the 8 rating scales presented in the user experience questionnaire.	31
4.1	System setup for Soft Brain-Machine Interface: translational movements of the robot in space are controlled by human gaze, while an EEG-driven unidimensional index regulates the robot Cartesian stiffness in real-time.	35
4.2	Information workflow between system components.	36
4.3	Graphical User Interface.	38
4.4	Results from system evaluation. Panels A-B: distance between current arm endpoint and selected target for high (panel A) and low (panel B) stiffness trials and corresponding estimated endpoint forces in the push direction (panels C-D). $t = 0$ corresponds to Kuka receiving movement command. Black triangles indicate the approximate contact moment between soft hand and object. Panels E-H: distance traveled by arm endpoint since $t = 0$ in the vertical direction, for high (panel E) and low (panel F) stiffness trials and corresponding estimated endpoint forces, in the vertical direction. $t = 0$ corresponds to Kuka receiving movement command. Contact between grasped object and obstacle occurs almost immediately after movement start. Blue (orange) line depicts trials performed by experienced (naive) user (S1, S2 respectively).	40

4.5	Screen shots of the heavy object pushing (Task 1) and collision (Task 2) tasks in active mental state (stiff) and neutral mental state (compliant). For the second task, two different examples of the active (stiff) case for the two subjects are provided.	42
5.1	Experimental protocol: (a) experimental setup; (b) scene at the beginning of a session; (c) scene at the end of a session.	49
5.2	Grand averages of filtered EEG data for one channel, FCz, in 1 s time window after stimulus onset. Columns refer to different paradigms for stimuli (respectively, only visual V, concordant visuo-tactile VT, discordant visuo-tactile VT stimuli). Blue lines represent the average of all trials following a correct cursor movement, while red lines depict averages of erroneous trials. Thick green lines represent the difference of the two signals (erroneous minus correct).	51
5.3	Classification results: (a) Classification rates for correct and erroneous classes, for all subjects during visual (V) and visuo-tactile (VT) stimuli sessions. Last group of bars represent mean classification rates across all subjects. Error bars represent standard deviations obtained from different repetitions of the classification algorithm (S01 to S12) or across subjects (mean group). (b) Box plots of observed AUC distributions for each subject, referring to visual only (V) and visuo-tactile stimuli (VT) conditions. Red (blue) box plots represent data obtained on subjects that underwent concordant (discordant) VT stimuli. Dashed lines in both panels represent average chance level classification rates or AUCs plus or minus one standard deviation. Chance level results were obtained by training the classifier on actual datasets with randomly shuffled labels.	52
5.4	Average ROC curves. Left graph reports curve obtained for trials during visual-only condition (V), middle and right graphs display ROC curves for data acquired during experiments with visuo-tactile stimuli (respectively, concordant VT and discordant VT). Red (blue) plots represent data obtained on subjects that underwent concordant (discordant) VT stimuli.	54
5.5	Distributions of changes in classification performance (AUC) with the addition of tactile stimulus, for concordant VT (left box), discordant VT (middle box) and combined sets (right box). Red line indicates median, blue box extends to first and third quartiles, whiskers reach most extreme data outside of box. Reported p-values are resulting from one-sided t-tests (* indicating significance at 5% significance level).	55
6.1	System components and information flow in ErrP-based robot learning scheme. Adapted from Iturrate et al., 2015.	58
6.2	Graphical User Interface (GUI) for teleoperation during: training (left), and testing phase (right).	59
6.3	Simulation results for route learning.	66
6.4	Simulation results for target learning.	66
6.5	Grand average of ErrPs (E-C) across all subjects and training trials for channel FCz. Panels (a) and (b) display average C, E, and ErrP for V and VT conditions. Panel (c) provides a comparison V and VT ErrPs. Panels (d-f) provide a graphical representation of ErrP in frequency domain, for V (d), VT (e), and VT-V (f).	67

6.6	Experimental results for route learning.	69
6.7	Experimental results for target learning. Red line indicates median, blue box extends to first and third quartiles, whiskers reach most extreme data outside of box not considered outliers, and the outliers are plotted individually using the '+' symbol.	69
7.1	Scalp electrodes setup: frontal area (F); central area (C); occipital area (O), Emotiv EPOC channels (E).	74
7.2	Classification accuracy using optimal features sets computed in time windows TW1-3 for subjects: Sa, Sb, Sf, Sg from full 59 channels (-all) and reduced to EPOC channels (-EE) Dataset I- BCI Competition IV; S01, S02, S03 from Emotiv EPOC dataset.	80
8.1	Scheme of adaptive classifier functioning. EEG signals are used both to extract an active control signal (from a motor imagery task), and a passive information (ErrP) on user's evaluation of the MI classifier's output (after feedback is provided). The output of static ErrP classifier is then used to update the MI adaptive classifier's parameters, and to improve its performance over time.	82
8.2	Block diagram of adaptive classifier algorithm presented in Llera et al., 2011, and used in the present work.	83
8.3	Experimental protocol. After 1.5 s from cue onset, a green arrow indicating which motor imagery task to performs appears for 4 s. After 1 s break a feedback, simulating MI classification output, is presented. It consists in the movement of a virtual cursor in either the correct direction or one randomly chosen among the other ones (erroneous).	85
8.4	Variation in classification accuracy from static to adaptive MI task classifier, as function of the learning rate and considering 100% ErrP detection accuracy, for all time windows, in V feedback condition.	89
8.5	Variation in classification accuracy from static to adaptive MI task classifier, as function of the learning rate and considering 100% ErrP detection accuracy, for all time windows, in VT feedback condition.	90

List of Tables

3.1	Performance data - means (M) with standard deviations (SD).	29
3.2	Questionnaire data - means (M) with standard deviations (SD) - expressing the agreement of the subject (from 0 for "strong disagreement" to 100 for "strong agreement") with the statements in Figure 3.3 about different aspects of user experience.	30
5.1	Classification performance for concordant stimuli	53
5.2	Classification performance for discordant stimuli	53
6.1	ErrP classification results during training and testing, for subjects with V feedback.	68
6.2	ErrP classification results during training and testing, for subjects with VT feedback.	68
7.1	Results of feature selection on (a) Dataset I-BCI Competition IV	77
7.2	Results of feature selection on (b) EPOC channels from Dataset I-BCI Competition IV	77
7.3	Results of feature selection on (c) Emotiv EPOC Dataset	78
7.4	Results of feature selection on (c) Emotiv EPOC Dataset	78
8.1	Classification accuracy for V condition with static ErrP classifier	86
8.2	Classification accuracy for VT condition with static ErrP classifier	86
8.3	Classification accuracy for V condition with static MI classifier	87
8.4	Classification accuracy for VT condition with static MI classifier	87
8.5	ANOVA results on classification accuracy change between V and VT condition for each subject. Statistical significance threshold was chosen as $p < 0.01$	88
8.6	Change in classification accuracy from static to adaptive classifier considering the optimal TW and relative η for each subject, in V and VT conditions, in case of ideal 100% ErrP accuracy, and for real values of α_n and α_p (Tables 8.1 and 8.2)	91

List of Abbreviations

AAC	A ugmentative and A lternative C ommunication
ALS	A myotrophic L ateral S clerosis
AT	A ssistive T echnologies
BCI	B rain- C omputer I nterface
BMI	B rain- M achine I nterface
BP	B and- P ower
CMI	C onditional M utual I nformation
CLIS	C omplete L ocked- I n S yndrome
ECoG	E lectro C ortico G raphy
EEG	E lectro E ncphalo G raphy
EMG	E lectro M yo G raphy
EOG	E lectro- O culo G raphy
ERD/ERS	E vent- R elated D esynchronization/ S ynchronization
ErrPs	E rror-related P otentials
ET	E ye- T racking
fMRI	f unctional M agnetic R esonance I maging
FN	F alse N egative
FP	F alse P ositive
GUI	G raphical U ser I nterface
IR	I nfra R ed
ITR	I nformation T ransfer R ate
LIS	L ocked- I n S yndrome
MEG	M agneto E ncphalo G raphy
MI	M otor I magery
NIRS	N ear I nfra R ed S pectroscopy
PET	P ositron E mission T omography
RL	R einforcement L earning
SCP	S low C ortical P otentials
SNR	S ignal to N oise R atio
SSEPs	S teady- S tate E voked P otentials
SSVEPs	S teady- S tate V isual E voked P otentials
TN	T rue N egative
TP	T rue P ositive
UI	U ser I nterface
VOG	V ideo- O culo G raphy

Part I

State of the Art and Contribution

Chapter 1

Assistive Technologies based on the BCI paradigm

1.1 Background

1.1.1 Assistive Technologies for Paralyzed People

Individuals with severe physical disabilities, whether congenital, traumatic or induced by a disease, have a limited independence due to lack of alternative means to interact with the surrounding world (Tai et al., 2008). In this context, Assistive Technologies (AT) aim at recovering a mean of interaction between the person and the external world, therefore allowing paralyzed individuals, who are often unable to speak, to restore expressive capabilities, and some degree of independence. This is a crucial aspect to improve the quality of life of people with Locked-in Syndrome (LIS), showing complete paralysis except for vertical eye movements and blinking but preserved consciousness, and Complete Locked-in Syndrome (CLIS), with total immobility and loss of eye movements but preserved awareness and cognition (Bauer et al., 1979). Indeed, it has been shown that LIS patients can survive for many decades (Doble et al., 2003). In this period of their life, they almost completely depend on AT for communication and social interaction with their family and the external world.

In particular, technologies able to transfer the intention of a user with severe physical impairment into functional interaction (e.g. communication or environmental control) are referred to as access technologies (Tai et al., 2008). As reported in Fig. 1.1, an access solution is composed by an access technology and a User Interface (UI) technology. The first one includes sensors gathering the expression of a functional intent from the user, and a signal processing unit that transfers the input signal into a control signal. The latter is used as input for the UI, which triggers the execution of an appropriate functional activity, within a specific environment. The UI can be an iconic display for Augmentative and Alternative Communication (AAC), a front panel to allow environmental control, (such as TV, lights), or an on-screen keyboard to access a computer, browse on Internet and use social applications.

Based on the level of reliable physical movement exhibited by the user, different technologies can be used to implement the access technology component of an assistive interface. As visible in Fig. 1.2, if at least one reliable movement is available below and including the neck, mechanical switches, electromyography, and infrared sensing have been used as possible solutions.

Mechanical switches are the simplest access technology for those with at least one reliable voluntary movement due to the low cost, availability, robustness and operational simplicity. The actuation mechanism can be based on different mechanical stimuli, such as changes in displacement, tilt, air pressure or force. Some switches

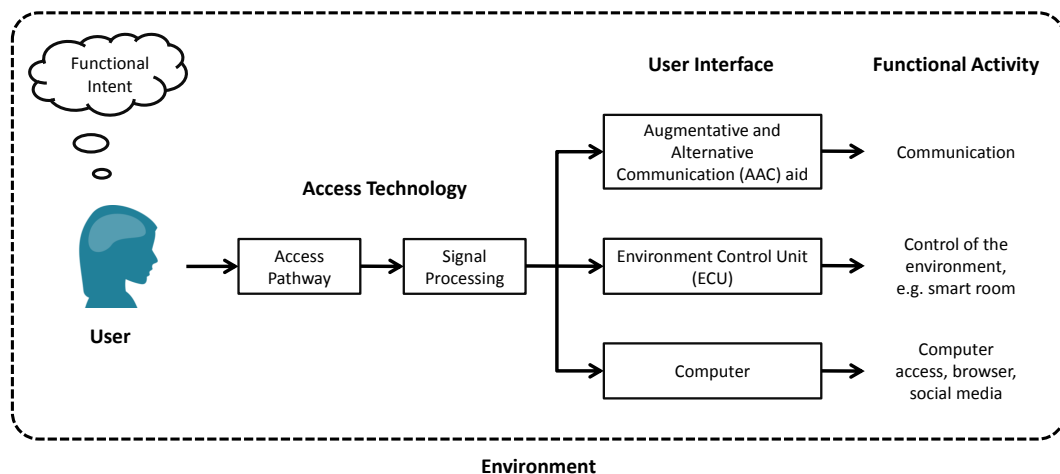


FIGURE 1.1: Access solution scheme, adapted from Doble et al., 2003.

are already available for individuals capable of some volitional movement, but novel switches and switch combination strategies have been proposed for customized solutions, suitable for people with severe motor impairments (Lancioni et al., 2006, Perring et al., 2003). The main limitation is due to the possibility of a challenging effort to develop positioning aids or mounting systems to secure the switch at the identified access site. Furthermore, the ability to exploit this solution can fluctuate due to mental (Kennedy et al., 2000) and physical fatigue (Evans et al., 2000), or changes in functional abilities of the user (Borasio et al., 2001).

Infrared (IR) technology can be used to produce low-cost interfaces (Evans et al., 2000), where the user mounts a transmission module on the head, to activate devices designed or modified to detect IR signals. An examples of this kind of assistive technologies is the eyeglass-mounted infrared system developed by Chen et al., 2004 and tested on nonverbal individuals with tetraplegia to activate a communication board. In the same vein, IR has been used as single switch AT to detect eye-blinks (Lancioni et al., 2005).

Electromyography (EMG), i.e electrical activity generated by muscles during contraction, recorded by means of surface electromyographic electrodes, can be used to generate a control signal for an access technology based on residual volitional muscular contraction, when physical movement is too weak to activate a mechanical switch. Many studies reported an effective control of myoelectric switches and interfaces using hand muscles activation (Gryfe et al., 1996), voluntary facial movements (Huang et al., 2006) and a combination of facial EMG and eye-tracking (Surakka et al., 2004). Practically, the effectiveness of EMG control depends on the signal-to-noise ratio, i.e. the strength of the muscle contraction, and is affected by motion artifacts and variations in electrode/skin contact impedance between electrode applications in long-term usage.

When the available motor control is limited to the muscles above the neck, communication and environmental control can be achieved by means of eye or face fine movements tracking systems based on Eye-Tracking (ET) technology or computer-vision. Gaze-based communication systems map eye movements or the point of gaze to the position of a cursor on a computer screen, allowing for selection of gaze-sensitive screen items by means of fixation for a predefined dwell time. Commercially available eye-trackers are typically based on Video-oculography (VOG) or

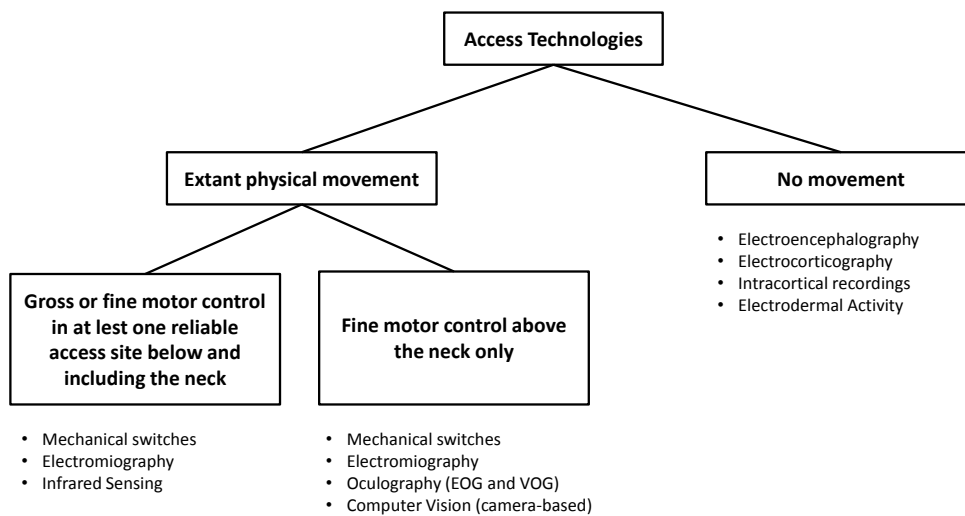


FIGURE 1.2: Categorization of access technologies based on the source used to generate the UI control signal expressing a functional intent. Adapted from Doble et al., 2003

Electro-oculography (EOG) technologies. In VOG systems gaze direction is detected by measuring the offset between corneal reflection and pupil center, exploiting a IR light source and a camera mounted on a computer. Due to the non-invasiveness and high accuracy, this technique is dominant in ET market (Bates et al., 2005). In EOG-based systems (Di Mattia et al., 2001), gaze direction is measured by means of electrodes placed around the eyes, exploiting shifts in potential difference between the cornea and retina that occur when user changes gaze direction. ET systems allow for a fast control, comparable to that achievable by means of a hand mouse. In Abbott et al., 2012, they proposed a ultra-low-cost binocular eye-tracker produced by using mass-produced video-game hardware at a cost of about 30 USD, with an information throughput of 43 bit/s, that yielded effective real-time closed loop control of external devices after few minutes of training. The system allowed to track gaze position in 3D, making it suitable to provide also direct interaction with the environment beside canonical control via computer display. Though, this technology is affected by some limitations, that restrict its practical effectiveness in computer access tasks. The main drawback is that only one channel is exploited for both observation and control, making ET suffering from the "Mida's Touch" problem (Jacob, 1991), i.e. incorrect selections arising when the system misinterprets user input activity. Furthermore, ET is not usable in case of insufficient range of eyes motion, and other factors such as calibration drifts, fatigue, artifacts (in case of EOG), can limit the system's usability.

A computer vision-based access system tracks the location of features identified on user's face, (e.g. pupils, eyebrows, or eyelids for blink detection) via a camera. Position changes are then translated into cursor movements on a computer screen, or used as switches. Thanks to the decreasing hardware costs, the widespread availability of inexpensive USB web-cameras, and the recent fast progress in the development of robust computer vision algorithms based on deep learning (facing challenges such as features invariance to orientation changes, occlusion, variation in ambient lighting), computer vision-based solutions can become the most affordable access alternative for people with some repeatable neck or facial movements.

Finally, for individuals who cannot control any physical movement, in the most

severe cases of paralysis, such as LIS and CLIS, there is the possibility of decoding functional intent through the analysis of various biopotentials, namely brain signals or other physiological signals. In the first case, the system is called Brain-Computer Interface (BCI), and exploits either invasive, i.e. electrocorticography and intra cranial recordings, or non-invasive, such as Electroencephalography (EEG), technologies to record brain signals, and translate them into control input for an external device. In the present work, assistive technologies developed for people with LIS (residual muscular control of eye movements) and CLIS (no muscular control) are taken into account, and in particular technologies based on non-invasive (EEG) BCI paradigm. The state of the art of this kind of technology is described in the following paragraph.

It is worth mentioning that also other physiological signals can be used as input for access technologies. These include electrodermal activity and galvanic skin response, measured as changed in skin conductivity mediated by the peripheral nervous system, that can be either consciously raised by a user after a specific training, or passively generated in response to stress and fatigue. However, the exploration of psycho-physiological input modalities other than EEG signals is out of the scope of the present work. This will only focus on the subset of access technologies corresponding to assistive EEG-based BCIs.

1.1.2 Brain-Machine and Brain-Computer Interfaces

A BCI was defined in Wolpaw et al., 2002, as a communication system in which messages or commands that an individual sends to the external world do not pass through the brain's normal output pathways of peripheral nerves and muscles. In Donoghue, 2002, a Brain-Machine Interface (BMI) definition was introduced as a system which has the goal of providing a command signal from the brain cortex to control disabled body parts or physical devices, such as computers or robotic limbs. Generalizing, the terms BCI and BMI both describe a communication system between the brain and a computer/external device. In the following the term BCI will be used to express the general concept, while BMI will refer specifically to a system including a physical external device, thus including a BCI component in its architecture. The control of an external device by means of a BCI necessarily implies the availability of a technology to acquire brain signals, in a way that enable their elaboration and translation to control commands. The development of EEG by Hans Berger in 1929 (Tudor et al., 2005) was a decisive step towards this direction, enabling the non-invasive recording of neuroelectrical signals from the human brain (Chaudhary et al., 2016). The first scientific report showing the volitional regulation of human brain oscillations (alpha waves) in a neurofeedback experiment was published in 1969 by Kamiya, 1969, while in 1973 a system able to translate EEG signals into computer control signals was presented by Vidal, 1973 with the coined term "Brain-Computer Interface". In the following decades, BCI field underwent an extensive progress, driven by advances in fast computing, real-time analysis, neuroscientific knowledge of brain functions, and the increasing number of available recording techniques. Nowadays, BCI research is in a quite mature phase, with many prototypes developed in different applicative fields, from assistive technologies, e.g. to control a neuroprosthesis (Müller-Putz et al., 2005a), drive a wheelchair (Millán et al., 2009), select letters from a virtual keyboard (Birbaumer et al., 1999), to rehabilitation (Chaudhary et al., 2016), and entertainment (Millán et al., 2010).

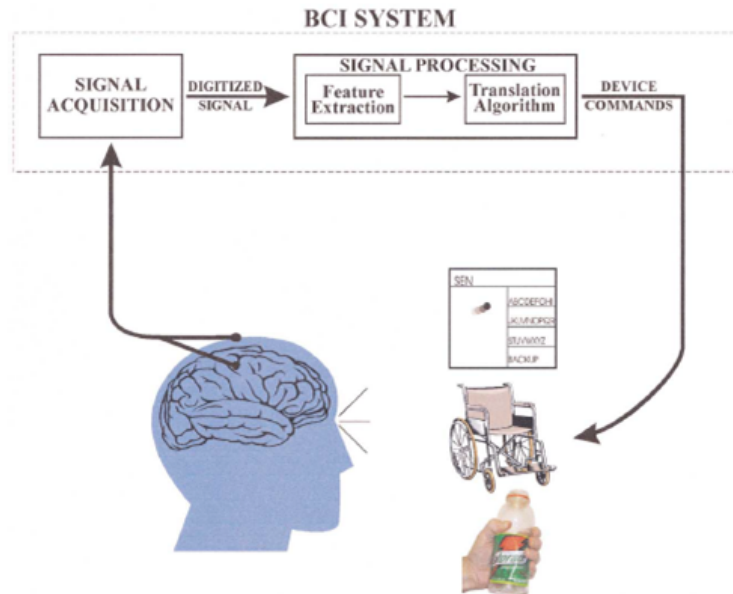


FIGURE 1.3: Components of a Brain-Computer Interface system (Wolpaw et al., 2002).

System Architecture

A Brain-Computer Interface system includes all software and hardware components from the brain signal acquisition to signal processing that allows to generate control signals for a computer or an external device. The general architecture of a BCI system is described by Wolpaw et al., 2002, and reported in 1.3, from the same work. The signal is acquired from electrodes placed on the human scalp or head by means of invasive or non-invasive techniques. After digitalization, acquired signals processed in order to remove noise and artifacts and to extract significant features, that encode user intent. Such features are then translated into commands for an external device. Such translation algorithm usually implies a supervised learning technique, thus requiring a training phase to achieve a reliable performance. An extensive review of signal processing and classification algorithms used in BCI can be found in Bashashati et al., 2007 and Lotte et al., 2007.

BCI Classification

In Fig. 1.4 a useful classification of BCI systems, first formalized by Lotte et al., 2015, according to the characteristics of dependability, invasiveness, and synchronization, is reported. These three categories of BCI are briefly explained in the following.

Dependent and independent: Based on the availability of user's residual motor functions, BCIs can be categorized in dependent or independent. Dependent BCIs can help the user to perform some tasks, but they rely on a certain level of motor control. Independent BCIs are those designed to work without any need of motor control, thus being usable by people with CLIS.

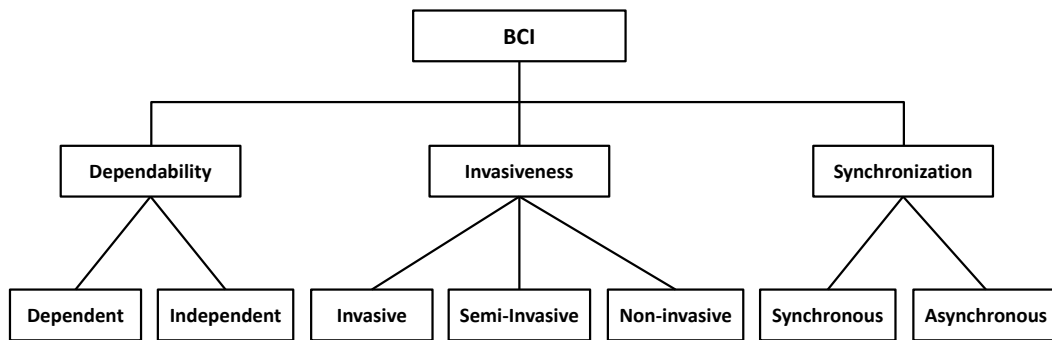


FIGURE 1.4: BCI classification according to (Ramadan et al., 2017).

Invasive and non-invasive: According to the method used to measure the brain activity, BCI are classified into invasive, non-invasive, and semi-invasive. In semi-invasive BCI, the electrodes are implanted in the brain surface epidurally or subdurally, and signals are recorded by means of Electrocorticography (ECoG). In alternative electrodes can be chronically implanted in the cortex, penetrating beyond the surface of the brain, and in this case the acquisition method falls into the category of Intracortical Recordings (invasive). In ECoG the signal has a broader bandwidth, higher spatial resolution, and higher Signal to Noise Ratio (SNR), compared to EEG. Furthermore, using intracortical recordings, the activity from a population of neurons, or even single-cell activity can be extracted (e.g. to drive a prosthetic device in Schwartz, 2004). The biggest limitations of invasive and semi-invasive techniques are the need for the patient to undergo neurosurgery for electrode implantation, the impossibility to change electrodes positions to other areas and the difficulty of substituting them when deteriorating. Furthermore, long-term effects of electrodes implantation is not known in humans. On the other hand, in non-invasive BCI, the signals are recorded with superficial sensors. The most common techniques used for non-invasive BCI are EEG and Near InfraRed Spectroscopy (NIRS). The signals in this case present a lower quality in terms of temporal and spatial resolution, as well as SNR. However, non-invasive BCI are the preferred option, since they allow to avoid surgery and related complications.

Synchronous and asynchronous (self-paced): Finally, BCI systems can be categorized as synchronous or asynchronous. In the first case, user interaction with the system is time-locked. This means that information extracted from brain signal to generate a control command is generated by means of an external event, as it is the case for BCIs relying on evoked activity (see Mental Control Signal paragraph, and Fig. 1.5), i.e. features in brain signals arising as response to external stimuli. In these systems, the interaction time, in which a meaningful signal can be detected, is allowed for a predefined period of time. On the other hand, for asynchronous BCIs, the user is able to perform a mental task in any moment, and the system continuously detects brain ongoing activity, reacting when meaningful information is detected. In this case, the system is self-paced: the user decides when to send a command without external constraints. Asynchronous BCIs exploit spontaneous activity to generate the mental control signal (see Fig. 1.5).

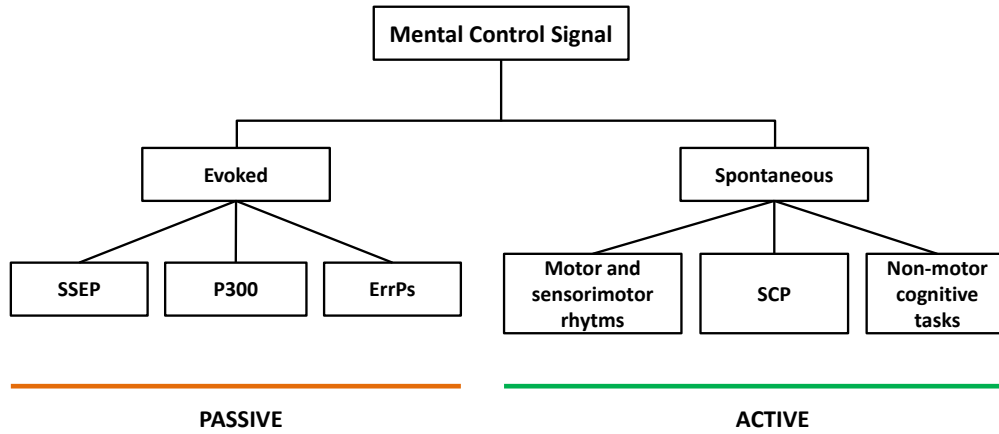


FIGURE 1.5: Active and Passive BCI classification based on EEG activity exploited to generate mental control signal (adapted from Ramadan et al., 2017). Among evoked activity, the most used paradigms include Steady-State Evoked Potentials (SSEPs), P300, Error Potentials (ErrPs). Among spontaneous activity, modulation of sensorimotor rhythms, Slow Cortical Potentials (SCPs) and non-motor cognitive tasks are the main control strategies.

Neuroimaging Methods

Recording of brain activities can be done by direct monitoring of electrophysiological signals, generated by potential actions or changes in the blood flow. The most used non-invasive methods are: EEG and ECoG (semi-invasive) among techniques recording electrical activities, and Magnetoencephalography (MEG), Positron Emission Tomography (PET), functional Magnetic Resonance Imaging (fMRI), optical imaging (i.e., NIRS and functional NIRS) among techniques recording metabolic activities. However, MEG, PET, fMRI and functional NIRS are not matching the requirements for a domestic BCI because of the high cost, technical complexity of instrumentation, and low time resolution due to the underlying metabolic process slow responsiveness. For their characteristics of low cost, portability and possibility of rapid communication, mainly EEG (spatial resolution 1 cm, temporal resolution 1 ms) and NIRS (spatial resolution ~ 2 cm, temporal resolution ~ 1 s) are used for the development of effective non-invasive BCI systems. In this work, just EEG-based BCIs are considered.

Mental Control Signal

Following the categorization proposed by Ramadan et al., 2017, EEG-based BCIs can be distinguished based on the kind of control signal extracted from brain activity. As reported in Fig. 1.5, mental control signals are mainly based either on evoked or spontaneous activity. This categorization can be used to distinguish between *passive* and *active* BCIs, respectively. In fact, evoked signals are generated unconsciously by the person, when receiving external stimuli, thus allowing control in a passive vein. On the opposite, spontaneous signals are generated by the subject voluntarily and without any external stimulation, allowing for an active control. Due to the underlying mechanism, passive BCIs are generally synchronous, while active BCIs work as self-paced systems. In the following, the principal evoked and spontaneous signals used in BCI applications are listed.

Passive control signals: Among evoked signals the most used are Steady State Evoked Potentials (SSEPs) and P300. SSEPs are brain signals that are generated during the presentation of a periodic stimulus, either visual, e.g. a flickering image in Steady-State Visual Evoked Potentials (SSVEPs) Müller-Putz et al., 2005b, a modulated sound in auditory SSEPs (Nijboer et al., 2008), or vibrations, as in somatosensory SSEPs (Breitwieser et al., 2012). When a person is subjected to a high-frequency periodic stimulation, the EEG signals power in the brain area related to the sensation process involved, tends to reach the stimulus frequency. This phenomenon can be exploited in SSEPs-based BCI to generate a control signal. One of the most common application is based on SSVEP, and consists in a Graphical User Interface (GUI) with some buttons, each one of them flickering at a certain frequency (typically between 6-30 Hz). When the subject focuses on one of the buttons, the equivalent frequency can be detected on EEG signals recorded over the occipital cortex, and used to select the button (Zhu et al., 2010). The P300 evoked brain potential is an EEG signal occurring ~300 ms after the subject is exposed to an infrequent or surprising stimulus. When the person recognizes one rare relevant stimulus, among a random sequence of stimuli, this triggers the P300 EEG signal (Polich, 2007). The P300 paradigm is the most used in BCI spelling applications: patients select a letter from a matrix of transiently illuminated rows and columns by focusing on it. The illumination of the desired letter arises an EEG P300 that triggers the letter's selection. Evoked signals do not require any training from the subject. However, repetitive stimuli and the passive nature of the control can be tiring and uncomfortable for the subject. Furthermore, P300 and SSVEPs-based BCIs require intact vision and attention capabilities, which instead are often compromised in patients with severe neurological disorders at late stage.

In this work, also Error-related Potentials (ErrPs) have been included into the category of evoked activity that can be exploited as passive control signal. ErrPs are event-related potentials detectable in EEG activity in the fronto-central areas, in human-computer interaction tasks where the user becomes aware of a wrong issued command, or misinterpreted intention in a BMI system (Chavarriaga et al., 2014). These signals have been used in BCIs to provide corrective signals or error-driven learning of an intelligent device, in order to improve the overall system's performance. Even if ErrP alone cannot be used to provide a control commands, it can be used as a passive feature in BCIs relying on another passive or active control paradigm.

Active control signals: Spontaneous signals used to drive BCI systems are the Motor and Sensorimotor rhythms, Slow Cortical Potentials (SCP)s, and Non-motor cognitive tasks. Motor and sensorimotor rhythms consist in ongoing activity over the motor cortex (Golub et al., 2016), with frequency bands defined as μ (8–13 Hz) and β (13–30 Hz). The amplitude of these rhythms vary when performing a physical or mental task related to movements. It is possible for a person to learn to control sensorimotor rhythms by means of operant conditioning or motor imagery (Ramadan et al., 2017). In the first case, the subject learns to voluntarily change amplitude of μ and β rhythms using a personal mental strategy, by means of long training (weeks or months). In motor imagery paradigm, the change of power in μ and β bands when related to movements (typically limbs movements) imagination or intent can be exploited to generate a suitable control signal for e.g. controlling a mouse or a computer game. Also motor imagery requires training, since optimal features are

often subject-specific and non-stationary over long periods of time. Modern machine learning and artificial intelligence techniques can be used to shorten the training period, as better explained in the following sections. SCPs are low frequency potentials, i.e. below 1 Hz (Kübler et al., 2001), that can be detected in the frontal and central parts of the cortex, reflecting a very slow variation, positive or negative, of the cortical activity. The subject can control generation of such signals using operant conditioning, but a long training, often longer than for sensorimotor rhythms is required. Finally, also non-motor cognitive tasks, such as music imagination, visual counting, mental rotation, and mathematical computation (Dobrea et al., 2009), can be used to drive a BCI.

1.1.3 Applications for Paralyzed People

Restricting the focus to BCI applications aiming at improving the life quality of people with severe motor impairments, two principal areas can be distinguished, as reported in Chaudhary et al., 2016: assistive BCI and rehabilitative BCI. Assistive BCIs are designed to enable paralyzed patients to communicate or control external assistive devices, while rehabilitative BCIs are intended to facilitate recovery of neural functions.

The clinical population benefiting from assistive BCIs include patients with severe impairments in communication and motor functions. Most of the existent BCIs for communication have been developed for people with Amyotrophic Lateral Sclerosis (ALS), but in general also people with damages to the central nervous system, e.g. stroke and spinal cord injuries, can benefit from this technology. ALS is a progressive motor neuron disease leading to complete destruction of the peripheral and central motor system (Chou et al., 1993). In the late stages of the disease people become unable to speak at all, reaching a condition of total paralysis except vertical eye movements and blinking (LIS), and eventually they can also lose eye movements (CLIS). Even in these late stages though, consciousness and cognitive capabilities are preserved, allowing these patients to exploit access technologies based on brain processes. Using invasive BCIs (based on ECoG) demonstrated the possibility for patients with tetraplegia to learn the use of neural interfaces to control a computer cursor movements, or a robotic hand movements in all directions (Hochberg et al., 2006). Successful clinical applications of non-invasive EEG-based BCIs were shown starting from 1999 to enable LIS patients to select letters on a computer screen using SCP (Birbaumer et al., 1999) and sensorimotor rhythms (Wolpaw et al., 2004). Spellers based on the EEG-P300 paradigm were successfully used by the majority of LIS patients affected by ALS, but with functioning vision and eye control (Sellers et al., 2010). On the other hand, attempts to use both invasive and non-invasive BCIs for communication in CLIS patients has been unsuccessful (Murguialday et al., 2011, Thorns et al., 2010). The first case of successful communication from a patient with CLIS as result of ALS came from the use of a BCI-based fNIRS with classical conditioning learning over a long time period (Gallegos-Ayala et al., 2014). Alternative learning methods and neuroimaging methods could be necessary for this kind of patients.

Beside communication, assistive BCIs have been used to provide motor substitution in paralyzed patients as a results of ALS, stroke, or spinal cord injury. On-line brain control in combination with functional electrical stimulation, has been demonstrated on patients with spinal cord injury to control movements of upper limbs (with both invasive and non invasive techniques, Pfurtscheller et al., 2003, Enzinger et al., 2008), and lower limbs (with non invasive techniques, King et al.,

2015). BCIs have been used with paralyzed patients also to enable neural control of a robotic arm, using both invasive and non-invasive systems (Hochberg et al., 2012, Pfurtscheller et al., 2000), and to control a wheelchair, using EEG-based BCI (Nguyen et al., 2013).

Finally, BCIs for rehabilitation have been used mainly by patients with stroke. In fact, the learning of neuroprosthetic control has been shown to induce the reorganization of cortical networks, helping motor rehabilitation in stroke patients without residual movements (Ganguly et al., 2011). A detailed review of rehabilitative BCIs is out of the scope of the present work, that focuses on assistive applications. A complete review of the state of the art is available from Chaudhary et al., 2016.

1.2 Current challenges

Up to date, BCIs, especially based on non-invasive signals, suffer from a number of limitations that prevent them to be produced as stable assistive products. In the following, the principal issues connected to non-invasive EEG-based BCIs, that are the ones considered in the present work, will be discussed.

In independent, asynchronous systems, one of the main problems is the need of a training phase each time a subject uses the system, to avoid a low signal classification performance. On the other hand, long training time decreases the system's usability, due to the effort required from the subject, thus reducing user engagement. There are also some limitations intrinsically related to the electrophysiological signals, which are the low signal-to-noise ratio and non-stationarity of EEG. Furthermore, changes in electrodes positions, differences in user internal mental activity, both compared to other people and in time, can cause a decrease of BCI system performance in online sessions as well as during inter-sessions. To cope with this issue, adaptive techniques and algorithms are required to ensure a robust signal classification over time.

One of the standard performance measures for a BCI system is the Information Transfer Rate (ITR), which is determined by the three factors: target detection accuracy, target detection time, and number of classes. A higher information rate can thus be achieved by acting on target detection accuracy, i.e. enhancing SNR and the considered classes separability, by means of preprocessing, filtering and features extraction techniques, to convert multi-channels EEG data in low-dimensional signal associated with cognitive states relevant to the task. Another way to enhance the ITR is by reducing the target detection time, by means of machine learning and adaptive methods (e.g. dynamic stopping) for asynchronous systems, or by means of an optimized design stimulus presentation in synchronous BCIs. For asynchronous systems, a higher number of discriminable classes result in a higher number of control degrees of freedom, thus corresponding to higher ITR and faster control.

Another BCI challenge concerns the development of invasive and noninvasive more accurate and portable sensors. Currently, for EEG-based BCIs, gel electrodes are required to achieve acceptable performances in terms of minimum SNR and high ITR. Nonetheless, dry electrodes are a mandatory requirement for the development a portable and usable technology. Future advancements in sensing technology and the inclusion of artificial intelligence into electrodes design, are expected to enable in the next years smart electrodes with wireless communication, with reduced dimension and high sensing and adaptive capabilities.

Overall, to bring BCIs into real life assistive applications, a robust system performance must be achieved, with the development of portable platforms with an

affordable hardware and software cost. The non-invasiveness of the sensing modality can push for the development of a practical technology, accessible by a large population (Milan et al., 2010). Furthermore, an asynchronous design of the system is preferable for the BCI usability and comfort, allowing the subject to achieve a control based on its own time. Though, the design of self-paced control systems poses some challenges, due to the difficulty of discriminating an idle state from a meaningful activity in EEG-based BCIs. Nonetheless, these characteristics promote the transition to user-centric BCI applications, in which the user needs, preferences and limitations are put as the center of the implementation process towards more effective and acceptable technologies (Lightbody et al., 2010).

1.3 Towards Intelligent Assistive BCIs

In order to overcome the current limitations and bring the BCI technology out of the lab, into real-life applications, Millán et al., 2010 reviewed the state of the art of EEG-based BCIs in the field of ATs, and outlined the principal research directions where an essential progress can be expected in the next years. These include:

- The development of hybrid BCI (hBCI) architectures, exploiting different physiological signals and/or different brain processes together, as input for the control.
- The design of user-machine adaptation algorithms, to endow BCI devices with self-adaptive capabilities.
- The exploitation of user mental states (mental workload, stress level, attention level, tiredness) as measures of reliability and confidence for the BCI.
- The incorporation of principles of human-computer interaction to improve BCI usability and the UI design.
- The development of better EEG sensing devices.

According to Millán et al., 2010, advances in these directions are a key factor towards the goals of: obtaining a more robust control signal, with increased degrees of freedom for the control, increasing reliability, easiness and performance of brain-computer interaction, reducing user's cognitive effort and improving system accessibility. Sharing the above mentioned view, in the present work the hybrid and adaptive approaches were considered, in order to contribute to the state-of-art of current EEG-based assistive BCIs. These two research directions are therefore better explained in the following.

1.3.1 Hybrid approach

A hBCI is defined as a system combining different input signals and including at least one BCI channel. The hybrid nature of the system can be achieved in different modalities.

A first approach consists in combining two different BCI channels (e.g. one passive and one active control signal). Examples of such implementations are the combination of motor imagery-based BCI with ErrP detection, for the automatic correction of wrongly detected mental commands (Ferrez et al., 2008a), or the combination P300 and SSVEPs to improve the performance of asynchronous control of a wheelchair (Li et al., 2013). The goal behind using two or more types of brain signals as input to

a BCI system is to improve the system reliability and to avoid the disadvantages of each type of signals.

A second kind of hBCI is the combination of BCI and another biosignal (e.g. EMG, mechanical switches or eye movements). This approach intends the BCI as an additional channel to enhance conventional assistive products, operated by residual muscular functions. The BCI control can be used to drive a different part of the assistive device, thus increasing the degrees of freedom for control, or improving the interaction, especially in applications for motor substitution. In alternative, all input channels can be combined to allow the user to switch from one modality to the other one depending on the personal preference and performance. This latter solution is particularly useful in cases of progressive loss of muscular activity (as in ALS), where early BCI training when the user can still exploit residual muscular activity will improve the transition between hybrid and pure BCI, once muscular control is lost, thus increasing long-term usability of the assistive device. Examples of this second category of hBCI are the combination of EEG with EMG activity (Leeb et al., 2010) or the use of EEG and eye gaze together (Danoczy et al., 2008).

Finally, hBCI could exploit different neuroimaging techniques simultaneously (e.g. EEG together with MEG, fMRI, NIRS).

Different input channels in hBCI can be weighted based on their reliability, that again can be determined from user mental state, exploiting some physiological measure, such as stress level or ErrP. Hybrid BCI systems are the preferred solution in case of control of complex devices, such as neuroprosthesis and mobile robotic systems (e.g. for telepresence, or wheelchair). For this reason, shared control and shared autonomy are a key component to allow an easy control of a complex intelligent device, with only high level control inputs from the user. Incorporation of artificial intelligence into the assistive device/interface, at both hardware and software level, will constitute the basis for the effective integration of BCI systems with AT. In Choi et al., 2017 and Müller-Putz et al., 2015 more extended and complete reviews of hBCI state of the art can be found.

1.3.2 Adaptation

The second pathway to the development of out-of-the-lab assistive BCIs is the integration of user-machine co-adaptation algorithms into the system design. The idea is that of changing the nature itself of the assistive interface/device from a passive executer of user commands, to an active assistant, able to interact with the user and to co-evolve with him/her, in order to learn and optimize its behavior towards user-directed task solving. Again, towards this objective, intelligence must be included into the interface and control loop design. Adaptation can be achieved at different levels of the system.

A first level of self-adaptation can be included into the BCI through the hybrid approach, allowing the user to dynamically choose the best interaction channel at any time, as well as the EEG phenomena that better suites the user (Millán et al., 2010). The second aspect where adaptation can strongly improve BCI performance concerns the online calibration of the decoding module, which translates EEG signals into control input for an external devices. To cope with EEG non-stationarity over time, and differences in optimal features from subject to subject, online adaptive techniques at this level could reduce the need of long calibration sessions, and improve system precision. This adaptation can be carried out at different modules of the BCI: in the feature extraction stage, in order to select information discriminative to the task and stable over time (Vidaurre et al., 2009); in the spatial filtering, to

extract uncorrelated information (Vidaurre et al., 2010), or at the classification side, e.g. performing online learning or retraining. Adaptation at all modules level can be carried out in both supervised (task known in advance) and unsupervised way (when no class labels are available). An example of semi-supervised classifier adaptation is shown by Llera et al., 2011, where ErrP detection in a motor imagery task is used to update classifier's parameters.

The selection of stable and discriminant features and BCI online adaptation, in one or more modules, allow for simultaneous co-adaptation of the BCI to the user and viceversa. Indeed, they allow to accelerate user training, also helping to provide a more stable feedback, thus making easier for the person to learn to modulate his/her brain activity.

Chapter 2

Contribution and Objectives

The present work focuses on the development of adaptive control strategies and hybrid systems to advance the state-of-art of assistive BMIs. The work was developed in the framework of the TEEP-SLA project ¹ (Empathic and Expressive Technologies for people with ALS). TEEP-SLA is a 3-year (from December 2015 to November 2018) collaborative project, involving the Istituto Italiano di Tecnologia (IIT) and Fondazione Sanità e Ricerca, and funded by Fondazione Roma. It aims to create novel assistive technologies for ALS patients. In particular, this project looks at satisfying the patients social interaction and communication needs with innovative interfaces and associated assistive robotic technologies. For this reason, the population target of the presented work is that of people with LIS or CLIS, and the considered access technologies are restricted to those exploiting eye movements and brain signals (Eye-tracking and BCI). Non-invasive sensing methodologies were chosen, and in particular the neuroimaging technique used in all studies is limited to EEG signals. This choice is motivated by the goal of developing a portable and affordable technology, with an overall cost sustainable by the Italian Sanitary System to assist ALS patients.

The strategies followed to bring innovation into the state of the art of assistive BCIs were inspired by the research paths presented in Section 1.3: development of hybrid and multimodal interfaces, using different input biosignals and different brain mechanisms together, and the inclusion of user-machine adaptation algorithms into the assistive interface architecture. The contributions collected in this thesis converge towards the development of a co-adaptive assistive hybrid BMI, exploiting active and passive control signals. The concept is shown in Fig. 2.1. In such interface, two kinds of active control signals, namely gaze and motor imagery, are exploited to generate control commands for an assistive device (either a communication interface or an assistive robotic arm). The hybrid approach is here intended as the simultaneous use of a BCI channel and gaze signal, which is one of the long lasting motor capabilities in LIS patients. The purpose is to increase the degrees of freedom available for the control, and the UI usability, as well as to gradually introduce the use of BCI for patients with progressive loss of all motor functions, making easier the transition to a pure BCI control in late stages of the disease. Furthermore, a passive EEG mechanism, i.e. error detection (ErrP), is exploited to endow the system with co-adaptive capabilities. Co-adaptation between the user and the device is realized at two levels:

- Exploiting the information on user mental state (error awareness) related to the evaluation of a semi-autonomous assistive device behavior, to achieve error-driven learning. Here, the autonomous robotic device learns how to adapt its behavior according to the information retrieved from user's brain activity. This

¹<http://www.teep-sla.eu/>

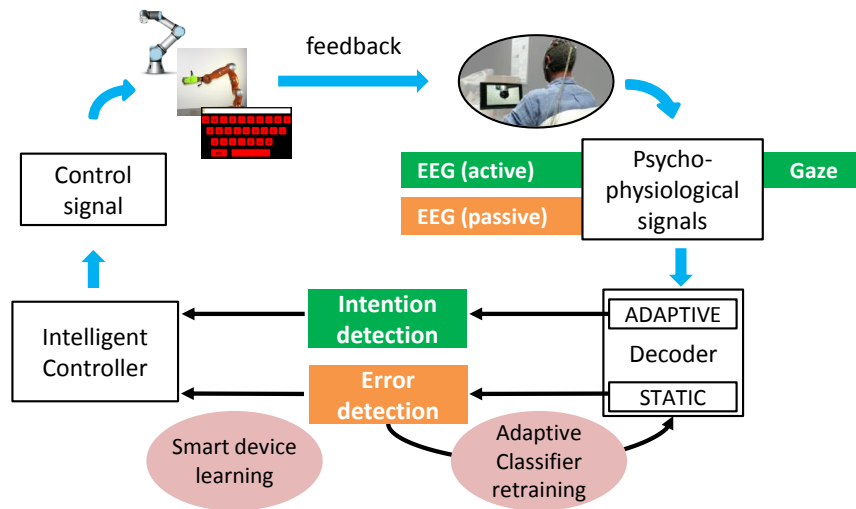


FIGURE 2.1: Co-adaptive assistive BMI.

is implemented in a reinforcement learning framework where ErrP detection is used to provide a negative reward signal.

- The second adaptive behavior is designed at the level of decoding of user's intention. Here, the detection of an ErrP on the feedback related to motor imagery classification is exploited for online automatic recalibrating/retraining of the classifier.

It is worth noting that the proposed architecture heavily relies on the capability of detecting error potentials with sufficient accuracy. Since error perception by the user is based on the feedback over an action (robot action or motor imagery classification output), some work has been devoted to the design of effective feedback modalities, able to enhance ErrP online detection.

The thesis structure is summarized in Fig. 2.2. Contributions are grouped in three main parts (II-IV). Part II presents two works developed following the hybrid ET-BCI approach, to generate active control signals for a communication interface (Chapter 3) and an assistive robotic arm (Chapter 4), respectively. Part III explores the use of passive signals (ErrP) as a reinforcement learning reward function for error-driven learning of a semi-autonomous device. In Chapter 5 a study on the effect of tactile feedback on ErrP single-trial detection is presented, while Chapter 6 reports results from a real-time implementation of ErrP detection for robot learning of target identification and reaching task in a bi-dimensional space. Part IV includes two studies on the use of both active (motor imagery) and passive (ErrP) EEG signals, to include adaptation at the levels of feature extraction and classification of the BCI motor imagery decoder. The first study (Chapter 7) explores an offline method for selection of subject-specific stable and discriminant features, with the goal of facilitating user-interface co-adaptation to shorten the training phase and increase the BCI system's accuracy. The second study (Chapter 8) simulates the effect of using ErrP detection for online updating of classifier parameters in a two-classes motor imagery task.

Outcomes of this work include the production of novel EEG datasets related to ErrP (Chapter 3 and 4), both on training and testing phases, and to motor imagery (Chapter 8), recorded using a professional acquisition system. These are or will be made publicly available for the BCI research community.

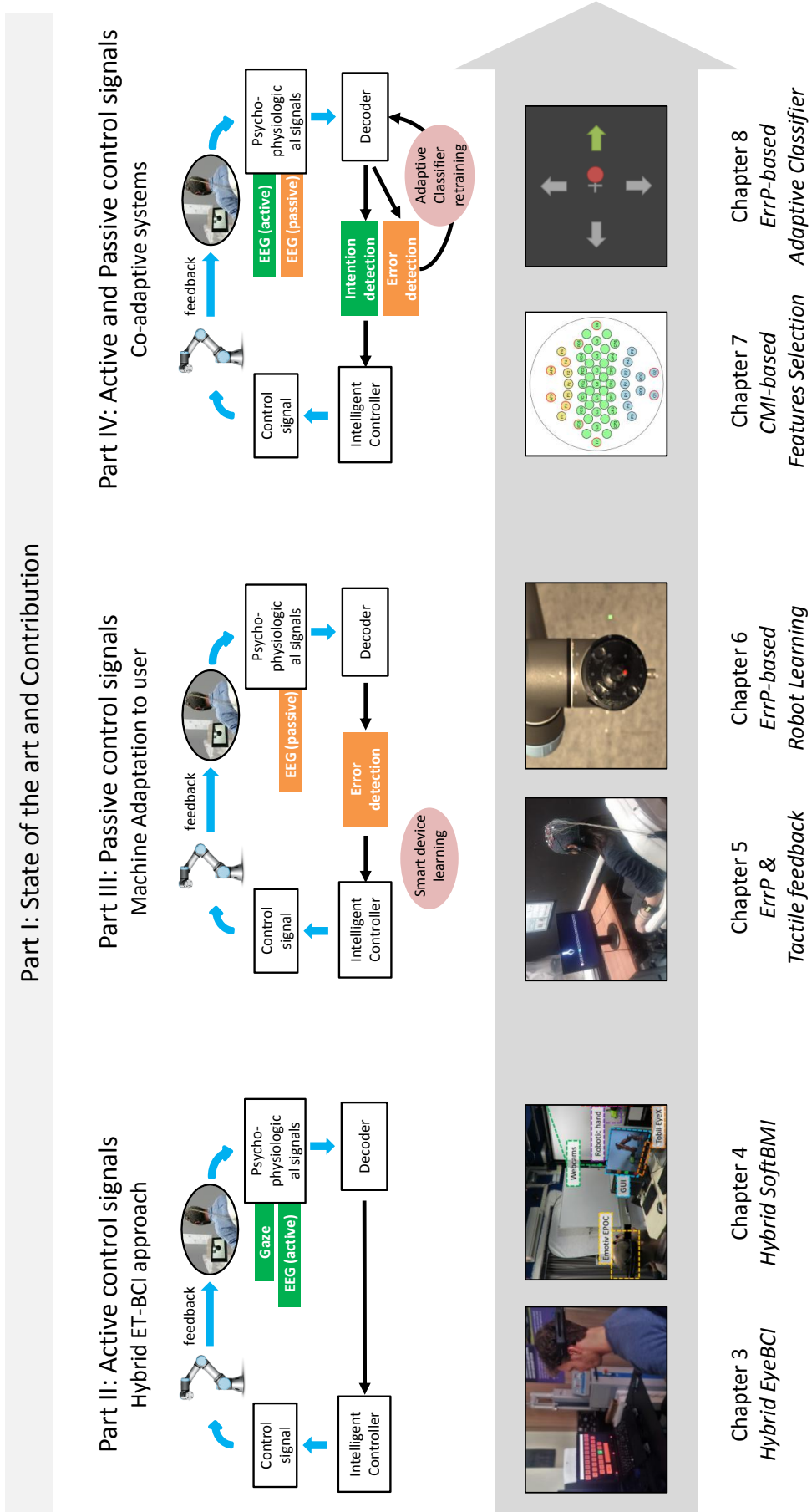


FIGURE 2.2: Contributions and thesis structure.

Part II

Active Control Signals: Hybrid ET-BCI Approach

Chapter 3

Focus Sensitive Dwell time in Eye-BCIs

This chapter introduces an hybrid ET-BCI solution - labeled as EyeBCI (Barresi et al., 2016) - in order to improve the performance and the usability of ET. A novel interaction concept is introduced to adapt the duration of the dwell time to the level of mental focus of the user of EyeBCI when he/she wants to select and activate a UI item: the dwell time shortens according to the raise of the observer's concentration, improving the system precision and responsiveness. The capability of this new interaction paradigm to be self-adaptable to the user's goals has the potential to greatly enhance the usability of ET solutions for patients with LIS.

This work has been published as : Barresi, G., Tessadori, J., Schiatti, L., Mazzanti, D., Caldwell, D. G., & Mattos, L. S. (2016, September). Focus-sensitive dwell time in EyeBCI: Pilot study. In Computer Science and Electronic Engineering (CEEC), 2016 8th (pp. 54-59). IEEE. - The final files for this publication are available from IEEE via: <http://dx.doi.org/10.1109/CEEC.2016.7835888>

3.1 Introduction

Current technologies for human-computer interaction offer different strategies for augmentative and alternative communication (AAC) (Beukelman et al., 2005) to assist people with severe motor impairments. For instance, many patients with locked-in syndrome (LIS) (Laureys et al., 2005) benefit from eye-tracking (ET) (Poole et al., 2006) cameras in order to move a cursor across a user interface (UI) by means of their gaze movements, and to activate any gaze-selected UI item by maintaining the gaze on it for a defined dwell time. This paradigm provides an intuitive control modality appreciated by many users. Nevertheless, the (unnatural) dual function of gaze (observation and control) in ET-based UIs can lead to stressful conditions, which can make the ET paradigm prone to errors and, by consequence, risk to present low performance, usability, and user experience. This typically happens when the user is not satisfied by the settings of the dwell time, which indeed should be calibrated and optimized according to the patient's skill and stamina: when the dwell time duration is shortened too much for the user, the ET control could become too challenging; when it is increased excessively, the user's engagement and motivation could decrease dramatically. Considering the potential of brain-computer interface (BCI) systems in monitoring parameters like user's attentive effort (Szafir et al., 2012), it is possible to design hybrid ET-BCI solutions (Vilimek et al., 2009), labeled as Eye-BCI in this work. Such solutions can improve the performance and the usability of ET, modulating its functioning according to the intentions of the users to control or explore the UI.

In this study, an interaction concept of EyeBCI is introduced to adapt the dwell time duration to the level of user's voluntary mental focus: the dwell time shortens according to the increase in concentration of the user. The result is an EyeBCI enriched by adaptive qualities that aims at decreasing the risk of errors in UI control and at improving user experience. In order to test this approach, implemented in a low-cost setup, a pilot study based on a series of comparisons between different ET and EyeBCI conditions was performed. The study considered performance metrics (correct characters per second, mean activation times, number of errors) and user experience indices (questionnaire scores). After describing the background of this investigation and the features of the novel "focus-sensitive dwell time" paradigm for EyeBCI, the experimental procedure and results are described and discussed, showing the potential of the proposed solution.

3.1.1 Background: EyeBCI Paradigms

As introduced above, ET systems offer easy and intuitive procedures of interaction by means of the detection of the user's ocular movements (Duchowski, 2002), often maintained in many cases of LIS (e.g., people with amyotrophic lateral sclerosis, ALS, can experience this kind of LIS before reaching total-LIS condition, which paralyzes also the ocular muscles, Spataro et al., 2014). Such systems are less demanding and more widely adopted solutions than BCIs, which enable paralyzed people to express thoughts and voluntary acts (decoded for instance from brainwaves in Moghimi et al., 2013). BCIs require more complex calibrations and trainings than ET, making their usage a highly difficult experience for the patients. Nevertheless, it must be observed that ET has its own costs (Majaranta et al., 2002), which include the effort required from the user for performing repetitive eye movements during hours of activity and for maintaining the gaze on a certain UI item until the end of a dwell time to activate it without producing accidental selections and activations.

In order to overcome such limitations, the approach of hybrid BCI (hBCI) can be introduced. hBCI systems (Henshaw et al., 2014) are designed for integrating different human-machine interfaces combined sequentially (when the output of one device becomes the input of the other) or simultaneously (when their data are processed in parallel). For instance, the hBCI perspective offers the opportunity to integrate ET and BCI (e.g., Cipresso et al., 2011) obtaining an eye-brain-computer interface, a category of hBCI labeled in this work as *EyeBCI*, designed for LIS patients who maintain a certain degree of ocular control. This solution can offer higher usability than each of its own components, improving the interaction capabilities of the users: ET can ease the pointing operation for selection, lowering the time for the calibration and training, while a BCI can ease the activation of the process triggered by the user in the observed location without a dwell time. Nevertheless, this hybrid approach can be severely influenced also by the limitations of its sub-components, in particular the BCI (Kos' Myna et al., 2013): the effort of triggering the activation of a UI item selected by the gaze can be affected by factors like the calibration of the BCI system or by the training of the user.

Considering such issues, this study defines a novel potential relationship between ET and BCI, aiming at designing more user-centered ET-based interactions.

3.1.2 Introducing a Focus-Sensitive Dwell Time in EyeBCI

The adaptive EyeBCI paradigm described in this work is based on two modalities of UI control: the ET enables the user to select an item of the UI, and the BCI enables

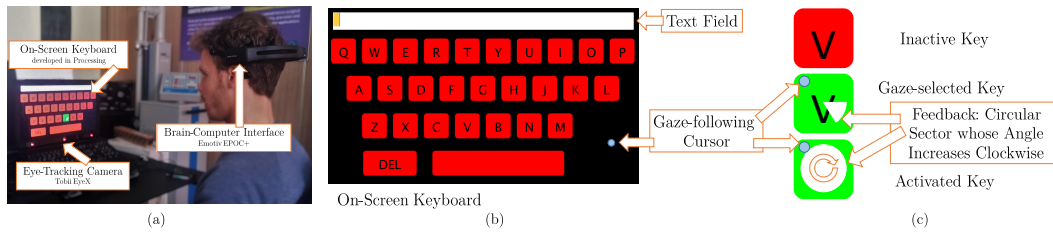


FIGURE 3.1: (a) Experimental setup, (b) on-screen keyboard and (c) states of a key.

him/her to shorten the dwell time for activating it according to his/her mental focus (representing the intention to activate the UI item). First of all, this solution fits with the natural dissociation between the activities of observation and control: when the user intends only to observe the UI, the dwell time will be long enough to avoid any accidental activation of its functions; on the other hand, if the user requires to interact with the UI, the dwell time will be reduced in order to facilitate the task.

The pilot study in this work evaluates this adaptive EyeBCI paradigm by comparing an implementation of it with 3 ET control paradigms and with a trigger-based EyeBCI technique. The 3 ET paradigms used for comparison are characterized by different dwell times, while the trigger-based (first action: gaze to select; second action: focus to activate) EyeBCI technique uses mental focus as a mean to activate gaze-selected UI items (as in typical paradigms involving the BCI device used in this investigation). Next sections will describe the pilot study conducted to evaluate how this adaptive EyeBCI can be comparable to ET and to trigger-based EyeBCI in terms of performance and user experience, estimating its actual functioning in adapting the dwell time to user's goals (observing vs. activating the UI).

3.2 Methods

In order to test the interaction paradigm proposed here, an experimental setup was designed and developed. The implementation of such paradigm is based on specific hardware and software solutions, which will be addressed in this section.

The context of the experiment was characterized by a setup in which the user controlled the selection and activation of on-screen keys either by means of ET or EyeBCI paradigms to accomplish the task of correctly writing 2 words. The experiment was performed on 14 healthy subjects (12 males, 2 females), with average age of 29.64 years (SD=3.88 years).

3.2.1 Setup

The complete setup is shown in Figure 3.1 (a), including an eye-tracker, a BCI, and an on-screen keyboard.

For all conditions, the commercial system Tobii EyeX¹ was used, including both hardware and software (i.e. EyeX SDK) components. The Tobii EyeX is used to track the eye movements and gaze point of the user. It is connected to the PC via USB 3.0 port, and it has to be mounted at the bottom of the screen, pointing towards the user's eyes from below. Its near infrared micro-projectors create reflection patterns on the cornea and pupil of the user's eyes and two optical sensors capture images of

¹<http://www.tobii.com/xperience/>

such reflection patterns. Advanced processing algorithms are then used to estimate the position of the eye in space and the point of gaze.

In order to detect the level of mental focus of the user, the electroencephalographic (EEG) headset Emotiv EPOC+² is used as the BCI hardware, together with the Emotiv control panel provided by the company as processing software. The neuroheadset includes 14 electrodes located in the positions AF3, F7, F3, FC5, T7, P7, O1, O2, P8, T8, FC6, F4, F8, AF4 according to the 10-20 International system, recording EEGs at a sampling rate of 256 Hz. This low-cost neuroheadset and its features, including the placement of electrodes, were extensively tested in past studies, considering also its previous version (Stytsenko et al., 2011). Its performance was proper for the pilot study presented here and for evaluating the chance of developing low-cost implementations of the novel EyeBCI paradigm. The Cognitiv suite of the Emotiv control panel was used to extract the Cognitiv value that represents the level of mental focus used as control signal during the experiment. The software provides a Cognitiv value from 0 to 1, corresponding to the degree of matching between a recorded calibration pattern of EEG activation (the subject was requested to focus on a UI item, recording a pattern of task-related high mental focus as in Barresi et al., 2015) and the present one. This calibration was performed alternating neutral and active trials lasting 8 seconds each. During neutral trials the user was asked to relax without moving any muscle, while during active trials the user was asked to concentrate on the action of pushing a computer-generated moving cube within the control panel. During the experiment, the value of the Cognitiv variable used to detect subjects level of mental focus was transmitted from the Emotiv control panel to the application via the open source software Mind Your OSCs³. The Cognitiv variable was low-pass filtered: current and previous Cognitiv value weights were the only two parameters of the filter and they were set to 0.01 and 0.99, respectively. Update of Cognitiv value occurred each time a new sample was acquired by the Emotiv (i.e. around 4 ms). Weights were chosen to provide an acceptable user experience during previous studies. Furthermore, Cognitiv was forced to zero after each key activation, to avoid erroneous multiple selections with activation.

The UI consisted of an on-screen keyboard, with red keys, including space, shift, and delete commands, and an upper bar where the typed text was shown. It was developed by means of the Processing⁴ environment, and it was presented to the subjects on the 15.6" screen of a laptop running Windows 7. A blue dot was displayed as a cursor to track the filtered user's gaze across the keyboard. Each key became green while the cursor was over it, showing a white circular sector whose angle increased clockwise as feedback until becoming a full circle when the activation condition was achieved. Figure 3.1 (b) depicts the on-screen keyboard and Figure 3.1 (c) the different states of the keys, from inactive to gaze-selected, to activated. Finally, the key restored its red color after the cursor moved away. It must be noted that, after the raw gazing coordinates were transmitted from the Tobii EyeX engine to the Processing application, such coordinates were filtered to stabilize the gazing task. A simple auto-calibration feature adds an offset to current coordinates so that eventually they match the center of the currently selected key. Similarly to the case of the Cognitiv variable, the estimated offset was also slowly changed in time, with weight of 0.9 and 0.1 for previous and current estimations, respectively.

²<http://emotiv.com/epoc-plus/>

³<https://sourceforge.net/projects/mindyouroscls/>

⁴<http://processing.org>

3.2.2 Task

The task consisted in correctly writing 2 words, “*cognitive robotics*”, using the ET or the EyeBCI control paradigm. The subject was warned with an error beep each time a mistake was detected. Each trial ended when the complete correct sentence was typed.

3.2.3 Experimental Conditions

Each subject performed the task in the conditions described below, according to a within-group experimental design with 5 levels of the independent variable “*UI Control*” and 5 repeated measures. The repeated measures correspond to 5 trials of writing 2 words as task using the system in each *UI Control* condition. Objective (performance) and subjective (user experience) measures were collected. All subjects performed the task under the following 5 different conditions of the independent variable *UI Control*:

Dwell times in ET conditions were defined after previous user trials, considering also the opinion of patients and healthcare professionals with experience with ET. In *EyeBCI trigger* the BCI triggered the activation of the key highlighted via ET by the user’s gaze, when the filtered Cognitiv value overcame the threshold of 0.3 (following the typical threshold-based activation paradigm used with the Emotiv EPOC+). In *EyeBCI dwell* the BCI reduced the duration of the ET dwell time according to the user mental focus. In particular, dwell time varied from 3 s to 0.75 s (a range defined based on preliminary user trials) according to the Cognitiv value and following the cumulative distribution of a beta function with $B(2, 15)$.

3.2.4 Experimental Procedure

Before the session started, and according to the ethical protocol, the subjects of this pilot study received information about the experiment and they signed an informed consent document. After this, the calibration of both ET and BCI was performed. ET was calibrated using Tobii EyeX Engine. BCI was calibrated using Emotiv Cognitiv suite, alternating neutral and active 8 s trials, for about three-five minutes, until the subject felt confident with the Cognitiv variable control level. After calibration, and before the first session, each subject was asked to perform two short training trials, typing the word “*hello*”, under conditions *ET 1.5 s* and *EyeBCI trigger*, to understand the most typical functioning of ET and of EyeBCI with the Cognitiv threshold paradigm.

Each subject ran 2 sessions of 5 trials each one, corresponding to 3 ET-based (*ET 3.0 s*, *ET 1.5 s*, *ET 0.5 s*) and 2 EyeBCI-based (*EyeBCI trigger*, *EyeBCI dwell*) controls. In the first session (*familiarization*) the conditions were presented in the same order within their block: a block with the ordered set 1-*ET 3.0 s*, 2-*ET 1.5 s*, 3-*ET 0.5 s*, and a block with the ordered couple 1-*EyeBCI trigger*, 2-*EyeBCI dwell*. In order to control potential effects of the sequence, half of the subjects experienced the ET block before the EyeBCI block, and the other half the EyeBCI before the ET. In the second session (*evaluation*) the five conditions were presented in random order, to check the potential effects of repeated measures.

1. *ET 3.0 s*, based on ET control with dwell time of 3s;
2. *ET 1.5 s*, based on ET control with dwell time of 1.5s;
3. *ET 0.5 s*, based on ET control with dwell time of 0.5s;

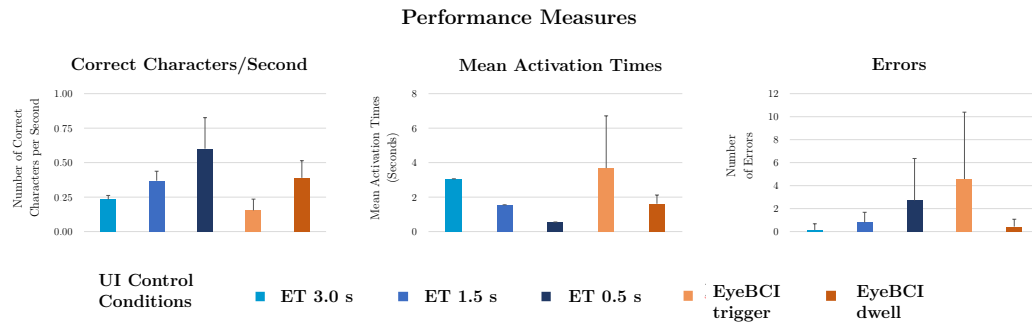


FIGURE 3.2: Performance indices - means (across users in each trial, representing a condition) with upper standard deviation bars.

4. *EyeBCI trigger*, based on the BCI triggering the activation of the key highlighted via gaze;
5. *EyeBCI dwell*, based on the BCI shortening the duration of the ET dwell time.

3.2.5 Measures

Objective Measures of Performance

From the *evaluation* session the following performance measures were extracted per each trial, that is constituted by the task of writing “*cognitive robotics*”: (a) the number of correct characters per second, computed as the total time required to accomplish the task divided by the number of correct characters activated during each trial; (b) the mean activation time, computed as the mean time elapsed between gaze moving inside a key and its activation during each trial; (c) the number of errors, i.e. erroneous activated characters during each trial.

Subjective Measures of User Experience

After each trial of the *evaluation* session, the subject was asked to fill out a questionnaire based on 8 statements (Figure 3.3) on different dimensions of user experience. Considering each completed trial, the subject was asked to mark on a continuous-like rating scale his/her level of agreement with each statement. Each scale consisted in 100 points: it was divided in 100 intervals by small lines and with increasing values from left to right. The 1st, 25th, 50th, 75th, and 100th lines are bigger than the others to provide intuitive reference points for the subject (similar to a 5-point Likert-type scale). The resulting pattern is perceptually similar to visual analogue scales (Jaeschke et al., 1990) that allow to perform properly a wider range of analysis techniques than the discrete scales with few points.

3.3 Results and Discussion

Since ANOVA could not be used (assumptions of normality and sphericity are violated because of high variability of the data, probably due to the small number of trials and subjects in this pilot study), Friedman’s chi squared was used to compare the effects of different conditions on each performance measure, considering also the repeated measures (each condition was tested in a different trial). No effect of

TABLE 3.1: Performance data - means (M) with standard deviations (SD).

Performance Indices	Correct Characters/s		Mean Activation Times (s)		Errors	
	M	SD	M	SD	M	SD
<i>ET 3.0 s</i>	0.23	0.03	3.05	0.00	0.14	0.53
<i>ET 1.5 s</i>	0.37	0.07	1.55	0.00	0.79	0.89
<i>ET 0.5 s</i>	0.60	0.23	0.55	0.00	2.71	3.65
<i>EyeBCI trigger</i>	0.15	0.08	3.69	3.03	4.57	5.81
<i>EyeBCI dwell</i>	0.39	0.12	1.61	0.51	0.43	0.65
Friedman's chi squared (4)	43.26		40.97		15.67	
<u>p<0.01</u>	<u>9.15e-09</u>		<u>2.73e-08</u>		<u>3.5e-03</u>	

repeated measures was found. Table 3.1 and Figure 3.2 depict the results of performance measures (number of correct characters per second, mean activation time, number of errors) in terms of means and standard deviations (in each trial, across users). Table 3.1 presents also the Friedman's chi squared values in the comparisons across all conditions, with p-values with 0.01 as significance threshold. Significant differences in Friedman's chi squared were found in each comparison across all conditions. Pairwise tests allowed to evaluate further the differences between conditions in terms of preliminary observations according to the goals of this pilot study. Overall, the condition *EyeBCI trigger* showed the smallest number of correct characters per second, the longest mean activation time, and the highest number of errors. Comparing the two *EyeBCI* conditions, it can be observed how the BCI worked better in all performance indices when used to shorten the dwell time instead of triggering the activation of the gaze-selected UI item. *ET 0.5 s* resulted in the best overall performance in terms of number of correct characters per second, with the lowest mean activation times, but such advantages showed also costs in terms of number of errors. *EyeBCI dwell* is far less prone to error than *ET 0.5 s*. It is also slightly less fallible than *ET 1.5 s*, but this is not statistically significant. *ET 1.5 s* and *EyeBCI dwell* are similar in terms of correct characters per second and mean activation times. *ET 3.0 s* showed a non-significant advantage in terms of number of errors over *EyeBCI dwell*, without improving the number of correct characters per second (also because of the long mean activation times).

A within-subject ANOVA (Table 3.2) was performed (assumptions were checked) for each scale of the questionnaire about user experience, comparing the effects of control conditions on their scores. No effect of repeated measures was found. Significant effects of the different conditions in *UI Control* variable occurred in all scales but the 7th ("The time required to select a symbol was too short"). Considering also the post-hoc tests, it was possible to highlight how the *EyeBCI trigger* was the worst condition overall, while the *EyeBCI dwell* was appreciated in terms of speed, ease of use, and proneness to errors. Nevertheless, it must be noted the level of mental effort and fatigue expressed in scales 2 and 6: *EyeBCI dwell* was probably affected by the limitations in BCI control (effort in mental focus), even if they are influencing the interaction less than in *EyeBCI trigger*, where the activation of the key is completely controlled by the BCI without a dwell time.

TABLE 3.2: Questionnaire data - means (M) with standard deviations (SD) - expressing the agreement of the subject (from 0 for "strong disagreement" to 100 for "strong agreement") with the statements in Figure 3.3 about different aspects of user experience.

Scales	1		2		3		4		5		6		7		8	
	M	SD														
<i>ET 3.0 s</i>	55.4	35.0	27.2	28.3	27.3	26.2	66.4	28.3	83.4	17.8	23.3	23.8	17.4	26.3	18.5	28.6
<i>ET 1.5 s</i>	35.5	26.3	14.0	11.9	10.4	11.3	72.9	27.0	82.1	14.9	16.6	15.4	22.4	23.8	21.1	22.8
<i>ET 0.5 s</i>	8.4	8.5	7.9	9.0	14.8	13.0	80.4	18.0	77.9	21.2	19.5	18.9	41.8	34.6	50.5	34.5
<i>EyeBCI trigger</i>	60.5	32.3	69.6	30.4	60.1	31.8	50.5	31.7	33.0	25.2	51.9	31.2	23.3	24.8	54.9	34.8
<i>EyeBCI dwell</i>	24.8	22.7	34.5	30.6	25.2	22.8	62.9	29.8	67.1	29.6	34.5	26.5	22.3	16.0	24.1	20.5
$F(4,52)$	10.9		15.18		12.03		4.05		12.45		6.46		2.13		5.03	
$p < 0.01$	<u>1.7e-06</u>		<u>2.8e-08</u>		<u>5.4e-07</u>		<u>6.3e-03</u>		<u>3.6e-07</u>		<u>2.7e-04</u>		<u>9.1e-02</u>		<u>1.7e-03</u>	

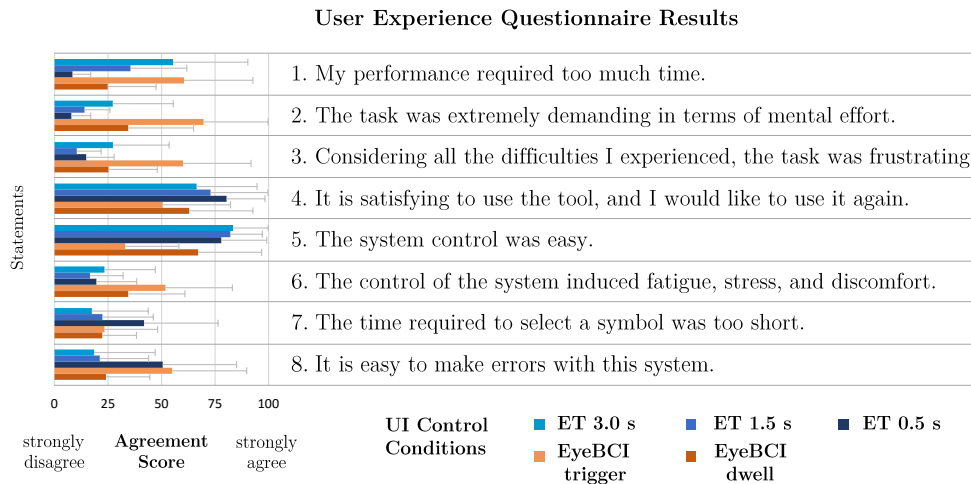


FIGURE 3.3: Scores - means with upper standard deviation bars, across subjects - of the 8 rating scales presented in the user experience questionnaire.

Apparently, the most important advantage of the *EyeBCI dwell* was the low perceived proneness to errors, on the same levels of *ET 3.0 s* and *ET 1.5 s* ET conditions. The *ET 0.5 s* is perceived as quite demanding in temporal terms, and as prone to errors like the *EyeBCI trigger* probably because of the risk of selecting a word when the Cognitive value is already over threshold.

The analysis of performance and user experience data showed that the *EyeBCI dwell* condition was less prone to errors than the fastest ET condition. In addition, it has overcome, in all indices, the *EyeBCI trigger* condition, which implemented a more typical ET-BCI control. Thus, *EyeBCI dwell* offers high precision and responsiveness, similar to (and, in terms of errors number, slightly better than) an ET with average dwell time. In addition to this, *EyeBCI dwell* paradigm has the potential of obtaining even shorter mean activation times, while in typical ET they are obviously constant. The fatigue and frustration of the users in *EyeBCI dwell* is higher than in ET conditions: it depends probably on the BCI control, which requires more advanced methods of EEG interpretation than the default ones offered by the low-cost Emotiv EPOC+. Nevertheless, such fatigue and frustration are smaller than the ones produced by *EyeBCI trigger*. Such observation, alongside the ones about performance, suggests to design EyeBCI paradigms with an adaptive relationship between ET and BCI that is based on a flexible facilitation of ET according to the user's intentions (which increases the potential self-customization of ET) instead of EyeBCI paradigms with a prone-to-errors pure sequential control of gaze-selection followed by focus-activation.

3.4 Conclusions

In this study, an interaction concept of focus-sensitive dwell time in EyeBCI (UI dual control based on ET and BCI) is introduced to adapt the duration of the dwell time to the level of mental focus of the user: the dwell time shortens according to the increase in concentration of the user in order to improve the system performance and the user experience.

This approach was evaluated by means of a series of experimental comparisons within a pilot study that considered 5 UI control conditions, 3 based on ET (differing

by duration of dwell time: 3 s, 1.5 s, 0.5 s) and 2 based on EyeBCI (in one case the BCI triggers the activation of the UI item observed by the user, in the other the BCI lowers the dwell time for the activation of the observed UI item according to the level of mental focus of the user). The task was based on the selection and activation of keys on an on-screen keyboard to write 2 words. The comparisons considered performance measures (correct characters per second, mean activation times, number of errors) and user experience measures (questionnaire scores).

The tested implementation of the novel EyeBCI surpassed, in all considered aspects of user experience and performance, an EyeBCI based on a typical BCI-trigger to select the keys. It obtained selection times and performance levels similar - and slightly superior in terms of errors - to the ones of ET with medium dwell time (1.5 s). Nevertheless, the effectiveness of the novel EyeBCI is shown alongside higher fatigue than the one experienced by subjects under ET conditions. Next investigations will consider this issue while improving the capabilities of self-customization in the algorithms for EEG interpretation: a faster recognition of the user's intentions should lower his/her fatigue, maintaining the same levels of precision or raising them further. Indeed, the results of this pilot study were obtained by means of a low-cost implementation of the paradigm, which did not allow a specific study of EEG signals to customize the recognition processes. Yet, the potential of the focus-sensitive dwell time paradigm for EyeBCI was confirmed because it actually shaped the dwell times according to the requests of the user, avoiding too long or too short durations as pure ET paradigms cannot do. While it is obtaining performance results similar to ET paradigms, it is also minimizing the errors that can be produced without modulating the dwell time according to the real time changes of users' goals (observing or activating the UI).

Chapter 4

Soft Brain-Machine Interfaces for Assistive Robotics

This chapter aims at exploring the potential of a novel hybrid Brain-Machine Interface - labeled as SoftBMI (Schiatti et al., 2017) - composed of an eye-tracking system, for an intuitive and reliable control of a robotic arm system's trajectories, and a BCI unit, for the control of the robot Cartesian stiffness, which determines the interaction forces between the robot and environment. The latter control is achieved by estimating in real-time a unidimensional index from user's EEG signals, which provides the probability of a neutral or active state. This estimated state is then translated into a stiffness value for the robotic arm, allowing a reliable modulation of the robot's impedance, and its adaptation to dynamic constraints of different tasks. The potential of the proposed approach resides in exploiting the BCI as an additional channel, enhancing the degrees of freedom available for control over both kinematic and dynamic behavior of an assistive device.

This work has been published as : Schiatti, L., Tessadori, J., Barresi, G., Mattos, L. S., & Ajoudani, A. (2017, July). Soft brain-machine interfaces for assistive robotics: A novel control approach. In Rehabilitation Robotics (ICORR), 2017 International Conference on (pp. 863-869). IEEE. - The final files for this publication are available from IEEE via: <http://dx.doi.org/10.1109/ICORR.2017.8009357>

4.1 Introduction

The applications of robotic arms in assistive domains have demonstrated a high potential in improving the patient's quality of life by reducing their degree of dependence on caregivers, aiding them in activities of daily living (ADLs), such as self-care and pick-and-place tasks (Tsui et al., 2008). Patients who can benefit from this technology include those with upper body disabilities, such as traumatic spinal cord injuries (SCI), paraplegic and tetraplegic patients (Kim et al., 2012). To make robotic arms suitable for the execution of a large class of daily tasks, intuitive and user-friendly human-robot interfaces must be designed to associate the residual capabilities of the users with disabilities to appropriate robot functions.

There are many studies aiming at improving the usability of commercially available robotic arms in assistive scenarios, by designing control interfaces able to reduce user's cognitive burden and time required to accomplish a task. Such interfaces often rely on teleoperation or shared control paradigms. Typically the partially or fully autonomous robot behavior is adapted to the user's high level inputs, based on his/her residual limb motor capabilities, to enhance the task execution performance. An example of implementation is shown in Jain et al., 2015, where shoulder movements are detected and mapped into high level control signals for a robotic arm.

Here a shared-control framework for assistive manipulation is built on the concept of autonomous piecewise trajectory segments. In a similar vein in Jiang et al., 2013a, a haptic 3D joystick was adapted to directly control a robotic arm movements, enhancing the performance of traditional arm joystick control. In Jiang et al., 2013b, a hand gesture recognition interface was combined with robot embedded object tracking and face recognition to control a wheelchair-mounted robotic manipulator.

However, for people suffering from more severe forms of motor disabilities, the above mentioned Body-Machine Interface examples cannot be exploited to drive a robot function. To address this issue, former studies explored the use of gaze (Dziemian et al., 2016) or brain signals, through eye-trackers and Brain-Computers Interfaces (BCI) respectively, to produce robot control by means of non-muscular channels. Robotic systems driven by brain signals, also known as Brain-Machine Interfaces (BMI), typically exploit P300 (Palankar et al., 2009), steady-state visual evoked potentials (SSVEP) (Petit et al., 2014), or motor imagery (Meng et al., 2016) paradigms, to generate high level commands to control a robot. However, despite the continuous improvements, BCI systems are still far behind those based on Body-Machine Interfaces in terms of performance and reliability. This is due to well-known issues, such as high cognitive loads on the user, especially in continuous control schemes, low performance in high degrees of freedom control, and lack of flexibility given that user choices are mostly predefined. To overcome the limitations of pure BCI systems, hybrid interfaces have been proposed that exploit a combined use of EEG and another biosignal, as those based on BCI and gaze, to enhance communication (Barresi et al., 2016) or robot control (Wang et al., 2015).

It is worth mentioning that most of the existing solutions focus on aspects related to the ease-of-use and intuitiveness of the user interface rather than on the control of physical interaction capabilities of the robot. The latter feature can contribute to enhanced interactions in the human-robot-environment loop, and the underlying safety. When developing a robotic assistive tool, a safe behavior must be guaranteed e.g., for eating/drinking or personal hygiene tasks, as well as in case of accidental arm collisions with the environment (Vogel et al., 2015). A well-known strategy to ensure safety in a robotic system is the active impedance control, which regulates the interaction between the robot and its environment, including a virtual compliance at the joint level between the motor and the output, which causes the human operator to perceive a softer arm.

Within this context, the concept of Teleimpedance control (Ajoudani et al., 2012) has been recently proposed for the control of teleoperated robots, not only by means of kinematics quantities, to drive robot position and trajectory, but also regulating dynamic aspects like its stiffness or full impedance parameters during the task execution. Through this framework, the robot is able to adapt its physical behavior to various interaction scenarios, by replicating the master's real-time measured trajectories and limb impedance, usually estimated by processing electromyographic (EMG) signals (Ajoudani, 2016). Nevertheless, as mentioned above, the use of EMG cannot be considered for patients with severe motor disabilities.

To address these issues, in this work we present a hybrid BMI for real-time planning of a robotic arm movements and its physical interaction behavior. Our contribution is two-fold. (1) We use gaze signals for continuous robot position control, to explicitly select the target in reaching and grasping tasks. In this way, the developed interface can be used by severely motor-impaired people, since gaze control is a long-lasting motor process in most motor diseases. Moreover, the gaze constitutes an intuitive and reliable input to control the robot motor planning in the 3D space,

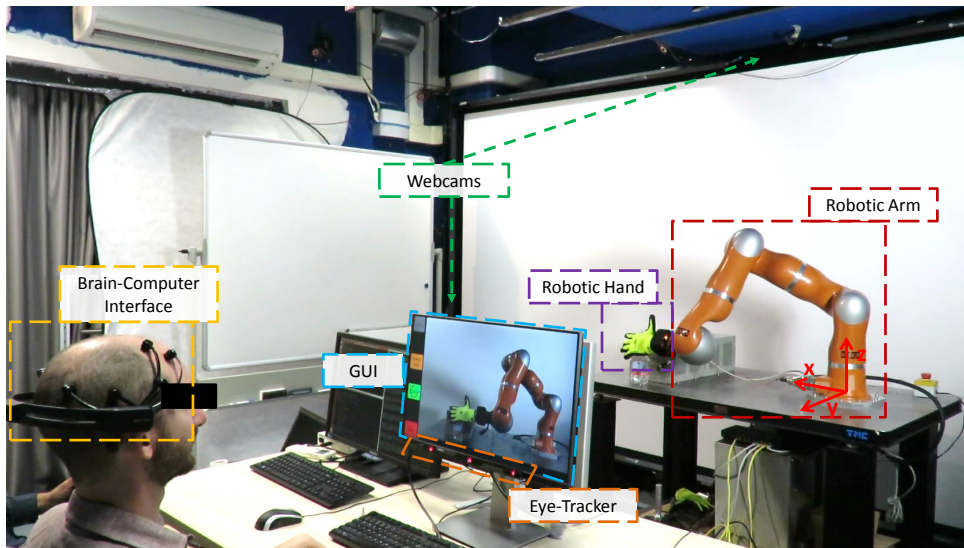


FIGURE 4.1: System setup for Soft Brain-Machine Interface: translational movements of the robot in space are controlled by human gaze, while an EEG-driven unidimensional index regulates the robot Cartesian stiffness in real-time.

overcoming the limits and constraints of a BCI system, which we use instead for low-dimensional control. (2) We introduce the novel idea of exploiting EEG signals as an input for active impedance control of assistive robots. To the best of our knowledge, it is the first attempt in the literature. This approach will enable motor-impaired users to achieve also a dynamic control of the robot interaction behavior (stiff/soft). Considering this feature, we call the presented system "Soft BMI". The control of robot Cartesian stiffness profile is simultaneous to the kinematic gaze-driven position control, in a seamless way, and the BCI is used to command a less crucial aspect of robot behavior, for which an estimation error does not contribute to a substantial reduction of the robot performance.

The proposed technique is implemented in an assistive robotics application: using a robotic arm to grasp and move objects in tasks with different constraints. In our setup (see Fig. 4.1), the user can drive a compliant robot using gaze and move it in an unstructured environment to establish a soft contact or avoid high interaction forces during collision. If there is a requirement for a higher interaction force profile, the operator can increase the robot stiffness to accomplish the task, by means of a mental command. A unidimensional index corresponding to the probability of command detection is associated to the regulation of the robot's Cartesian stiffness components in all translational and rotational directions. This allows for a higher task accuracy, as it is well-known that an enhanced movement accuracy or increased force capability in humans or robots can be achieved by stiffer profiles of the human and the robot joints (Gribble et al., 2003).

4.2 Methods

Fig. 4.2 introduces the system, which consists of three main parts: Input block, which includes two web cameras, an eye-tracker, and an EEG headset to achieve the BCI functions; Control Interface, implemented in Processing programming environment, for the real-time processing of the input data to generate suitable control outputs for the third block; and the Actuated System, a 7-DoF torque controlled robotic arm

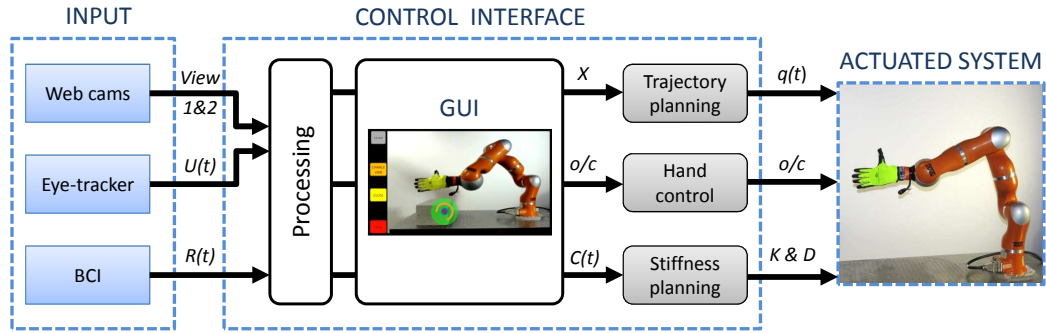


FIGURE 4.2: Information workflow between system components.

equipped with the Pisa/IIT SoftHand (Catalano et al., 2014). The components of the system and the flow of information between them are described in detail in the following sub-sections.

4.2.1 Web cameras

Two low-cost Logitech web cams were used to monitor the robot position from different angles and allow the user to plan 3D translational movements of the robot end-effector. Cameras were placed on top and to the side of the setup, so that each view allows for a clear selection of a coordinate pair. A Logitech B525 HD webcam was set above the robot, to capture xy view in robot coordinates system (view 1 in Fig. 4.3), while a Logitech HD C270 webcam was put in front of the robot, to catch xz view (view 2 in Fig. 4.3). An autonomous algorithm was implemented to build the mapping from the gaze coordinates on the screen to the robot coordinates for each camera. To this purpose, in the calibration phase (executed only once, depending on the placement of the cameras), the operator selected a few points on the screen, with known coordinates on the KUKA frame of reference, for each view. The rest of the mapping, i.e. the identification of two homogeneous transformations, was done autonomously using the algorithm.

4.2.2 Eye-Tracker

The eye-tracker employed in this work was the commercially available Tobii EyeX, both in its hardware and software (i.e. EyeX SDK) components. The system consists of two infrared micro-projectors that are used to illuminate user's eyes, while two optical cameras record the reflections of visible and infrared light on corneas and pupils. A USB 3.0 connection is required to connect the sensor system to the computer, in order to transfer the data collected by the imaging sensor. This information is processed by the dedicated software to provide the screen coordinates of the user's current gaze target. The gaze target coordinates provided by the Tobii system were transmitted via UDP to the Control Interface script at 30 Hz frequency, and filtered using the following equation:

$$X_i(t) = X_i(t-1)(1 - \sqrt{V(t)}) + U_i(t)\sqrt{V(t)} \quad (4.1)$$

in which X_i denotes the filtered i^{th} coordinate, with $i=1,2$, $U_i(t)$ is the Tobii estimation at time t and $V(t)$ is an estimation of the movement speed of the gaze target in the

current step. More specifically, $V(t)$ was defined as:

$$V(t) = \sqrt{\sum_{i=1,2} \left(\frac{X_i(t-1) - U_i(t)}{X_{max_i}} \right)^2} \quad (4.2)$$

where X_{max_i} is the largest value the i^{th} coordinate can assume (i.e. the screen resolution along each dimension). With this normalization, $V(t)$ varies in the $[0, 1]$ range. Intuitively, this filter was designed to cancel out minor gaze fluctuations, while leaving performance on fast movements as unchanged as possible.

4.2.3 Brain-Computer Interface

The unidimensional index for the impedance control was estimated through the combined use of the EEG system Emotiv EPOC+ and its accompanying software. The Emotiv EPOC+ is a low cost EEG wireless headset with 14 electrodes located at the positions AF3, F7, F3, FC5, T7, P7, O1, O2, P8, T8, FC6, F4, F8, AF4 according to the International 10-20 system, communicating with the PC via bluetooth. Sampling rate is 256Hz. Given the final goal of developing an affordable and usable assistive technology, Emotiv EPOC was chosen in this study for his significant advantages in terms of cost, portability, robustness and user customization. Although it lacks in reliability and signal quality compared to existing medical EEG interfaces, it has already been used in robotic applications both exploiting its embedded muscular measurements (Ranky et al., 2010) and EEG signals (e.g to control a 7 dof robotic arm in Ouyang et al., 2013).

The Emotiv software includes a control panel, which encompasses a Cognitiv suite. The latter evaluates user's real time brainwave activity to discern the user's conscious intent to perform physical actions on a real or virtual object. Up to four actions can be recognized at any given time. The detection system outputs a single action or neutral (i.e. no action) at a time, along with an action power, a unidimensional scalar index ranging between 0 and 1 representing the detection certainty that the user has entered the mental state associated with that action. For the present work, only one action, corresponding to the "push" mental command was trained and used. Training was performed using the Cognitiv suite, and consisted in alternation of neutral and active states in trials lasting 8 s each one, for some minutes, until user felt comfortable with the state control. In neutral trials the user was asked to relax and avoid moving, while during active trials the user had to focus on the action of pushing a 3D object (cube) represented on the screen.

An open source software (Mind Your OSCs) was adopted to transmit via OSC protocol the Emotiv readings to the Processing Control Interface. To limit quick fluctuations in the estimation of the mental action state index, the raw value provided by the Cognitiv suite was low-pass filtered with a leaky integrator:

$$C(t) = \min(1, R(t) + A \times C(t-1)) \quad (4.3)$$

Here, $R(t)$ is the reading provided by the Emotiv system at time t , while $C(t)$ is the filtered index describing user's concentration (neutral or active) state. The parameter A has a value ranging in the $[0, 1]$ interval, with typical values around 0.5. This parameter was introduced in order to compensate for widely varying performances observed across different users and sessions and it was re-calibrated before each session in order to provide an acceptable user experience. Finally, the upper limit of

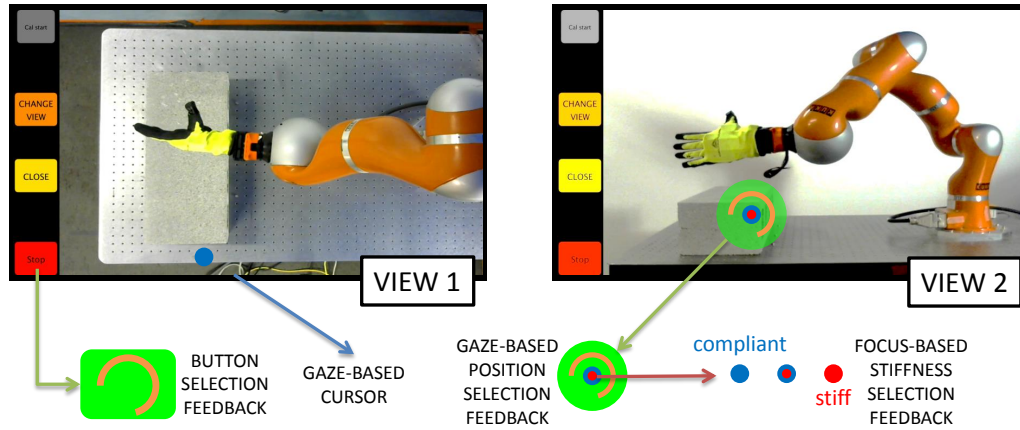


FIGURE 4.3: Graphical User Interface.

1 was imposed to the C value in order to keep its range consistent with the input variable R .

4.2.4 Graphical User Interface (GUI)

The GUI itself consisted of a vertical panel on the left margin of the screen including four buttons (from top to bottom: calibration start/stop, change view, open/close and stop), while most of the monitor was displaying the live feed from the currently selected camera (Fig. 4.3). The buttons on the left allowed the user to:

- start and stop the calibration to map each webcam screen view coordinates with corresponding robot workspace coordinates;
- switch currently selected camera;
- open or close the Pisa/IIT SoftHand;
- stop the robot movement in case of wrongly issued command.

An interactive cursor was constantly indicating gaze target and current mental state: the cursor was a blue dot when C was zero (neutral state) and it progressively became red with increasing current values of C . A button was selected when the gaze-controlled cursor rested within it for longer than 1.5 s (this dwell time was shortened to 0.5 s for the stop button in the lower left corner). A circular progress bar provided the indication of elapsed and total dwell time required.

The selection of the desired target robot position was enabled by fixing gaze on the corresponding point in the webcam screen view: if gaze velocity $V(t)$ fell below a certain threshold while on top of a specific point on the webcam image, a virtual circular button appeared and its progress bar started filling as for the buttons of the left panel. If the user did not divert its gaze from the button, when the bar was filled the target point coordinates X were sent to the robot controller. Diverting gaze caused the virtual button to disappear. Rigidity of the robot during each movement was a function (see text below) of the concentration index C at the time instant in which the progress bar filled completely.

4.2.5 Actuated System

System evaluation was carried out using a 7-DoF KUKA lightweight robotic arm. The robot was controlled in torque mode and a Cartesian impedance controller was developed to achieve the operator's planned trajectories through the eye-tracker, in KUKA frame of reference (using two transformations, as explained above). A fifth order polynomial model generated online smooth Cartesian trajectories in between two selected points on the screen, every time the operator's gaze target point on screen was detected by the User Interface. This consideration was to achieve smooth trajectories in a suitable time, that was estimated according to the distance from the final destination.

The Cartesian stiffness of the robot was allowed to vary between a minimum (K_0) and maximum (K_m) value of 300 to 2000 $\frac{N}{m}$ for all translational components (k_t), and 50 to 250 $\frac{Nm}{rad}$ for rotational ones (k_r), respectively. The exact value was estimated in real-time from the concentration index, using a linear mapping:

$$K_{t,r} = K_{0,t,r} + C(t)(K_{m,t,r} - K_{0,t,r}) \quad (4.4)$$

This profile enables the robot to establish a soft contact in case of lower stiffness values, while demonstrating a stiff behaviour when a higher precision or force generation is required by the task. The Cartesian damping matrix D was obtained from the desired K using the double diagonalisation design as explained in Albu-Schäffer et al., 2003.

The robot was equipped with the Pisa/IIT SoftHand, an under-actuated and synergy driven robotic hand. The embedded adaptivity of the robotic hand made this choice ideal for the grasping of objects with various shapes since only one actuator input was controlled. The hand unit and power driver for the motors (SoftHand and force feedback cuff) are custom control boards based on the Texas Instruments Luminary DSP chip LM3S8962. The DSP control loop is executed at 1KHz while the communication with the host PC is achieved through a real time Ethernet link. Motor current measurement is performed by a hall effect based current sensor (ACS714, Allegro Microsystems Inc.) and appropriate signal conditioning integrated in the motor power driver module. The robot control script was implemented in C++ environment, running in a separate PC and receiving the user input from the Processing script via UDP. A data package included the selected target gaze coordinates X with a flag indicating if they are expressed in view 1 or view 2, a control bit indicating open or close state of the hand, and the concentration index $C(t)$ describing user's mental state.

4.3 System evaluation

The presented Soft BMI system was tested on two different subjects (aged 24 and 33), who were asked to control the robot in two different tasks. One subject had previous experience with both the Tobii eye tracker and the Emotiv BCI system, while the second was a naive subject. Operative tests were preceded by a calibration session for both the eye-tracker and the BCI, with the standard procedures implemented in the software suites of the two systems. Both subjects were able to control the GUI of the robot within minutes: they could deliberately fixate gaze on any given point on the screen in order to select it as a robot target position while maintaining the chosen mental state, corresponding to concentration index equal to 0 for neutral or a scalar between 0 and 1 for active state, or divert gaze to prevent undesired commands.

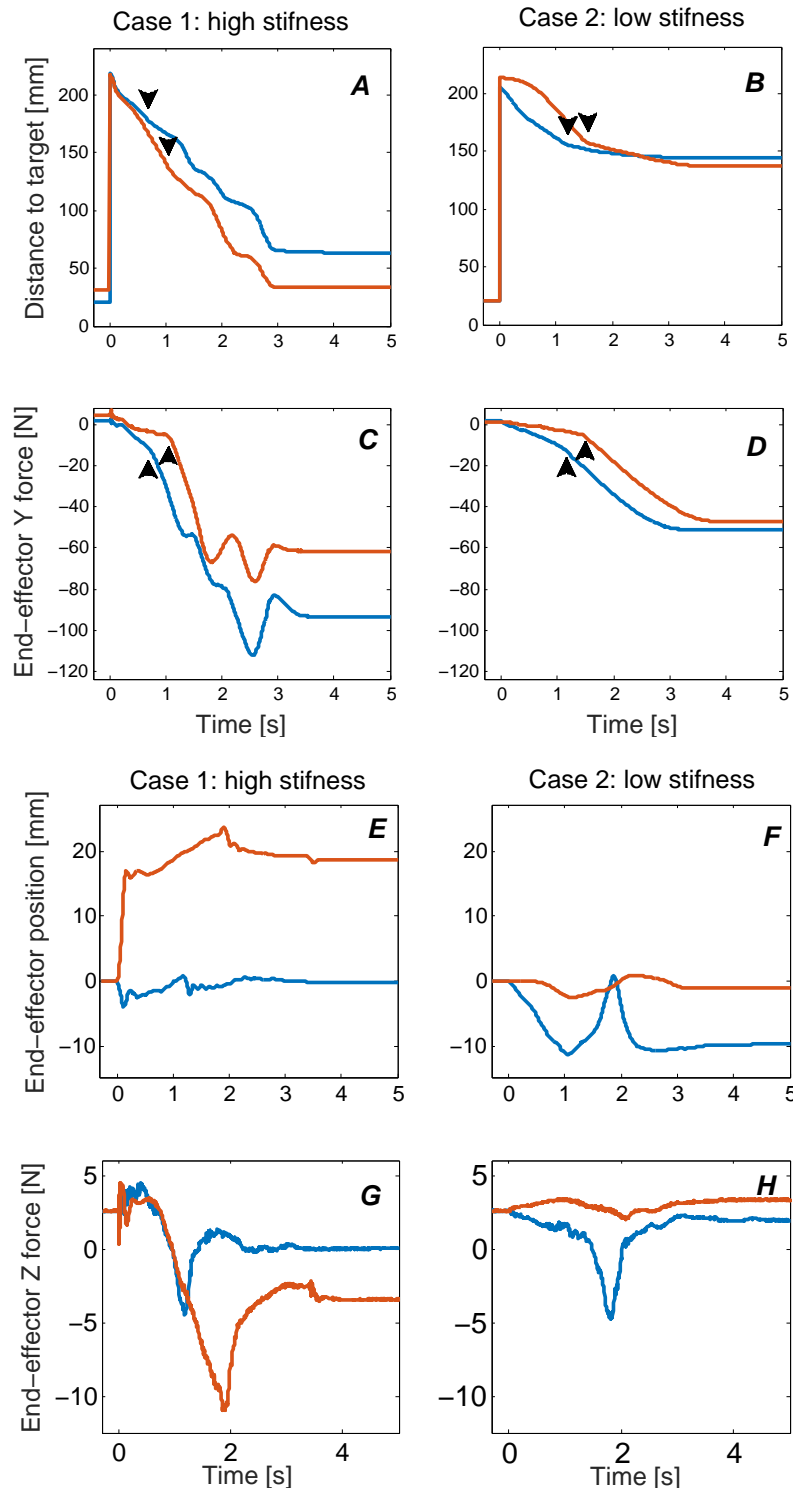


FIGURE 4.4: Results from system evaluation. Panels A-B: distance between current arm endpoint and selected target for high (panel A) and low (panel B) stiffness trials and corresponding estimated endpoint forces in the push direction (panels C-D). $t = 0$ corresponds to Kuka receiving movement command. Black triangles indicate the approximate contact moment between soft hand and object. Panels E-H: distance traveled by arm endpoint since $t = 0$ in the vertical direction, for high (panel E) and low (panel F) stiffness trials and corresponding estimated endpoint forces, in the vertical direction. $t = 0$ corresponds to Kuka receiving movement command. Contact between grasped object and obstacle occurs almost immediately after movement start. Blue (orange) line depicts trials performed by experienced (naive) user (S1, S2 respectively).

4.3.1 Tasks

Two complementary tasks were considered to evaluate the effectiveness of the proposed interface for the online control of the robot trajectories and physical interaction behavior.

Heavy object pushing: The purpose of this task was to demonstrate the need for force production capabilities of robots when dealing with precision tasks. In this task, the user was asked to position the robotic hand beside a heavy brick (about 8 kg), and push it aside by selecting a target position around 15 - 20 cm inside the brick from the top view (please refer to the accompanying video, see Fig.5 caption). The user was asked to perform the task in both neutral and active mental state in order to select low and high robot Cartesian stiffness profile, until the task was accomplished.

Object grasping and environment collision: This task was designed to stress the need for a compliant behavior of the robot when dealing with an unstructured environment, in which collisions with obstacles are likely to occur. The user was requested to control the robot in order to grasp a partly full plastic water bottle (around 0.2 kg), lift it and then move the arm such that the part of the bottle sticking out below the hand would hit a rigid, immovable obstacle. As for the previous task, the user was asked to repeat this test in two conditions, with the lowest and highest possible levels of robot stiffness respectively. Our objective was to examine the effectiveness of the proposed interface in allowing the user to control robot behavior adaptability to the environment constraints¹.

4.4 Results and Discussion

Heavy object pushing: Fig. 4.4 illustrates results of two repetitions of the task, performed by the two subjects. Panels A-C and B-D represent data collected during the active and neutral mental state, corresponding to high and low stiffness respectively. In particular, panels A and B show the distance, expressed in millimeters, between gaze-selected target and robot endpoint current position, while the second row presents the endpoint forces produced by the Kuka robot in the y (pushing) direction. Different colors correspond to trials performed by different subjects.

Since the robot started in the position of the last selected target, the distance to target was approximately 0 at the beginning of the trial. At $t = 0$, a new target was chosen in order to push the object forward and the robot started moving. Impact occurred around 1 s later in all presented trials, as evidenced by the black triangles in Fig. 4.4. After touching the obstacle, the robot sharply increased the applied force in y direction to reach its intended target, as visible from the sharp change in force slope, in panels C-D (see Fig. 4.5 upper block for the snapshots of this experiment). In the high stiffness case ($C = 0.8, 1$ at the moment of selection for subject S1, S2 respectively), the total force produced was high enough to overcome statical friction between the object and the underlying surface, and a stick-slip movement phase occurred, characterized by oscillations in force and irregular robot speed, until the endpoint was close to its final intended target. In the low stiffness scenario ($C = 0$ for both subjects at the moment of selection) the applied force was sufficient to distend the fingers of the SoftHand (hence the small reduction in distance to target after reaching the object, panel B), but never overcame the static friction threshold. It is worth noting that even in the high stiffness case the robot was not perfectly rigid

¹A video of the system evaluation is available at the following link: http://y2u.be/k6DyosvWB_s

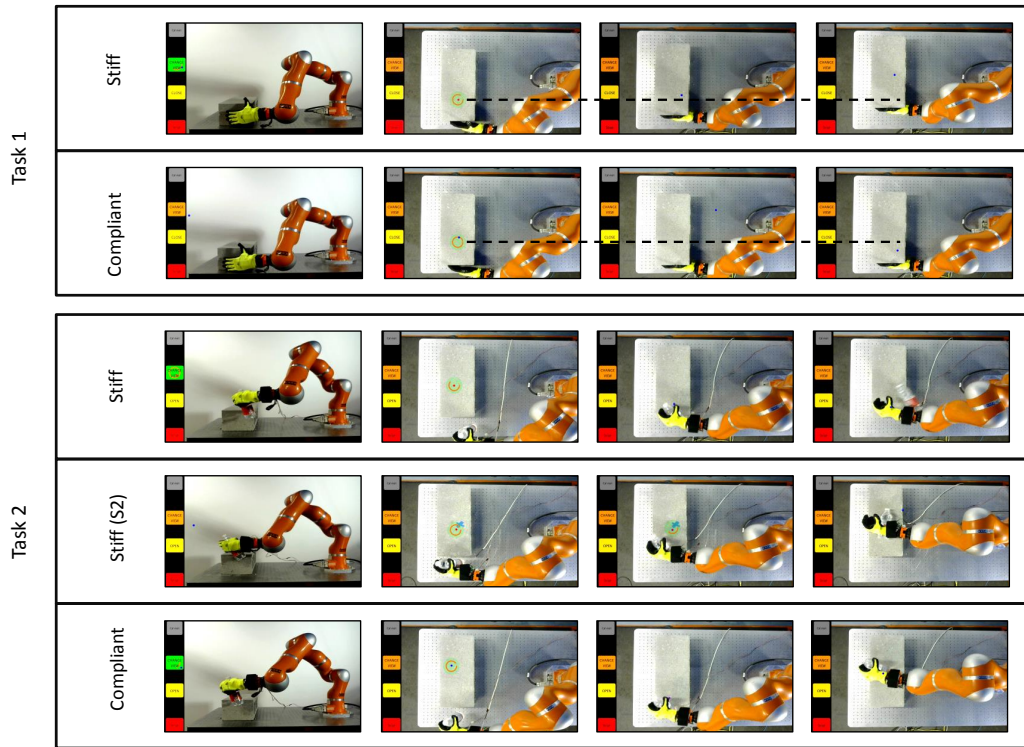


FIGURE 4.5: Screen shots of the heavy object pushing (Task 1) and collision (Task 2) tasks in active mental state (stiff) and neutral mental state (compliant). For the second task, two different examples of the active (stiff) case for the two subjects are provided.

and therefore it stopped slightly short of its target and it kept applying force against the obstacle.

Object grasping and environment collision: Similarly to the previous case, subjects performed the task in two conditions: panels E-G on Fig. 4.4 display results for a high-stiffness (active mental state) trial, while panels F-H on the right side present the low-stiffness (neutral mental state) case. The first row shows the z coordinate of the Kuka endpoint recorded starting from the moment of the impact of the grasped object against an obstacle, while panels G and H show the corresponding estimated forces in vertical z direction.

As before, $t = 0$ indicates the time in which the movement command is received by the robot. Impact against the obstacle occurred almost immediately, with very different outcomes depending on robot arm rigidity: for both subjects low-stiffness trials ($C = 0$) resulted in the bottle being successfully held on to, whereas high-stiffness trials ($C = 1$) resulted in the dislodgement of the bottle from the soft hand grip. Moreover, the high-stiffness case present a strong difference for the two subjects: in the case of subject 1 (S1, blue line), the bottle rolled away after being dislodged, whereas for subject 2 (S2, orange line) the plastic bottle was stuck between the robot arm and the brick (see Fig. 4.5 lower block for the snapshots of this experiment). The different behavior is clearly shown in the graphs: in the stuck-bottle case (panel E, orange line), the robot endpoint was sharply pushed upwards by the bottle itself, while for the rolling-bottle case (panel E, blue line) the impact caused only a minor readjustment in the robot trajectory. The corresponding force graph (panel G) shows a value of about 2.5 N at the beginning of both subjects trials, which was force required to keep the bottle lifted and steady. During the impact, forces at the

endpoint turned negative, as the distal end of the robot arm was pushed upwards by the interaction between held bottle and obstacle. After the bottle was dislodged, the estimated force was around 0 N if the bottle rolled away (blue line) or negative when the robot was actually pushing downwards on the stuck bottle (orange line).

In the low stiffness case, the bottle remained within the hand for the whole trial, as the robot arm adapted its path according to the imposed environment constraints. In particular the robot endpoint moved downward when it was rotating around the bottle-obstacle contact point for both users (first negative peak, panel F), then it moved slightly above target as the bottle was dragged on the surface of the obstacle (positive peak, panel F). The final position of the robot endpoint, as well as the forces expressed at the end of the trial (panel H), vary slightly according to the final relative angle between the bottle and the obstacle it was resting on.

4.5 Conclusions

In this study, a preliminary study demonstrated the possibility of controlling both kinematic and dynamic parameters of a robotic arm through a hybrid BMI - Soft BMI - that only exploits eye-movements and brain signals. These features allow the interface to be accessible to patients with severe motor disabilities, where residual muscular functions (excluding ocular control) cannot be exploited. The main contribution, compared to the state of the art of brain-controlled assistive robotics, lies in the introduction of an additional degree of control for the user, enabling the adaptivity of the robot behavior during physical interactions with the environment.

The eye-tracking system is very intuitive in its use, as it can be calibrated and proficiently driven by a user with no previous experience within minutes, while maintaining a high degree of precision in the selection of desired targets. On the other hand, the BMI was designed in order to take advantage of the fact that tasks requiring a higher degree of mental concentration are typically those that require stiffer movements (e.g. very precise displacements or heavy object moving). Therefore the robot has a default soft and safe behavior. The BCI channel is normally inactive, and it is just used in tasks where high accuracy is required. Compared to systems where the eye-tracker alone is used for position control, this introduces a remarkable advantage. During a drawing/writing task, for instance, as the one presented in Dziemian et al., 2016, a stiff behavior is advisable. On the other hand, when changing task, e.g. to self-feeding, robot stiffness should be reconfigured to a lower level by a caregiver, to allow safety. The solution proposed in this study, allows for a further degree of control and therefore independence for the patient.

The control of the robot proved to be quite easy to learn, as a naive subject learned to perform a relatively complex task such as grabbing an object and moving it around with a given degree of rigidity within his first session. At the moment, however, evoking a desired mental command required effort from the user and, sometimes, multiple attempts. This could be ascribed to the limitations connected to the use of the commercial EPOC software and hardware.

The controller presented in this work was intended as a proof of concept for a novel kind of interface that could help to integrate a higher degree of autonomy in assistive applications of soft robotics for severely disabled patients.

Part III

Passive Control Signals: Machine Adaptation to User

Chapter 5

The Effect of Tactile Feedback on ErrP Single-Trial Detection

This chapter evaluates the effect of tactile feedback on Error-related electroencephalographic potentials detection. The goal is to explore new interaction protocols able to enhance ErrP single-trial detection accuracy, in view of online applications, where information about user awareness of erroneous responses can be used to improve the reliability of BCI-based assistive systems. In the present work (Tessadori et al., 2017), two hypothesis were tested: 1) whether the addition of tactile feedback can improve the detection of ErrP, when used in combination and not alternatively to visual feedback; 2) whether a mismatch between the two different sensory channels can enhance ErrP detection.

This work has been published as : Tessadori, J., Schiatti, L., Barresi, G., & Mattos, L. S. (2017, October). Does Tactile Feedback Enhance Single-Trial Detection of Error-Related EEG Potentials? In Systems, Man, and Cybernetics (SMC), 2017 International Conference on (pp. 1417-1422). IEEE. - The final files for this publication are available from IEEE via: <http://dx.doi.org/10.1109/SMC.2017.8122812>

5.1 Introduction

Brain-computer interfaces (BCIs) offer the possibility to improve the degree of autonomy of people suffering from severe motor disabilities, but without cognitive impairments, e.g. Amyotrophic Lateral Sclerosis (ALS) patients, by providing them with a non-muscular channel for communication with the outside world and control of external devices (Wolpaw et al., 2002). Usually these systems exploit non-invasive (mainly electroencephalographic - EEG) measures of brain signals, and extract significant features out of them, in order to infer the subject's intention. These features are then forwarded to a classifier, which translates them into a control signal for a communication interface or any other kind of assistive device (Millán, 2002). Despite recent advances, BCIs still suffer from a lack of reliability, preventing them to be exploited as everyday life widespread products. Indeed, these systems, as well as other interaction technologies based on physiological signals, are prone to errors in recognition of subject's intent. One of the modern challenges of this research domain is consequently to increase the successful classification rate of subject's intention, without intensifying user mental effort or decreasing the communication rate (as would be the case for verification procedures where the output of classification is validated on two subsequent trials as in Wolpaw et al., 1998).

A unique advantage of the use of brain data as input for interaction technologies is that they can provide at the same time both information from which mental control commands can be derived and information about cognitive states, that are passively

elicited during human-machine interaction. Such information can be exploited to improve the interaction quality, as well as the rate of correct intention detection itself. To this aim, previous studies explored the use of one of these cognitive states, namely the awareness of error responses, as a way to improve the performance of BCIs (Chavarriaga et al., 2014).

The presence of error-related potentials in EEG recording right after people realize that they made an error was shown in different physiological studies in the last few decades (Carter et al., 1998). Depending on the context, slightly different kinds of ErrPs have been observed: "response ErrP", arising after the subject's incorrect motor action, e.g. pressing the wrong command key (Falkenstein et al., 2000); "feedback ErrP", in typical reinforcement learning tasks, following the presentation of a stimulus that indicates incorrect performance (Holroyd et al., 2002). Beside ErrPs elicited in case of errors made by the subject himself, the presence of an "observation ErrP" was also proved when the subject is observing errors made by an operator during a choice reaction task (Schie et al., 2004). The main components of response ErrP in the EEG are a negative potential at 80 ms followed by a larger positive peak between 200 and 500 ms after the incorrect response, while feedback and observation ErrPs are characterized by a negativity at 250 ms after presentation of incorrect performance feedback. All ErrPs have a fronto-central scalp distribution, and are probably generated in the anterior cingulate cortex (ACC), which regulates emotional responses (Holroyd et al., 2002).

Recent studies, exploring the feasibility of the inclusion of such ErrPs in BCI applications, demonstrated the existence of a so called "interaction ErrP", in which the error is not made or observed by the subject but by the interface, during the recognition of the subject's intention (Ferrez et al., 2005, Ferrez et al., 2008b). This latter ErrP shows a similar shape to the one of response ErrP, with mainly a negative and a subsequent positive peak, whereas the timing is similar to the feedback and observation ErrPs, since the first negative peak occurs around 250 ms after presentation of error feedback.

The attempts of integration of ErrPs in the context of BCIs so far encompassed two main applications: correction of wrong action and the use of ErrP for error-driven learning. In the first case the interaction ErrP has been used e.g. as correcting signal in a motor imagery-based BCI to control one-dimensional step-wise movements of a cursor, by canceling the selected action if an error was detected (Ferrez et al., 2008a); or in a P300-based speller, to improve the spelling accuracy by means of online error correction (Margaux et al., 2012). The second approach has been applied to implement adaptive capabilities in BCIs, either updating the BCI classifier (Artusi et al., 2011), or improving the behavior of a semi-autonomous system (Chavarriaga et al., 2010).

Some studies explored the patterns of interaction ErrP when using a different feedback modality, i.e. tactile instead of visual, to provide error signal (Lehne et al., 2009). In Chavarriaga et al., 2012 ErrP classification results were evaluated through a comparison between visual and tactile feedback modalities, both for an active and a monitoring task. Erroneous and correct trials were classified above random level (ROC curves AUCs between 0.7 and 0.8) for all conditions, even if visual modality always resulted better than the tactile one.

In this study, we aimed at testing whether the use of a supplementary sensory feedback channel beside the visual one, namely tactile feedback, can improve the single-trial detection of the interaction ErrP for BCI applications. In this case, the tactile feedback is intended to increase the saliency of the visual one, and not to replace it, as investigated in the works described above, in which visual and tactile stimuli

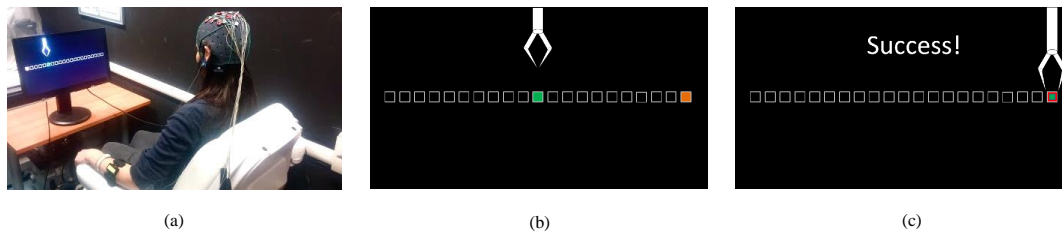


FIGURE 5.1: Experimental protocol: (a) experimental setup; (b) scene at the beginning of a session; (c) scene at the end of a session.

were never used together. To this purpose, we implemented a passive EEG acquisition protocol, where the subject was asked to monitor mono-dimensional cursor movements towards a target on a computer screen, with sporadic erroneous movements. The subject possibly received tactile stimulation on either forearm during cursor movements. Three conditions were tested: i) only visual stimuli; ii) tactile stimuli concordant with visual stimuli both in case of correct and erroneous behavior, and iii) tactile stimuli discordant with the visual stimuli during erroneous actions (i.e. tactile stimuli always in the direction of the correct action).

Our research questions are: 1) whether tactile feedback can improve the detection of interaction ErrP, thanks to a more engaging interaction in view of real BCI application for paralyzed patients; and 2) whether a mismatch between two different sensory channels can enhance ErrP detection. The latter is motivated in view of a possible future implementation of error-driven learning: e.g. a shared control scenario in which ErrPs are used to improve the behavior of a semi-autonomous system. In this case, visual feedback would be provided to the user by direct system observation (e.g. system movements direction), while tactile feedback could match some other input modality corresponding to user’s high level intention, e.g. desired movement direction inferred by detection of motor imagery (exploiting the same BCI system used for ErrP), or gaze direction, with an eye-tracking system.

5.2 Methods

5.2.1 Experimental protocol

In order to test the influence of tactile feedback on interaction ErrP, we simulated errors made by a BCI in recognizing subject’s intents in a one-dimensional control task. The implemented protocol was similar to the ones already presented in previous studies on ErrP inclusion in BCI applications (Iturrate et al., 2012). Specifically, the acquisition protocol was developed to simulate a human-robot interaction task, where the user wishes to move the robot towards a target either on the right or left side of the working space (in this case the computer screen) by means of discrete steps. In our paradigm the subject did not actually control the interface; rather, the robot spontaneously moved towards the intended target with sporadic direction errors. We then tested the presence of ErrP generated by a movement in the wrong direction, simulating an error made by the interface in the recognition of subject’s intent. The choice of not implementing a real motor intent detection in this experiment was motivated by the purpose of isolating the problem of tactile feedback effect on ErrP (i.e. our experimental question) from the more complex and general problem of implementing a complete BCI system.

The experimental setup is shown in Fig. 5.1a, and consisted of 16 active gel electrodes (g.LADYbird from g.tec) located at Fz, FC3, FC1, FCz, FC2, FC4, C3, C1, Cz, C2, C4, CP3, CP1, CPz, CP2 and CP4 according to the standard 10/20 international system, connected to a g.USBamp biosignal amplifier for EEG signals acquisition. Ground and reference were respectively placed on the forehead (AFz) and left ear lobe. Hardware filters were set to perform a bandpass between 0.1 and 30Hz. Signals were sampled at 256 Hz. Experiments were started only after impedance of all electrodes was stably under 5k Ω . Two Myo (Thalmic Labs) armbands positioned on the subject's forearms were used to provide tactile stimuli, consisting in 0.5 s of vibration on either armband, simultaneously to robot movements.

The graphical stimulation protocol was developed in Matlab, while data acquisition occurred through a Simulink model that handled the g.USBamp amplifier. The experiment scene is shown in Figure 5.1b and c, at the beginning and at the end of a session (robot reaching target), respectively. Each trial consisted of a cursor (green square) and robot arm movement between current position (among 21 possible positions) and the next one. Timing was set so that movement was followed by a pause of random duration between 1.5 and 2.5 s. Trials were repeated until the target (orange square) was reached. Then, the target was randomly positioned either at the far right or left side of the screen and cursor was placed at the middle position. At the end of each session a simple animation showed the robot extending and grasping the target. The task was performed in three conditions:

- **Visual stimuli (V):** the task was performed with no armband activation;
- **Concordant visuo-tactile stimuli (concordant VT):** the subject received a vibration from the armband placed at the side corresponding to cursor movement direction;
- **Discordant visuo-tactile stimuli (discordant VT):** the subject received a vibration from the armband placed at the side corresponding to target position, i.e. an erroneous movement caused cursor to move left (right), and right (left) armband to activate.

Twelve healthy subjects (31.9 ± 4.2 y.o., 8 males and 4 females) participated in the study. Each subject tested a visual-only feedback condition and one of the two visuo-tactile conditions. Each condition lasted about half an hour, with pauses every 6 reached targets, and encompassed 750 trials with 20% of error probability (cursor movement in the opposite direction of target). Before the experiment started, all subjects agreed with experiment guidelines, and signed an informed consent document¹. All anonymized experimental data are available online².

5.2.2 EEG signal processing

Error related potentials

EEG data were spatially filtered by common-average re-referencing (CAR), then band-pass filtered between 1 and 10 Hz with a 4th order Butterworth filter, since EEG error correlates are known to be slow potentials. Time windows between 150 ms and 850 ms after each cursor movement were considered for subsequent analysis, after baseline correction (baseline estimated as the mean value in the 100 ms-long

¹IIT ADVR TEEP01 protocol, approved by the Ethical Committee of Liguria Region on June 14th, 2016.

²<http://teep-sla.eu/index.php/results/40-smc2017-dataset>

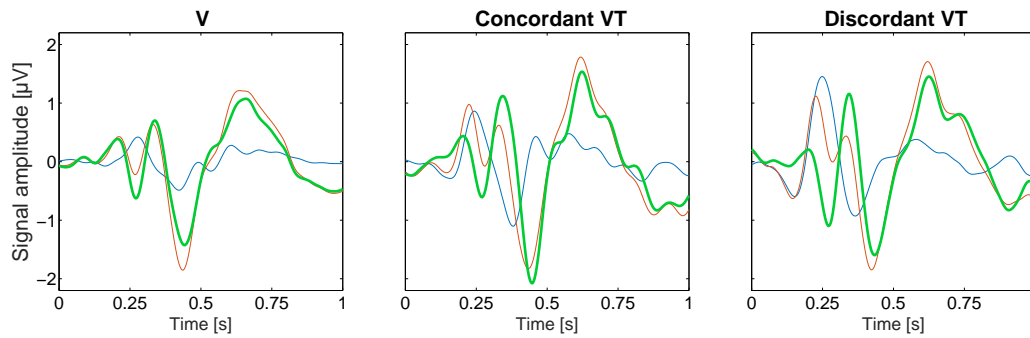


FIGURE 5.2: Grand averages of filtered EEG data for one channel, FCz, in 1 s time window after stimulus onset. Columns refer to different paradigms for stimuli (respectively, only visual V, concordant visuo-tactile VT, discordant visuo-tactile VT stimuli). Blue lines represent the average of all trials following a correct cursor movement, while red lines depict averages of erroneous trials. Thick green lines represent the difference of the two signals (erroneous minus correct).

interval before stimulus). Since in this study we considered different stimuli conditions, possibly leading to ErrP variations, both time and frequency features have been computed. In fact it has been demonstrated that the addition of frequency features (theta band spectral power) increases the task-generalization capabilities of ErrP classification based on temporal features alone (Omedes et al., 2013). This is explained by the fact that ErrP mainly vary in latency but not in amplitude among different tasks. Time features were obtained by sub-sampling signal in time windows by a factor of 4. Frequency analysis was performed selecting non-overlapping 2 Hz-wide power spectrum bands between 2 and 10 Hz, on the same time window mentioned above, after filtering with a Blackman window. This procedure led to 45 time and 4 frequency features per channel.

Classification

Several different classifiers were tested (feature selection based on z-scores followed by linear discriminant analysis, learners trees, Gaussian mixture models) and the best single-trial classification results were achieved with a linear support vector machine (SVM). In order to compensate for the unbalanced number of samples in the correct and error classes, synthetic data of the minority class were generated with the SMOTE algorithm (Chawla et al., 2002). In line with the use of such an algorithm, the misclassification costs for the correct and error classes were respectively set to 0.4 and 0.6. The classifier was trained separately for each subject and type of stimulus. Classification performance was assessed using a 10-fold cross-validation procedure, and it is expressed by means of the correct identification ratios of correct and error classes, while the area under the ROC curves (AUC) was adopted as a single parameter expressing the overall classification accuracy. Early analysis proved that the random nature of both the SMOTE algorithm and partitioning of training and testing sets had a meaningful effect on the observed results. In order to reduce uncertainty, 100 hundred repetitions of the above procedure have been performed, and average classification results are shown and discussed in the following.

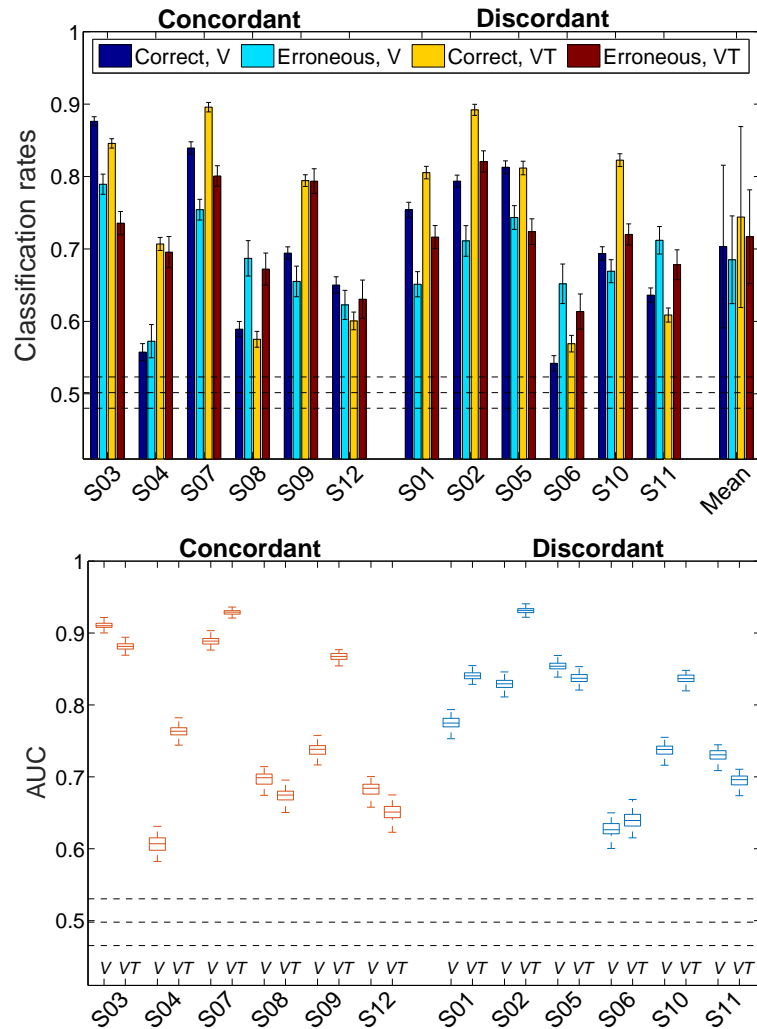


FIGURE 5.3: Classification results: (a) Classification rates for correct and erroneous classes, for all subjects during visual (V) and visuo-tactile (VT) stimuli sessions. Last group of bars represent mean classification rates across all subjects. Error bars represent standard deviations obtained from different repetitions of the classification algorithm (S01 to S12) or across subjects (mean group). (b) Box plots of observed AUC distributions for each subject, referring to visual only (V) and visuo-tactile stimuli (VT) conditions. Red (blue) box plots represent data obtained on subjects that underwent concordant (discordant) VT stimuli. Dashed lines in both panels represent average chance level classification rates or AUCs plus or minus one standard deviation. Chance level results were obtained by training the classifier on actual datasets with randomly shuffled labels.

5.3 Results and Discussion

5.3.1 Error related potentials

Figure 5.2 shows the grand averages of time features for one channel, FCz, under the three tested conditions (V, concordant VT and discordant VT) and for both classes (correct, C, and erroneous, E, cursor movement, respectively blue and red thin lines), as well as their difference (thick green line, erroneous minus correct). It is worth noting here that the left graph is obtained by averaging recorded data from 12 subjects,

TABLE 5.1: Classification performance for concordant stimuli

Subj.	V			VT		
	C[%]	E[%]	AUC[%]	C[%]	E[%]	AUC[%]
S03	88±1	79±1	91±1	85±1	74±2	88±1
S04	56±1	57±2	60±1	71±1	70±2	77±1
S07	84±1	75±1	88±1	90±1	80±1	93±1
S08	59±1	69±2	70±1	58±1	67±2	66±1
S09	69±1	66±2	75±1	79±1	79±2	87±1
S12	65±1	62±2	68±1	60±1	63±3	66±1
M±SD	70±12	68±8	75±11	74±12	72±7	79±11

TABLE 5.2: Classification performance for discordant stimuli

Subj.	V			VT		
	C[%]	E[%]	AUC[%]	C[%]	E[%]	AUC[%]
S01	75±1	65±2	76±1	81±1	72±2	85±1
S02	79±1	71±2	83±1	89±1	82±1	93±1
S05	81±1	74±2	86±1	81±1	72±2	84±1
S06	54±1	65±3	62±1	57±1	61±2	65±1
S10	69±1	67±2	73±1	82±1	72±1	84±1
S11	64±1	71±2	73±1	61±1	68±2	70±1
M±SD	71±9	69±4	76±7	75±12	71±6	80±10

whereas the middle and right column include data from 6 subjects each. The difference between classes present a similar pattern in all considered cases, and coherent in the shape to what expected from the literature: a first negative peak centered around 260 after stimulus onset, and a positive one centered around 330 ms. A second deep negative peak at 440 ms after stimulus, followed by a wider positive one between 500 ms and 750 ms are also visible for all conditions, and match the shape of the interaction ErrP described in Ferrez et al., 2008b. A slight difference is in that we observe a more evident last positive peak, as reported in Iturrate et al., 2010b, during observation of robot operation. Differently from what documented in Chavarriaga et al., 2012, where the ErrP (E-C) signal presented a shift of the first positive peak from 300 ms in case of visual feedback, to 400 ms in case of tactile feedback, we did not observe differences in latencies of V or VT ErrPs. Nonetheless, both C and E trials signals show larger amplitude peaks for VT conditions, and the first small positive peak of E trials is delayed in presence of tactile stimulus.

5.3.2 Classification

For the considered tasks, namely error monitoring during either V or VT stimuli, we found that classification results computed on both time and frequency features sets did not change noticeably compared to those achieved using time features only. Therefore, only results obtained by analysis in the time domain are reported. Figure 5.3 reports bar plots of the classification rates (panel a) for all subjects, classes (C and E) and tested conditions (with and without tactile stimulation), as well as

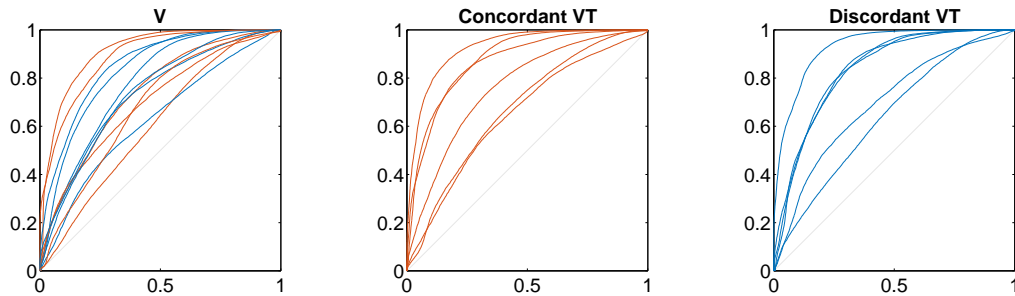


FIGURE 5.4: Average ROC curves. Left graph reports curve obtained for trials during visual-only condition (V), middle and right graphs display ROC curves for data acquired during experiments with visuo-tactile stimuli (respectively, concordant VT and discordant VT). Red (blue) plots represent data obtained on subjects that underwent concordant (discordant) VT stimuli.

the corresponding AUCs distributions (panel b). Obtained results are, furthermore, summarized in Tables 5.1 and 5.2. Specifically, table I lists the accuracy computed for each class (C and E), and the corresponding AUC value, for the subjects that underwent concordant stimuli condition, during both V and VT experiments. Table II shows the same values obtained for discordant stimuli. Classification performance varies greatly among subjects, ranging from very accurate (90% and 82% respectively for C and E classes, in the best case) to barely above or chance level (54% and 57% in the worst case). The overall classification performance, expressed in terms of AUC, is on average between 75% and 76% for V conditions, and increases to 79% and 80% for concordant and discordant VT conditions respectively, with a standard deviation ranging from 7 to 11 percentage points.

To check the correlation between classification performances on the V and VT sessions of the same user, the R-squared of the linear model linking results (in terms of AUC) was computed. It resulted in a value of 0.55, suggesting that, while introduction of tactile stimulation can significantly change classification results, classification accuracy is subject- or montage-dependent, rather than a random fluctuation (i.e. subjects obtaining good results during V condition, tended to do the same in the VT condition).

The inter-subject variability of results is also evident from the ROC curves, shown in Figure 5.4, and corresponding AUC values reported in Figure 5.5. Independently from the VT stimuli condition (concordant or discordant), the addition of tactile stimuli either leaves the performance mostly unchanged or it strongly improves classification performance. In particular, for the majority of subjects the classification performance increases several percentage points from V to VT condition, while for three subjects in the group of concordant stimuli and two subject in the group of discordant stimuli there is a slight decrease of classification accuracy.

The box plot depicted in Figure 5.5 illustrates the range of changes in classification performance (expressed in terms of AUC percentage points) following the addition of tactile stimulus to the visual one, and their statistical significance. The left box reports changes in AUC values for users subjected to the concordant tactile stimulation protocol, the middle one describes performance for discordant tactile stimulation, while the right column reports changes in AUC values for all VT conditions combined. Both tactile stimulation paradigms facilitate classification: discordant VT feedback causes an average increase of 4.6 points in AUC, while concordant stimulation changes mean AUC by $\sim 4\%$. One-sample t-tests confirmed results pointing towards a significant effect (mean greater than 0 at 5% significance level) for the first

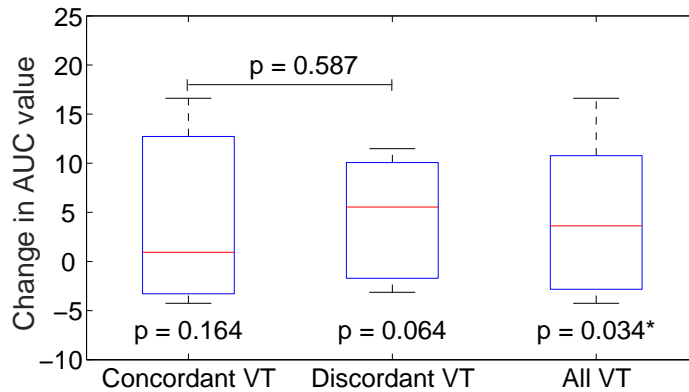


FIGURE 5.5: Distributions of changes in classification performance (AUC) with the addition of tactile stimulus, for concordant VT (left box), discordant VT (middle box) and combined sets (right box). Red line indicates median, blue box extends to first and third quartiles, whiskers reach most extreme data outside of box. Reported p-values are resulting from one-sided t-tests (* indicating significance at 5% significance level).

case ($p=0.064$) and with less evidence for the second ($p=0.164$). The difference in classification improvement, however, is not significant among the two tested conditions ($p=0.688$ from one-sided t-test on the hypothesis that AUC change from V to VT is greater for discordant than concordant stimuli condition). This can also be empirically observed in the EEG ErrP waveforms depicted in Figure 5.2: the amplitude of the peaks in the difference between correct and erroneous classes increases following the addition of tactile stimulus, but both curves for VT paradigms present very similar profiles. Considering all visuo-tactile sessions together, the mean AUC change compared to V condition results in a significant positive increase of 4.2 points ($p=0.034$).

Overall, these statistical results suggest that tactile stimulation can be helpful in increasing ErrPs classification accuracy. The described method of single-trial ErrP classification proved generally efficient, and the conducted experiments hint at the fact that providing mismatching sensory stimulation might be more effective than the simple involvement of an additional sensory pathway. However the number of subjects tested, given the high inter-subject variability observed, was too low to draw definitive conclusions. In fact, while top results (E and C classification rates ~ 80) matched literature gold standards (Chavarriaga et al., 2014), recordings on several trials yielded classification results scarcely above chance level. A possible cause for such discrepancies is the low involvement level of the subject during the experiment. This will be the focus point of the follow-up of this work, in which similar experiments, i.e. monitoring of an autonomous agent's correct or erroneous behavior, will be performed using a video game-like or real scenario.

5.4 Conclusions

Recent studies reported promising results on the feasibility of detecting single-trial erroneous responses during human-computer interaction, and the inclusion of ErrP detection was proven to lead to significant improvements in the performance of BCI systems. In particular, a new kind of error-related potential was found, called interaction ErrP, arising when the interface misinterprets the subject's intention. A still

open issue is how to increase the recognition rate of single-trial erroneous and correct responses, and specifically which kind of feedback, whether visual, auditory, somatosensory, or a mix of them, can elicit the strongest interaction ErrP.

Our study aimed at investigating this problem, looking for the effect of a combined visual and tactile stimulation on single-trial detection of interaction ErrP. Furthermore, we explored the effect on ErrP of both concordant and discordant presentation of stimuli from the two sensory channels. The first hypothesis, i.e. whether adding tactile to visual stimuli enhances ErrP detection, was confirmed, as the addition of a tactile stimulus significantly increased ErrP classification performance. The second hypothesis, i.e. whether a mismatch between the two feedback channels can elicit a stronger ErrP, was only partly supported by our study: the discordant VT condition indeed produced improvements in classification performance over V condition, but not significantly differing from the ones caused by the concordant VT condition.

In conclusion, the study presented in this chapter supports the idea that exploiting more sensory channels is a promising way to improve ErrP detection in real time BCI applications. This is in line with the research effort towards the inclusion of patients emotional and cognitive states into adaptive assistive interfaces, able to dynamically and automatically adjust their behavior to optimize performance and reliability, for out of the lab BCI technologies.

Chapter 6

EEG-based Reward Signal for Robot Learning

This chapter presents an implementation of ErrP detection to allow for error-driven learning of a semi-autonomous system. This concept forms the basis for an online robot-learning task, where a user's evaluation of the actions performed by a robot, in terms of detected ErrP, is exploited to update a reward function in a Reinforcement Learning (RL) framework. The presented results support the potential of human-robot co-adaptive and co-operative strategies to develop human-centered assistive technologies.

This work has been accepted as : Schiatti, L., Tessadori, J., Deshpande, N., Barresi, G., & Mattos, L. S. (2017, September). Human in the Loop of Robot Learning: EEG-based Reward Signal for Target Identification and Reaching Task. In Robotics and automation (ICRA), 2018 International Conference on. IEEE.

6.1 Introduction

In the context of assistive technologies for severely motor-impaired people, the development of Brain-Computer-Interfaces (BCIs) and neuro-prostheses offer new channels for communication and control of external devices (Wolpaw et al., 2002), bypassing the traditional muscular control and inferring user intentions directly from the ongoing brain activity. The brain signals are typically recorded by means of non-invasive techniques such as electroencephalography (EEG). However, a continuous delivery of mental commands for a brain-actuated device is highly demanding in terms of cognitive attention and effort. Moreover, the identification of user intention, especially when based on non-invasive recording techniques, is prone to errors, and allows for a very restricted number of discriminable states, and consequently, degrees of control. A viable solution to these issues was offered by the concepts of shared autonomy and shared control (Tonin et al., 2010). The continuous advances in autonomous robotics made possible applications such as semi-autonomous wheelchairs, prosthesis, or robots for telepresence (Vanhooydonck et al., 2003, Kim et al., 2006, Millan et al., 2004), allowing patients constrained from severe paralysis to join their relatives and friends in their activities, or to restore some degree of independence in their self-care. Studies involving disabled patients reported their preference for a semi-autonomous rather than fully autonomous approach, in which the intelligent system helps the human to cope with problematic low-level aspects of planning, while the person keeps as much control as possible on decision-making (Tahboub, 2001).

Following this idea, a novel classic approach for BCI-based interaction between human and an assistive system has been investigated during the last two decades.

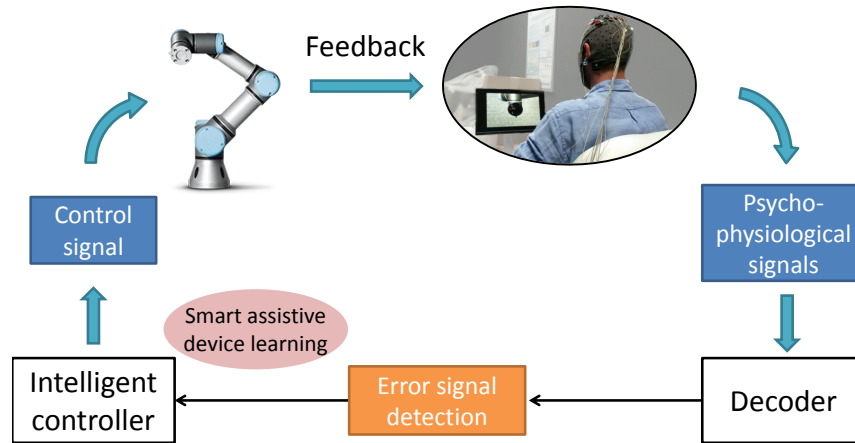


FIGURE 6.1: System components and information flow in ErrP-based robot learning scheme. Adapted from Iturrate et al., 2015.

This is based on the detection of electrophysiological correlations of error recognition in human brain, the so-called error-related EEG potentials (ErrPs). In this approach, systematized by Chavarriaga et al., 2010 and shown in Fig.6.1, the user monitors the performance of an autonomous system, acting like a critic instead of continuously generating control commands, and the user's spontaneous perception of an erroneous action is used to optimize the system behavior. This concept is built on the ability of recognizing ErrPs on a single-trial basis. ErrPs are electrophysiological responses arising in the fronto-central area of the cortex, and have been observed in response to awareness of erroneous actions made by the user (Falkenstein et al., 2000), observation of erroneous actions performed by an interface (Ferrez et al., 2005) or an external system, such as a robot (Iturrate et al., 2010b), when interpreting the user's intention. At the level of recorded EEG signal, ErrP response is typically characterized by a uniform sequence of evoked response potential (ERP) components, i.e. positive and negative peaks at fixed time delays from the stimulus onset. The ErrP typical waveform is derived by computing the average difference between erroneous and correct trials, and is characterized by an initial positive peak at about 200 ms after feedback presentation, followed by a larger negative deflection at about 250 ms and a third larger positive peak at about 320 ms (Chavarriaga et al., 2014).

ErrP single-trial detection has been implemented online in BCI applications for erroneous action correction, e.g. in P300-based speller (Margaux et al., 2012), for robot movements (Ehrlich et al., 2016, Salazar-Gomez et al., 2017), with reported classification accuracies between 70 and 80%. Some studies explored the use of ErrP signals for error-driven learning, e.g. for online re-training of a 2-class motor imagery classifier (Llera et al., 2012), or, as is the focus of the present work, to improve the behavior of a semi-autonomous system. A first implementation of this concept, with ErrP used as negative reward value in a RL scheme, was presented by Chavarriaga et al., 2010, in a mono-dimensional control task. An online evaluation of the same approach on two subjects monitoring a simulated robot was demonstrated by Iturrate et al., 2010a. In Iturrate et al., 2015 a study on ErrP implementation for robot RL of optimal policy for target reaching in a 2-D discrete space was carried out. The study, conducted with 12 subjects, reported algorithm convergence towards optimal behavior, even for targets unseen during training, with a 74.3% ErrP online classification accuracy. In Iturrate et al., 2013, a possible integration with shared control

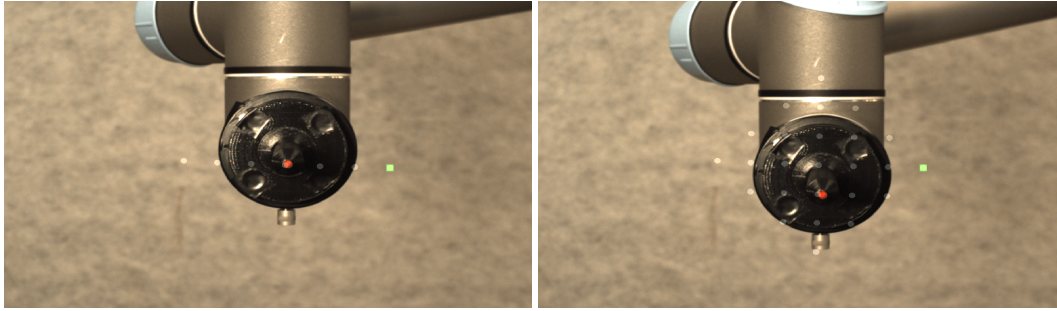


FIGURE 6.2: Graphical User Interface (GUI) for teleoperation during: training (left), and testing phase (right).

technique was shown, in a 2-D cursor-reaching task. Here ErrP was used to indirectly infer user-intended target location, selecting the corresponding control policy from a pre-defined repertoire.

The rationale behind these works lies in the fact that ErrP detection offers a natural framework for improving the performance of an artificial intelligence system in an RL scheme. Error identification through user monitoring can be exploited by the RL agent to learn an optimal behavior, by reducing the likelihood of repeating the same decision in the same context. This concept was originally presented by Iturrate et al., 2015, and it is adopted for the present work, as shown in Fig. 6.1.

In this work, we aim take the above mentioned works forward, by exploiting the concept of the EEG-based reward for robot RL, to implement a simultaneous learning of: 1) the optimal policy for reaching a target, and 2) the identification of user-intended target location, among a pre-defined set, and corresponding policy selection. Our main contribution is to provide a framework for simultaneous learning of the two problems mentioned above, and to test this framework in an online setting encompassing physical robot movements. We tested the proposed learning algorithm in a study involving 8 subjects, and the task consisted of tele-observation of the movements of a robotic manipulator towards a target, in a 2-D discrete space. Since ErrP detection accuracy above chance level (50-50) is a key aspect for RL algorithm convergence, we also tested two different feedback conditions (visual and visuo-tactile), aimed at improving ErrP online classification rate.

6.2 Methods

6.2.1 Experimental Protocol

Eight subjects (6 males, 2 females, aged 27.6 ± 1.7) participated in this study. Total duration of the experiment was about one hour, including half an hour of training and half an hour of testing, with pauses every 5 minutes. Before the experiment, all subjects agreed with experiment guidelines, and signed an informed consent document¹.

Training

A training phase was developed in order to collect EEG signals to train the ErrP classifier. During training, the subject was asked to observe, by means of a graphical

¹IIT ADVR TEEP01 protocol, approved by the Ethical Committee of Liguria Region on June 14th, 2016.

user interface (GUI) shown on a PC screen, a robotic arm moving towards a target. The arm motion was programmed, with sporadic direction errors, 25% of the time. The GUI included a discrete mono-dimensional grid, superimposed on the robot scene, with 7 positions. These corresponded to the positions that the robot could assume, as shown in Figure 6.2, left. The target position would be selected to be either of the two extreme positions on this 7-position 1-D grid, and highlighted in green color on the GUI.

The training session was composed of 600 trials, and each trial consisted of a single robot movement, i.e. movement between two adjacent positions. Time between two consecutive movements was set as 2.5 s. The sequence of robot's moves from the starting position, i.e. the middle of the 1-D grid, to the target (the length of which was varying according to the number of erroneous movements), was defined as an iteration. At the end of each iteration, the robot position was reset to starting point, and a new target was randomly selected.

Since during the testing phase the robot was allowed to move in a 2-D space, the training was divided in four sub-sessions, alternately showing horizontal and vertical 1-D grid orientation. This was done to let the training data include all four movement directions (left-right-up-down), and make the ErrP classifier scalable from training to testing data.

Testing

During the testing phase, the subject was again instructed to evaluate erroneous robot movements towards a target, but in this case ErrP was detected online using the classifier trained on training data.

During testing, the robot was allowed to move in a 2-D diamond grid with 25 positions, as visible in Fig. 6.2. The grid had two possible target positions, at either extreme vertical or horizontal positions that were alternated between subjects. Testing encompassed 600 trials, i.e. robot steps. The movements of the robot were dictated by the output of the RL algorithm, explained in detail in section 6.2.3. The RL algorithm took into account the result of the online ErrP classification. Therefore, contrary to the training session, in the testing phase the subject's brain activity directly influenced robot movement behavior.

Specifically, during the first 500 trials, the learning algorithm collected the subject's evaluations on erroneous movements to generate optimal step sequences toward each target (route learning), whereas in the last 100 trials, ErrP detection was used together with the information obtained in the route-learning phase, to identify which target was currently selected and to command the robot to move towards it. It is worth noting that the transition from the route-learning to the target-learning phase occurred without the knowledge of the subject.

Feedback condition

Each subject was tested in one of two feedback conditions: (i) the visual (V) condition or (ii) the visuo-tactile (VT) condition. In the V condition, a red cursor was superimposed on the robot position within the GUI. The cursor served the purpose of slightly anticipating the movement of the robot, i.e., the cursor instantly moved to the next commanded position when the robot movement command was issued. This feedback was introduced to improve the accuracy and generalization capabilities of ErrP classifier, since ErrP is a time-locked potential.

Subjects undergoing the VT feedback condition, were asked to wear vibrating bands on their wrists and ankles, and received 1-s vibrations on right wrist, left wrist, both wrists, and both ankles for movements towards right, left, up, and down direction respectively. The vibration command was delivered simultaneously with the motion of the red cursor, when the robot movement command was issued, therefore again slightly anticipating the robot motion itself.

6.2.2 Experimental Setup

The experimental setup (Fig. 6.1) included: (i) a robotic arm (UR5, Universal Robots), (ii) a HD camera (Prosilica GT1910 GigE Vision – 1080p, Allied Vision) for robot real-time video streaming and recording, (iii) a teleoperation GUI showing the robot movements on a PC screen, through a real-time Ethernet connection to the camera, and (iv) the EEG acquisition system. Two independent PCs were used in the setup, the GUI PC (control-side PC) and a robot-side PC.

During the experimental session, the EEG signals from the user's brain activity were recorded using a headset, which included 16 active g.LADYbird (g.tec) gel electrodes located at scalp positions Fz, FC3, FC1, FCz, FC2, FC4, C3, C1, Cz, C2, C4, CP3, CP1, CPz, CP2, and CP4 according to the standard 10/20 international system. The electrodes were connected to a g.USBamp biosignal amplifier. Ground and reference electrodes were respectively placed on the forehead (AFz) and left ear lobe. Hardware filters were set to perform a bandpass between 0.1 and 30 Hz. Signals were sampled at 256 Hz.

The robotic arm was the commercially available 6 degrees-of-freedom (DOFs) Universal Robot 5 (UR5) manipulator. The end-effector of the arm was modified so as to be seen as a single point easily distinguishable against the background in the GUI. The teleoperation GUI, EEG online processing, and the learning algorithm were implemented in MATLAB, while data acquisition was implemented through a Simulink model that handled the g.USBamp amplifier. The robot-side PC implemented the robot position controller, by means of a custom C++ script, and the motion commands from the control-side PC were received using simple UDP communications over a direct LAN connection.

A set of four custom-made silicone rubber (ACC Silicone M230) cuffs with embedded vibration motors (Precision Microdrives 304-116) was cast in order to provide tactile stimuli in the VT feedback condition, consisting of one second vibrations. The vibrations were synchronized with each robot movement, and commanded through serial communication over a direct USB connection with the control-side PC.

6.2.3 Algorithms

EEG Analysis

Pre-processing and features extraction

Following the state-of-the art for signal processing related to ErrP detection, EEG data were spatially filtered by common-average re-referencing (CAR), and then band-pass filtered between 1 and 10 Hz with a 4th order Butterworth filter, since EEG error correlates are known to be slow potentials. Time windows, 800 ms in length within each trial, were considered for subsequent analysis. Both time and frequency features were computed. Frequency analysis was performed by multiplying relevant signal intervals in time with a Blackman window, followed by computation of Fast

Algorithm 1 Route Learning Strategy

```

1:  $s_0 \leftarrow s_{start}$ 
2: for  $i = 1$  to  $N_{trials}$  do
3:   if  $s_i \neq s_{final}$  then
4:     Choose  $a_i$  from  $Q(a, s_i)$   $Q$  ( $\epsilon$ -greedy)
5:     Take action  $a_i$ 
6:     if  $ErrP = true$  then ▷ Error is detected
7:        $r_{i+1}(s_i, s_{i+1}) \leftarrow r_i(s_i, s_{i+1}) * 0.9 - 1$  ▷ Update reward for last transition
       (converging to -10)
8:       Update  $Q(s_i, a_i)$  according to Eq.(6.2)
9:        $r_i \leftarrow r_{i+1}$ 
10:       $s_i \leftarrow s_{i+1}$ 
11:   else ▷ Target is reached
12:      $r(s_i, s_{i+1}) \leftarrow 100$  ▷ Set environmental reward
13:      $s_i \leftarrow s_{start}$  ▷ Start a new iteration

```

Fourier Transform. Frequency features were then selected as non-overlapping 2 Hz-wide spectrum bands between 2 and 10 Hz.

Time features were obtained by sub-sampling signal in epoched time windows by a factor of 4, for a final sampling frequency of 64 Hz. This procedure resulted in 45 time features and 8 frequency features for each channel.

Offline classifier training

A linear support vector machine (SVM) was used to classify training trials, without prior feature selection. The unbalance in correct (C) and error (E) classes occurrence was compensated by random downsampling of the majority (C) class. Possible and unknown effects on the ErrP latency were considered, reflecting variations in user's perception possibly caused by the different V and VT feedback conditions, as well as originated by the physical delay in the robot movements execution.

To take this latter effect into account, feature sets were extracted as explained in the previous paragraph, considering time windows with different delays. Specifically, 10 possible delays ranging from 0 to 1 s after robot movement onset, in 100 ms steps, were considered for time windows epoching. Thus, relevant features were obtained in windows ranging from 0-800 ms to 1000-1800 ms after robot movement onset. A different SVM classifier was trained on the feature set corresponding to each considered time window. A 10-fold cross-validation was used to compute the classification performance, in terms of area under the ROC curve (AUC).

Online classification

For each subject, the time window (and therefore the time delay) that lead to the higher classification accuracy in the offline analysis was selected. A linear SVM was trained on all available training data (without performing cross-validation), on the optimal time window. During online classification, this classifier was applied to the features extracted on ongoing EEG data, in the time window selected according to the chosen optimal delay. The output of such classification was sent to the learning algorithm, in terms of a label $\in [0,1]$ indicating whether the last movement (EEG trial) belonged to correct (0) or error (1) class.

Robot Learning

In order to implement the robot learning, a reinforcement learning framework was chosen.

In an RL framework, an agent learns through interaction with environment, based on a reward signal (r), which recompenses or penalizes its actions. The analytical framework of an RL problem is a Markov Decision Process defined by the tuple $\{S, A, P, r, \gamma\}$, where S is the state-space (in the reaching problem described here, it corresponds to the set of all discrete positions that the robot can assume), A is the action-space (in this case movements in four directions), and $P : S \times A \rightarrow S$ are the transitions probabilities from one state to the next one, when executing a particular action a . The function $r : S \times A \rightarrow R$ defines the reward obtained by the agent when executing an action a at state s , and $\gamma \in [0, ..1]$ is a discount factor on the total accumulated reward. The goal of RL is to find a policy $\pi : S \rightarrow A$ to map each state to the action that maximizes the accumulated reward $R_i = \sum_{t=0}^n \gamma^t r_{i+1}$.

For discrete tasks, as the one considered here, the standard Q-Learning algorithm is the most suitable to compute the optimal policy Sutton et al., 1998. The so-called Q-function is used to compute the state-action map:

$$Q^*(s, a) = r(s, a) + \gamma \sum_{s' \in S} P(s, a, s') \max_{a' \in A} Q^*(s', a') \quad (6.1)$$

In Q-learning, the optimal Q^* function is estimated iteratively from empirical data. At each time step, the agent in state s_i executes an action a_i , that produces the agent being in a new state s_{i+1} . To this transition, corresponds a reward $r_{i+1}(s_i, a_i)$. The Q-function is updated according to:

$$Q_{i+1}(s_i, a_i) = (1 - \alpha_i) Q_i(s_i, a_i) + \alpha_i [r_{i+1}(s_i, a_i) + \gamma \max_{a' \in A} Q_i(s_{i+1}, a')] \quad (6.2)$$

where Q_i is the current estimate, at step i , of the Q-function, α is the learning rate, and γ is a coefficient $\in [0, 1]$, accounting for the importance of long-term rewards. During learning, it is necessary to choose a policy a , i.e. which action to perform, from a particular state s . In this work, an ϵ -greedy policy was adopted: the best action, obtained from the current policy (current Q-map values), is chosen $(100-\epsilon)\%$ of the times, while an exploration strategy (random action) is selected $\epsilon\%$ of times. When agent behavior approaches the desired one, ϵ is set to zero.

The Q-learning algorithm was used to implement both route learning, i.e. learning the optimal sequence of steps to reach each one among two available target positions, and target learning, i.e. once the routes towards the targets were sufficiently learned, the robot was allowed to choose which one of the two learned routes to follow, so as to match the will of the human observer. The learning strategies for the two tasks are explained in detail below.

Route Learning

The route learning strategy consisted in a slightly modified version of the basic Q-learning algorithm, and it is reported in Algorithm 1. For the discrete space of 25 positions considered for the task, the state-action Q-function consisted of a sparse 25x25 matrix representing the transition probabilities from each one of the possible 25 states to the sub set of 1 to 4 linked (reachable) states. The reward function r represented a 25x25 matrix of reward values assigned to each transition. Both matrices were initialized to zeros, and the initial state set to the central position of the grid, three steps away from each possible target.

Algorithm 2 Target Learning Strategy

```

1: Initialise  $Q_{target}(s_t, a_t)$  as zeros matrix
2: Initialise  $r_{target}(s_t, a_t)$  as zeros matrix
3: Randomly choose initial guessed target  $s_{t_j}, j \in 1, ..nTargets$ 
4: for  $step \in \{TargetLearningTrials\}$  do
5:   if  $s_i \neq s_{final}$  then
6:     Select route Q matrix corresponding to current guessed target,  $Q[s_{t_j}]$ 
7:     Choose  $a_i$  from  $Q(a, s_i)$   $Q[s_{t_j}]$  derived from  $Q[s_{t_j}]$  ( $\epsilon$ -greedy)
8:     Take action  $a_i$ 
9:     if  $ErrP = true$  then ▷ Error is detected
10:       $r_{target_{j+1}}(:, s_{t_j}) = r_{target_j}(:, s_{t_j}) - [Q[s_{t_j}](s_i, s_{i+1}) - mean(Q[s_{t_j}](s_i, \{s_k : k \neq i\}))]$  ▷ Penalize actions bringing to current guessed target
11:      for  $w \in \{1, .., j-1, j+1, ..nTargets\}$  do
12:         $r_{target_{j+1}}(:, s_{t_w}) = r_{target_j}(:, s_{t_w}) + Q[s_{t_w}](s_i, s_{i+1}) - mean(Q[s_{t_w}](s_i, \{s_k : k \neq i\}))$  ▷ Reward actions bringing to different guessed target
13:      Update  $Q_{target}(s_{t_{k1}}, a_{t_{k2}})$  using Eq.(6.2), for  $k1, k2 = 1..nTargets$ 
14:      Choose  $a_{t_j}$  from  $Q(a_t, s_{t_j})$  derived from  $Q_{target}$  (i.e always optimal action) ▷ Compute new guessed target
15:      Take action  $a_{t_j}$ 
16:      if  $s_{t_{j+1}} = s_{t_j}$  then ▷ Guessed target does not change
17:        Update route reward and state-action matrices corresponding to current guessed target  $r[s_{t_j}], Q[s_{t_j}]$ , as in lines 6:10 of Algorithm 1
18:         $r_{target_j} \leftarrow r_{target_{j+1}}$ 
19:         $s_{t_j} \leftarrow s_{t_{j+1}}$ 
20:      else ▷ Target is reached
21:        Execute lines 12:13 of Algorithm 1
22:        Execute lines 1:3 of Algorithm 2 ▷ Reset target learning data and start a new iteration

```

One iteration consisted of the sequence of robot steps from the starting position to the target. Both targets were alternately presented during subsequent iterations, until 250 trials (robot steps) were performed towards each target. At each robot step, the Q-matrix was updated using (6.2). The output of the online ErrP classifier provided information about user detection of an error in the last observed robot step, and was used to update the corresponding transition value in the reward matrix r , according to line 7 in algorithm 1, with the effect of discouraging that action. This allowed the implementation of a short-term negative reward. The r matrix was also updated with a positive value when the target was reached, thus allowing the forward term, multiplied by γ in (6.2), to start propagating information on the long-term environmental reward.

In this phase of the task, two Q matrices were learned, one for each target, and information on the current target was provided in a supervised way, by sending to the learning algorithm the true label for the current target. Learning rate was fixed to 0.7, while ϵ was initially set to zero (first iteration), to allow a faster learning of a possible route to the target, exploiting information provided by EEG ErrPs. After the first iteration it was increased to 0.4 to allow exploration of a route map robust to ErrPs misclassification, and for fast route correction in case of sub-optimal learned

route. When the best (3 steps-wide) route was learned, ϵ was set to 0.2, and then to 0 during target learning. Similarly, γ was initially set to 0.5 to avoid the strong learning of a non-optimal route, and then increased to 0.9 when the best route was found, in order to rapidly consolidate optimal information.

Target Learning

Once 500 route-learning trials were completed, target learning was activated during the last 100 trials. In this phase, the robot had to learn which one of the two available maps to choose, in order to reach the current target.

To achieve this result, the information on ErrP detection after each step was used, together with information provided by the learned Q-maps. As explained in algorithm 2, the target learning was restarted at each iteration: target learning, differently from route learning, should desirably be fast, without the possibility of exploiting accumulated information. For this reason, the relevant γ value was set to zero.

Similarly to the route learning case, a Q and r matrix were defined: Q was a 2x2 fully linked matrix with possible actions corresponding to conserving the guessed target or switching to the other one. The strategy used to make such a decision was based on the q-values accumulated in the Q matrices corresponding to the routes towards the two targets. Specifically, as explained in lines 9-10 of algorithm 2, after a robot step, if an error was detected, a negative reward was assigned to all actions keeping the same guessed target. This corresponded to the q-value for that transition in the route Q matrix of the current guessed target, discounted by the mean of q-values of all other possible transitions from that step's initial state. At the same time, a positive reward was assigned to all actions leading to changing the guessed target, proportional to the q-value for the same transition in the route Q matrix of the other target.

After reward updating, the target Q matrix was also updated using Eq. (6.2), with $\alpha = 0.7$, and the optimal action was always chosen ($\epsilon = 0$). If the selected action did not bring about a change in the current guessed target, ErrP detection was used to continue the corresponding route learning, according to algorithm 1.

It is worth noting that the learning strategy was based only on the error class detection, while no update was allowed for route or target reward functions based on the correct class detection. This choice was intended to reduce the weight of false negatives (erroneous trials classified as correct) on the degradation of the learning algorithm performance, since low classification accuracy is a known issue in ErrP detection, especially in real-time systems.

6.3 Simulation Study

Before practical implementation, the route and target learning algorithms described in Section 6.2.3 were tested in a simulation study, comparing their performance for different simulated levels of ErrP detection accuracy. Results for route learning and target learning are reported in Fig. 6.3 and 6.4, respectively.

For route learning, the number of steps taken from the starting position to the target, and the length (number of states crossed) of current best route, against number of iterations are reported in Fig. 6.3 left and right panel respectively, as average values and standard deviations over 50 simulations. Results are compared for ErrP detection accuracy=[100%; 80%; 60%], and for simple Q-learning (without using ErrP detection information for step-by-step reward updating). With 100% ErrP detection

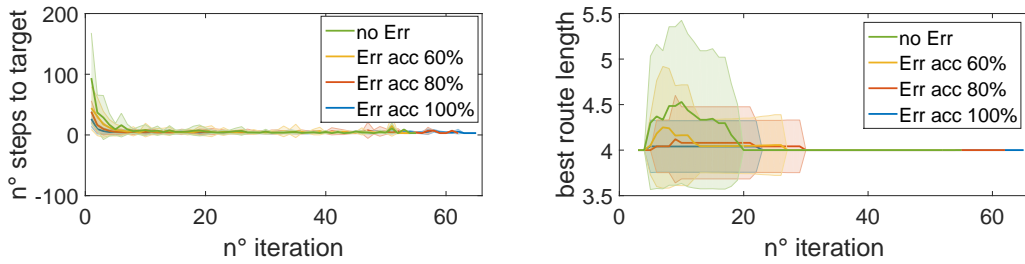


FIGURE 6.3: Simulation results for route learning.

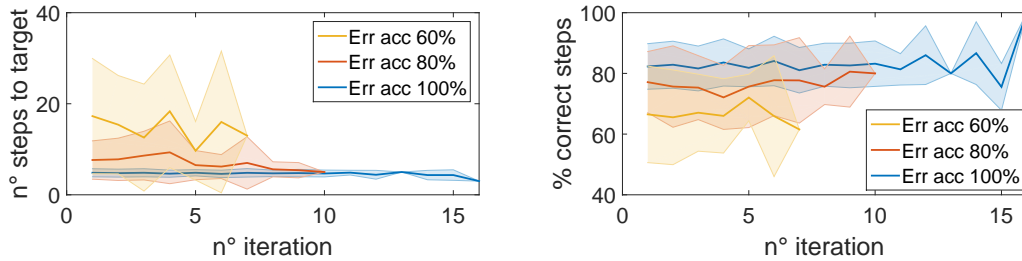


FIGURE 6.4: Simulation results for target learning.

accuracy, the inclusion of the negative step-by-step rewards reduces the number of steps required during the first iteration from 80 to 20, and considerably reduces the variability among task repetitions. Also, ErrP detection inclusion in Q-learning reduces the length of non-optimal learned routes during early iterations, though it does not fasten the route correction as compared to basic Q-learning. These results are consistent also when a mis-classification rate in ErrP detection is simulated, even if with a progressive decrease of performance. For 80% of ErrP detection accuracy, which corresponds to the state-of-the-art standard for ErrP detection in simulated tasks, the algorithm performance is very close to the 100% accuracy case. Even for lower accuracy in ErrP detection, the algorithm allows for a more efficient performance than a simple Q-learning algorithm.

For target learning, the number of steps taken from the starting position to the target, and the percentage of steps with correctly guessed target during each iteration, are shown in Fig. 6.4. In this case, simple Q-learning cannot be implemented, and in fact, one of the contributions of the proposed use of ErrP is the possibility of having an additional degree of freedom in the learning. Even in this case, an increase in ErrP classification accuracy reduces the number of moves necessary to reach the target, and increases the correct steps percentage, i.e., steps with correctly guessed target.

It is worth noting that for the considered task, the optimum value, in terms of number of steps to reach the target, is indifferently 3 or 5 steps, corresponding to 80% to 100% correct steps, respectively when the robot correctly guesses the target at the first step, and never receives an error signal, or when it initially guesses the wrong target, and it needs the first erroneous step to correct the identified target. For 80% accuracy, the mean number of steps to reach the target is 7, corresponding to 2 erroneous steps necessary to correct the target guess. For lower accuracies (50% and 60%), the correct steps % decreases to 60-70%, and the number of steps to the target increases to 15-25 on average, respectively.

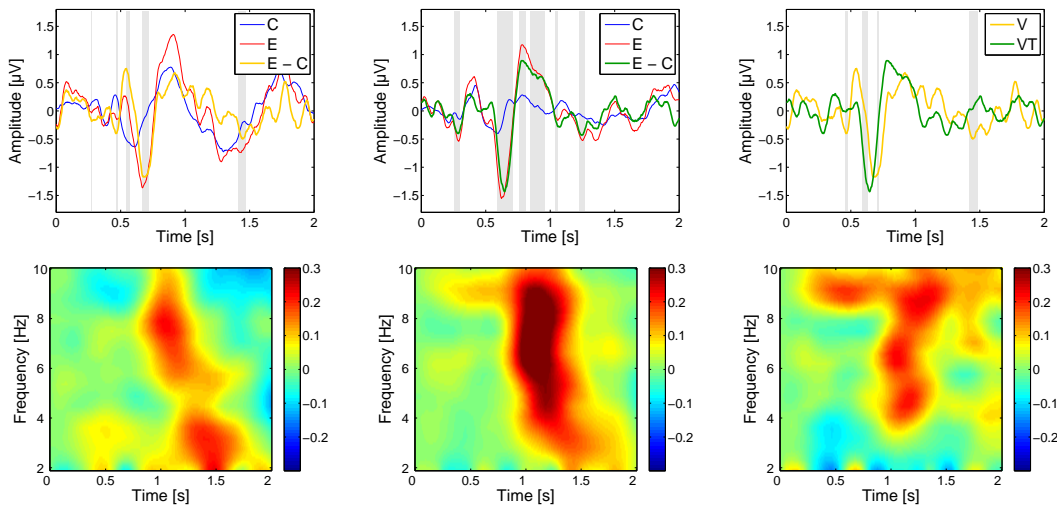


FIGURE 6.5: Grand average of ErrPs (E-C) across all subjects and training trials for channel FCz. Panels (a) and (b) display average C, E, and ErrP for V and VT conditions. Panel (c) provides a comparison V and VT ErrPs. Panels (d-f) provide a graphical representation of ErrP in frequency domain, for V (d), VT (e), and VT-V (f).

6.4 Results and Discussion

6.4.1 EEG Analysis

ErrP Detection

Fig. 6.5 shows the grand averages of E and C signals, together with ErrPs (E-C) across subjects and trials for V (a) and VT (b) conditions. The difference E-C is also reported in frequency domain for V (d) and VT (e). Right-column panels highlight the difference between ErrPs in the two feedback modalities, both in time (c) and frequency domain (f). Time-frequency graphs have been obtained by computing spectral densities of 1 s long windows, shifted by 50 ms, after multiplication with a Blackman window. Before averaging data from each subject, features have been normalized in amplitude by their value at $t = 0$. Shaded areas in time graphs represent time windows during which the difference between correct and erroneous responses is significant at a 5% level, according to t-tests (paired t-test for left and middle columns, unpaired t-test for right one).

The difference between classes present a similar pattern for both considered feedbacks: a first significant negative peak centered around 270 ms after stimulus onset is present for both feedback conditions as well as the largest negative peak, with center around 650 ms after stimulus presentation. All other significant features differ between conditions, with two relevant peaks in the V condition right before and after the 500 ms mark, while the VT condition still shows significant differences in the time window between 700 and 1200 ms. In general, recorded responses are very similar in shape to what was reported in literature Chavarriaga et al., 2014, but with a significant delay (around 200 ms). This reflects what was observed in previous works, reporting that the latency of ErrP waveform varies among different tasks, typically with increasing delay when coping with observation of physical movements or more complex tasks Iturrate et al., 2012.

On frequency domain, the most obvious feature, clearly visible both in V (Fig. 6.5 (d)) and VT (Fig. 6.5 (e)) responses is an increase of up to 30% in the spectral

TABLE 6.1: ErrP classification results during training and testing, for subjects with V feedback.

Subj.	Delay[s]	Training			Testing		
		C	E	AUC	C	E	AUC
S04-V	0.50	0.82	0.74	0.85	0.61	0.64	0.68
S06-V	0.60	0.59	0.61	0.62	0.52	0.49	0.52
S08-V	0.40	0.65	0.60	0.68	0.63	0.51	0.59
S010-V	0.60	0.67	0.71	0.75	0.6	0.59	0.62
Mean	0.53	0.68	0.67	0.73	0.59	0.56	0.60
Sd	0.08	0.08	0.06	0.09	0.04	0.06	0.06

TABLE 6.2: ErrP classification results during training and testing, for subjects with VT feedback.

Subj.	Delay[s]	Training			Testing		
		C	E	AUC	C	E	AUC
S05-VT	0.50	0.70	0.69	0.74	0.63	0.42	0.55
S07-VT	0.20	0.55	0.62	0.61	0.51	0.62	0.57
S09-VT	0.20	0.73	0.57	0.72	0.62	0.64	0.66
S011-VT	0.30	0.65	0.67	0.69	0.58	0.51	0.59
Mean	0.30	0.66	0.64	0.69	0.59	0.55	0.59
Sd	0.12	0.07	0.05	0.05	0.05	0.09	0.04

density power following stimuli. The center of this increase is almost exactly matching for both tested conditions and occurs around 1.1 s after stimulus, while the peak frequency involved is about 7 Hz. Despite the matching position in both time and frequency, this increase is about 50% more intense in the case of VT feedback. A marked difference in response, on the other hand, occurs earlier in time (around 0.5 s after stimulus) at a frequency of 9 Hz: while the VT feedback causes an increase of this response component, the visual-only response results weakened compared to baseline.

ErrP Classification

Classification results, in terms of AUC, are reported in tables 6.1 and 6.2 for V and VT feedback condition respectively.

It is possible to note how VT feedback generally leads to more consistent responses (smaller standard deviations) and classification accuracy tends to peak earlier for VT than V (0.3 s delay against 0.53 s).

Classification accuracy obtained from training data varies significantly between subjects, ranging from very good (highest AUC = 0.85), to discrete (lowest AUC = 0.61), with average values around 0.7 (0.73 and 0.69 for V and VT feedback). These values drop by almost 10% during testing phase, to 0.60 and 0.59 on average for V and VT conditions respectively. This is likely due to subjects' attention lapses, given the length of the experiment, and to the difference in task and errors occurrence moving from training to testing.

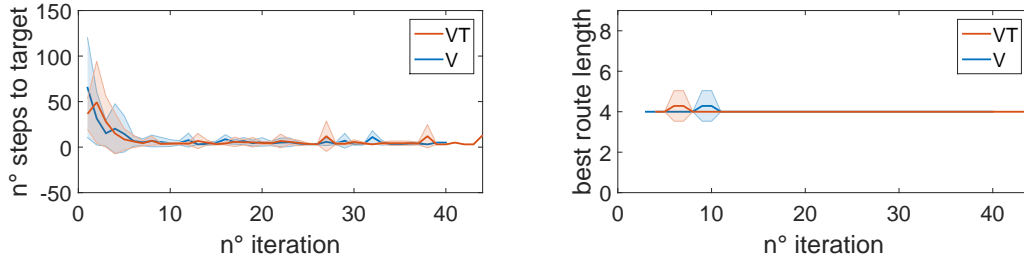


FIGURE 6.6: Experimental results for route learning.

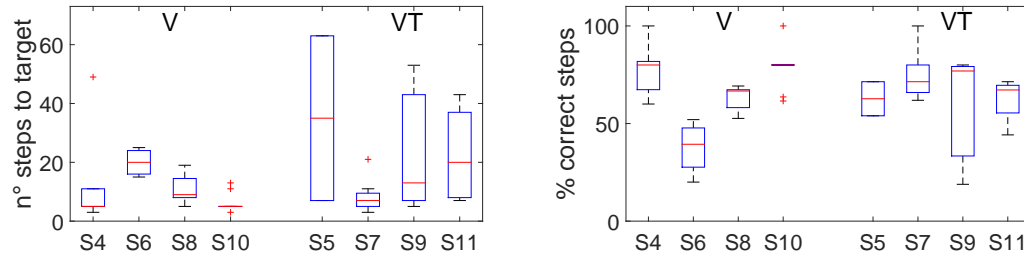


FIGURE 6.7: Experimental results for target learning. Red line indicates median, blue box extends to first and third quartiles, whiskers reach most extreme data outside of box not considered outliers, and the outliers are plotted individually using the '+' symbol.

6.4.2 Robot Learning

Results collected during online robot learning, considering separately route learning trials (250 trials per target), and trials in which also target learning was activated (last 100 trials), are reported in Fig. 6.6 and 6.7. Here, statistics shown are the same reported in the simulation study, Section 6.3.

Route Learning

The average number of steps to the target, and the average length of best route (number of crossed states) per iteration, are shown on left and right panel of Fig. 6.6 respectively. Results are shown in terms of mean across subjects and targets, considering V and VT feedback conditions separately.

While ErrP classification accuracy, in terms of mean AUC (see Table 6.1 and 6.2), was not varying among V (0.60) and VT (0.59) conditions, the average number of steps and the variability across subjects results lower for VT condition than for V (36.5 ± 16.9 against 65.3 ± 54.8), in the first iteration, where no exploration is allowed and only information from ErrP signal is used to update the reward and choose the best action. These values match respectively an accuracy of around 80% and 60% in the simulated data (see Fig. 6.3 left panel). This observation suggests that the ErrP classification accuracy could not be uniformly distributed over all experiment duration.

In both conditions, the number of steps converge to the minimum at around nine iterations, as in the case of simulated 60% ErrP detection accuracy. On the other hand, results related to best route length show the opposite trend: for the majority of subjects in VT condition the route correction happens between the 5th and the 8th iteration, while for V condition this is observed between 8th and 11th iteration. On

simulated data (Fig. 6.3 right), it appears that an earlier route correction happens for lower ErrP detection accuracy, since ϵ is higher and more states are explored in the first iterations compared to cases with high ErrP detection accuracy. In contrast with simulated data, on experimental data route correction for VT condition happens earlier but without requiring a higher number of steps.

Target Learning

Fig. 6.7 reports boxplots for distributions of number of steps to target, and % of correct steps across iterations, for each subject during robot target-learning, when route exploration is set to zero.

Comparing results from V and VT feedback conditions, a much bigger subjective variability of moves to the target is evident for the VT condition across iterations. This is in line with the lower accuracy observed in this phase of the experiment for ErrP detection. At the same time, the % of correct steps is on average between 60 and 80%, and more uniform across subjects undergoing VT condition compared to those with only V feedback. Also in this case, the experimental data are coherent to what expected from simulations, given the value of AUC expressing ErrP detection accuracy computed on testing data.

6.5 Conclusions

This work presented the evaluation of an ErrP-based reward signal for the inclusion of human implicit evaluation in the loop of robot learning, in order to: 1) improve a classic reinforcement learning (Q-learning) algorithm for robot target reaching, and 2) introduce the possibility of identifying, among a predefined set of possible targets, the one selected by the user, in a human-robot co-operative scenario.

The learning algorithm was evaluated offline simulating different levels of ErrP detection accuracy, showing a faster convergence to optimal behavior compared to basic Q-learning algorithm, and a correct target identification above 60% even for a ErrP classification accuracy slightly above chance level. The system was then evaluated through online experiments, involving 8 subjects, using two different feedback conditions superimposed on the robot movements, to give rise to the ErrP signal: visual (V) and visuo-tactile (VT) feedback. Results showed that transferring the ErrP classifier to the online task causes a decrease in the accuracy of the ErrP single-trial detection, when compared to training, from 70% to 60%. Even so, this value allowed for the convergence of the learning algorithm faster than classic Q-learning, and for successful target identification with a mean 70% accuracy. These results also pointed out some difficulties related to the real-time use of ErrP in a human-robot co-adaptive interaction framework. There is a need for exploring techniques towards improving ErrP classification accuracy as well as knowledge transfer (generalization) methods to make ErrP decoders robust to differences from the training task to different real-time tasks.

The comparison between V and VT feedback conditions did not result in significant variation of ErrP detection accuracy for the considered task, although it did produce some differences in the learning behavior.

Overall, these results confirm the high potential of introducing human psychophysiological signals in the learning process of an intelligent assistive agent, towards a human-centered design of interaction between a patient and an intelligent robotic assistive tool.

Part IV

Active and Passive Control Signals: Co-adaptive Systems

Chapter 7

Mutual Information-based Feature Selection for Motor Imagery

This chapter presents a feature selection algorithm based on mutual information and conditional mutual information. This is applied to electroencephalographic data acquired during three different motor imagery tasks from two datasets: Dataset I from BCI Competition IV including full scalp recordings from four subjects, and new data recorded from three subjects using the popular low-cost Emotiv EPOC EEG headset (Schiatti et al., 2016). The aim is to evaluate optimal channels and band-power features for motor imagery tasks discrimination, in order to select information discriminative to the task and stable over time. Results confirm the importance of applying user-adaptive feature selection algorithms towards the development of effective portable low cost BCI systems based on motor imagery.

This work has been published as : Schiatti, L., Faes, L., Tessadori, J., Barresi, G., & Mattos, L. (2016, August). Mutual information-based feature selection for low-cost BCIs based on motor imagery. In Engineering in Medicine and Biology Society (EMBC), 2016 IEEE 38th Annual International Conference of the (pp. 2772-2775). IEEE. - The final files for this publication are available from IEEE via:

<http://dx.doi.org/10.1109/EMBC.2016.7591305>

7.1 Introduction

A Brain-Computer Interface (BCI) extracts meaningful information from brain signals and convert it into control signals of an external device. Such system has the potential to allow people suffering from mobility impairments to restore a non-muscular channel for communication and control (Wolpaw et al., 2002). In this context low cost, ease of use, and portability are key factors for the development of 'out-of-the-lab' systems, accessible to people in their home environment and usable in everyday life. Among existent BCI paradigms, detection of motor imagery is well suited for the development of self-paced systems, allowing the user to perform the control at will at any time (Blankertz et al., 2002). These paradigms are based on the detection of event related desynchronization/ synchronization (ERD/ERS), indicating decrease/increase of signal spectral power in specific frequency bands ($\mu=8-13$ Hz and $\beta=13-30$ Hz), during movement imagination or intent (Neuper et al., 2006). Recently the interest towards low cost EEG systems has been growing, as attested by an increasing number of related publications (Duvinaige et al., 2013, Martinez-Leon et al., 2016). The most popular is the Emotiv EPOC¹, a wireless EEG headset including 14 sensors positioned as shown in 7.1 under label E. Recent works explored the

¹<https://emotiv.com/>

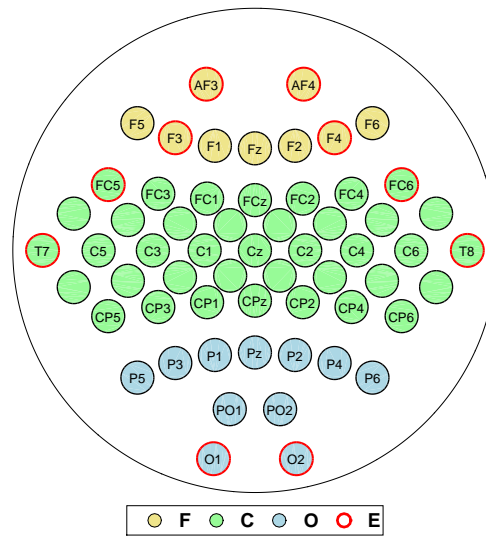


FIGURE 7.1: Scalp electrodes setup: frontal area (F); central area (C); occipital area (O), Emotiv EPOC channels (E).

possibility to develop motor imagery based on the EPOC system, obtaining encouraging results (Martinez-Leon et al., 2016, Mladenov et al., 2012).

Keeping a minimal number of electrodes is essential to develop a low cost and portable system. To this aim, several algorithms have been proposed to reduce the number of channels in BCIs (Barachant et al., 2011). Furthermore, optimal choice of frequency band and time segment reflecting ERD/ERS activation is highly subject-specific, and greatly affects the performance of the resulting BCI. The optimal combination of time, frequency and channel position, i.e. feature selection, is therefore essential in BCI design to achieve a good classification performance. In Hurtado-Rincón et al., 2014 a relevance analysis was applied offline to time and frequency domain parameters extracted from EEG data recorded with EPOC, and the resulting feature set was shown to allow left and right hand motor imagery discrimination.

In the present study a feature selection algorithm based on the conditional mutual information, originally presented in Tsimpiris et al., 2012, is applied to the Dataset I from the BCI competition IV and on new data recorded using the Emotiv EPOC headset. The method allows the selection of optimal features that are at the same time maximally relevant to the class variable, and minimally redundant among each other. Band-Power (BP) features are extracted from both datasets in different time windows during task execution. Optimal subsets of features are then selected to discriminate two out of three motor imagery classes, i.e. left hand, right hand, and foot, and results are validated in terms of classification accuracy.

7.2 Methods

7.2.1 Dataset

The first considered dataset is the 100 Hz version of the data from calibration session of the BCI Competition IV Dataset I (Blankertz et al., 2007). It consists of four subjects performing 100 trials for each one of two motor imagery tasks, respectively left hand

and foot for subjects Sa and Sf, and left and right hand for subjects Sb and Sf. At the beginning of each trial, a visual cue was provided in a computer screen to the subject, who then started to perform a motor imagery task for 4 s. Task periods are interleaved with 4 s long rest periods. EEG signals were recorded from 59 channels, mostly distributed over sensorimotor areas, labeled as F, C, and O in Fig.7.1. The second dataset was recorded at 128 Hz using the Emotiv EPOC headset (channels labeled as E in Fig. 7.1). It encompasses data from three subjects, S01, S02 and S03, performing 100 trials for each one of three motor imagery classes: left hand, right hand, and foot. The experimental paradigm was the same described for Dataset I. All subjects provided their informed consent to participate to the experiment.

7.2.2 Pre-processing

Raw signals were spatially filtered using common average re-referencing, and band-pass filtered using a zero-phase digital finite impulse response filter of 50th order, with Hamming window, to remove high frequency noise, slow artifacts, and extract information within the frequency bands of interest. Five frequency bands were considered for BP features extraction, covering μ and β bands, in which ERD/ERS phenomena connected to motor imagery are known to take place. Frequency bands were split as follows: $\mu=8-13$ Hz, $B1=13-18$ Hz, $B2=18-23$ Hz, $B3=23-28$ Hz and $B=13-30$ Hz. Three overlapping epochs after cue presentation were extracted from each record for BP analysis: $TW1=[0-2]$ s, $TW2=[1-3]$ s and $TW3=[2-4]$ s. Logarithmic BP features were extracted for each frequency band and time window, using Welch periodogram estimation.

7.2.3 Feature Selection and Classification

A feature selection algorithm based on estimation of conditional mutual information was used to select optimal features sub-sets, considering BP features extracted in three cases: (a) the set of all 59 channels from Dataset I; (b) the selection of 10 out of 59 channels corresponding to available EPOC electrodes locations from Dataset I; (c) the set of 14 Emotiv EPOC channels from the second dataset.

Given a set of M features $F = \{f_1, f_2, \dots, f_M\}$, and N cases (trials), a data matrix of size $N \times M$ is defined. In addition, the value of the corresponding discrete class variable C ($C = \{1, 2\}$ for the two-class problem) is assigned to each case. This allows defining the process of optimal feature selection as the problem of finding a feature subset $S \subset F$ that best classifies the N cases. Here, mutual information (MI) and Conditional Mutual Information (CMI) quantities were used to provide a feature selection criterion that evaluates two key properties of optimal features: the relevance of a feature to the class variable, and the redundancy of similar features. MI can intuitively be described as the information one variable carries about another variable and vice versa. For discrete variables, MI between each feature f_i and the class variable C , can be computed in terms of entropies:

$$I(f_i; C) = H(f_i) + H(C) - H(f_i, C) = H(C) - H(C|f_i) \quad (7.1)$$

for $i = 1, \dots, M$, where $H(f_i)$, $H(C)$, $H(f_i, C)$ are entropies of f_i , C . Redundancy and relevance, which together constitute the criterion for features selection, can be jointly formulated as the conditional mutual information $I(f_i; C|S)$, i.e. the MI of the candidate feature f_i and the class variable C accounting for the information shared

between each of them and the currently selected features set S . The CMI can be expressed in terms of entropies as:

$$I(f_i; C|S) = I(f_i; (C, S)) - I(f_i; S) = H(f_i, S) + H(C, S) - H(S) - H(f_i, C, S) \quad (7.2)$$

The progressive selection of features on the basis of MI and CMI can be summarized in the following steps:

1. Among all features $f_i \in F$ find the feature f^* most relevant to the class variable C as the one which minimize the conditional entropy $CE_i = H(C|f_i) = H(f_i, C) - H(f_i)$, thus maximizing the mutual information $I(f_i; C)$, computed as shown in Eq. 7.1. Set $S = f^*$.
2. To find the next optimal feature f^* to be added to S , compute for all candidate features $f_i \in F|S$ the CMI, $I(f_i, C|S)$, as in Eq. 7.2, and then select the one which maximizes it, $f^* = \operatorname{argmax}_{f_i} I(f_i; C|S)$.
3. Add f^* to S and repeat step 2 if CMI for f^* exceeds a threshold value, computed as the 95th percentile of a distribution of 100 estimations of CMI, each one derived using the values of f^* randomly permuted; otherwise stop the algorithm.

The CMI criterion in step 2 for optimal feature selection accounts for both relevance and redundancy: in fact, the feature selected is the one giving the largest amount of information about the class (relevance), which is not contained in the features already selected (redundancy). In this study, MI and CMI were estimated computing entropies from the probabilities assessed on the discretized values of the features. Discretization was performed by means of equidistant binning, using a number of quantization level $c = 4$. Such small value for c was chosen because it allows the selection of a higher number of features with an equal information gain.

The optimal sub-sets of features, selected for each subject and time window as described above, were used to train and test a linear SVM classifier, implemented according to a 10-fold cross-validation scheme, in order to show the corresponding optimal classification rates.

7.3 Results and Discussion

Results of the feature selection step are shown in Tables 7.1-7.4, considering the cases (a), (b), and (c) as starting datasets for the feature extraction and selection algorithms. For each time window and frequency band, the feature selected is indicated by the number matching its rank in the selection procedure, followed by a letter within brackets, indicating the area where the channel is located (F: frontal, C: central, O: occipital, see Fig.7.1). In Table 7.1, features relative to Emotiv EPOC electrodes locations are evidenced in bold type. Classification accuracies obtained using the optimal features sets in Tables 7.1-7.4 are reported in Fig. 7.2.

When using all channels from Dataset I, the highest accuracies for subjects Sa and Sg (0.79 and 0.83 respectively) were obtained for the window TW2, 1-3 s after cue (Fig.7.2). A high accuracy was shown also in TW3, 2-4 s, while a lower accuracy was observed immediately after the cue (TW1, 0-2 s). On the contrary, Sb and Sf showed higher accuracy in TW1 than in later time intervals (0.67 and 0.765 respectively), but comparable with Sa and Sg classification accuracies in the same time window.

TABLE 7.1: Results of feature selection on (a) Dataset I-BCI Competition IV

	<i>left hand-right hand</i>						<i>left hand-foot</i>					
	Sb_all			Sg_all			Sa_all			Sf_all		
	TW1	TW2	TW3	TW1	TW2	TW3	TW1	TW2	TW3	TW1	TW2	TW3
<i>Mu</i>	2(O)	2(C);3(C); 5(C)	1(C); 2(O)	-	-	-	1(C);2(C); 6(C)	1(C);2(O); 3(C);5(C);	1(C); 2(C)	1(C);3(C)	1(C);2(C); 6(O)	1(C)
<i>B1</i>	3(O); 4(F)	-	3(O)	1(C);3(O); 4(C)	4(O);5(F)	-	4(O)	4(C); 7(C)	4(F);5(C); 6(O)	4(C)	-	2(O); 4(C)
<i>B2</i>	5(C)	-	4(O)	2(C)	1(C); 2(C)	1(C);2(C); 3(C)	5(C)	6(C)	3(O)	-	5(C)	5(O)
<i>B3</i>	1(O)	1(O);4(C); 6(C)	-	5(O)	-	-	-	-	-	2(C);6(C)	3(C); 4(O)	6(C)
<i>B</i>	6(C)	-	5(C);6(C)	-	3(O)	4(O)	3(F)	-	-	5(O)	-	3(F)

TABLE 7.2: Results of feature selection on (b) EPOC channels from Dataset I-BCI Competition IV

	<i>left hand-right hand</i>						<i>left hand-foot</i>					
	Sb_EE			Sg_EE			Sa_EE			Sf_EE		
	TW1	TW2	TW3	TW1	TW2	TW3	TW1	TW2	TW3	TW1	TW2	TW3
<i>Mu</i>	-	-	-	2(O)	-	-	1(C)	1(C);2(F)	1(C)	1(F);2(O)	1(C)	-
<i>B1</i>	2(F)	-	-	-	2(F)	-	-	-	-	-	-	2(F)
<i>B2</i>	3(O)	-	-	1(C)	-	-	3(F);5(F)	-	3(O)	-	-	1(C)
<i>B3</i>	1(O)	1(O)	-	-	-	-	2(C);4(F)	-	2(O)	-	2(C)	-
<i>B</i>	-	-	-	-	1(F)	-	-	-	-	-	-	-

This suggests that features selected in late time intervals are more effective in capturing the ERD/ERS mechanisms leading to discriminate between motor imagery classes, independently from the considered task, (left-right hand, or left hand-foot discrimination).

Furthermore, the resulting accuracy depends more on the specific subject's brain patterns than on the type of imagined movements. Table 7.1 shows that the difference in task is captured by the frequency band of the optimal BP features selected. For left hand-foot discrimination the features with the highest rank are found in the μ band, while for left-right hand the most discriminative information is carried by features in low β band. Spatially, for both tasks the channels in central areas result as the most effective for discrimination. Higher classification accuracies were obtained when the first selected features are in central areas (Sa, Sf, Sg). For subject Sb, for whom the best accuracy was much lower than for other subjects, the first optimal feature was selected in occipital area, in β band (TW1).

When restricting the analysis to Emotiv EPOC channels, the best classification accuracies for subjects Sa, Sf, and Sg showed a decrease of about 20%, though remaining above the chance level (0.62, 0.615, and 0.63 respectively). On the contrary, for subject Sb, the best classification accuracy increased by 4% (0.695). This can be explained looking at the results of feature selection in Table 7.1-7.2. For subjects Sa, Sf, and Sg, when starting from the entire 59 channels set (Table 7.1), features in EPOC channels were selected with rank from 4 to 5, mostly in O and F areas. This indicates that for the tasks considered the 10 EPOC channels carry much less information than other channels of the full set of electrodes. On the other hand, for subject Sb most informative features were found in O, and coincident with EPOC electrodes also when starting from the complete 59 channels dataset (Table 7.1). Thus accuracy does not differ significantly when restricting the analysis to EPOC channels. The observation above highlights the influence of the first selected feature on the composition of the resulting optimal features set. When using the algorithm presented in Section II-C, all subsequent features are selected based on their relevance and redundancy compared to the already selected ones. This constraints the search potentially preventing the selection of the absolute best features set, as shown by the increase in Sb accuracy. The dimensionality of the optimal features set, leading to the best classification accuracy, when starting from the EPOC channels from Dataset I, ranged from 2 to 3. This suggests that the EPOC channels are able to determine features explaining most of the information connected to class discrimination, and that the first one or two selected features are mostly responsible for the final classification accuracy. Relevant information carried by subsequent features rapidly decreases with the number of features selected.

Best classification accuracies obtained on Emotiv EPOC dataset were 0.7, 0.615 and 0.67 for subjects S01, S02 and S03, achieved respectively for left hand-foot (TW1), left-right hand (TW1) and right hand-foot (TW2) discrimination (Fig. 7.2). As visible in Table 7.3 and 7.4, the corresponding first feature selected belonged to O area for all three subjects, in μ band for subjects S01 and S03, and in β band for subject S02. This confirmed that features in μ band are more effective in discriminating tasks involving foot motor imagery, while features in β band bring more useful information for left-right hand motor imagery discrimination. The importance of channels in C area was confirmed by the observation that best accuracies (0.7, 0.685) were obtained for S01 in both hand-foot tasks, in TW1, when also features in C are selected.

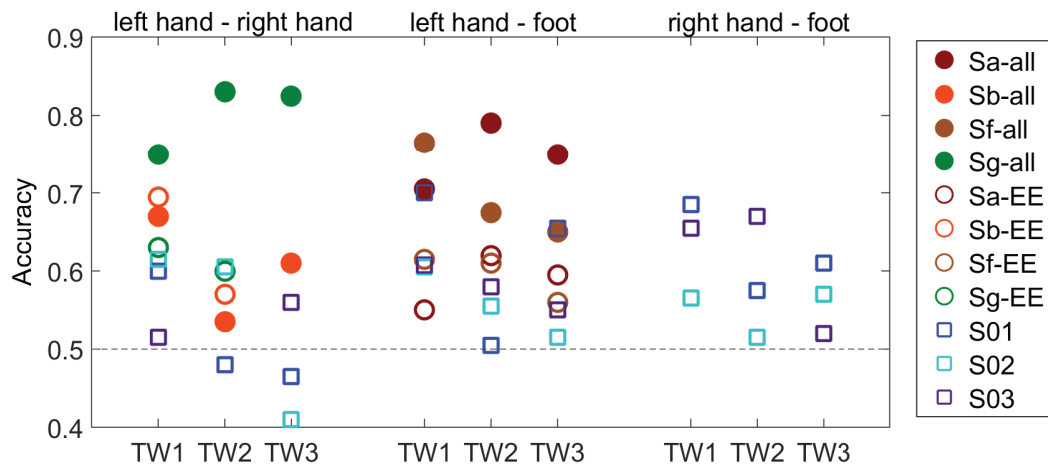


FIGURE 7.2: Classification accuracy using optimal features sets computed in time windows TW1-3 for subjects: Sa, Sb, Sf, Sg from full 59 channels (-all) and reduced to EPOC channels (-EE) Dataset I- BCI Competition IV; S01, S02, S03 from Emotiv EPOC dataset.

7.4 Conclusions

Results of feature selection on the 59 channels Dataset I from BCI competition IV showed that optimal features vary considerably across subjects, thus confirming the importance of subject-adaptive feature selection algorithms in the development of effective BCIs. The number of optimal features selected as relevant and not redundant varied from 5 to 7 for the best classification accuracy achieved on each subject data. This confirmed the feasibility of motor imagery-based BCI systems using a low number of EEG channels. Results also attested the usefulness of low cost EEG system like Emotiv EPOC, for the development of such BCIs. Even not encompassing electrodes in the motor area, BP features extracted from EPOC channels were found to be relevant, especially in hand-foot discrimination, allowing an offline classification accuracy of 70% using only 2 features.

Chapter 8

Tactile Feedback in Error-based Adaptive Classification of Motor Imagery

This chapter presents an implementation of ErrP detection to provide progressive adaptation of a motor imagery task classifier. The output of a static ErrP classifier is used to provide information about correctness of the motor imagery classification output. This is then exploited to update the task classifier's parameters, thus allowing for adaptation to new data. The main contribution of this work is in the evaluation of the effect of vibrotactile feedback on both ErrP and motor imagery classification, and on the adaptive classification performance. Results confirm the potential of self-adaptive techniques to improve motor imagery classification, and support the design of tactile feedback into BCIs to improve both static and adaptive performance.

8.1 Introduction

The development of Brain-Computer Interfaces (BCIs) offers the possibility to restore a non-muscular channel for communication and control to people with severe motor disabilities (Wolpaw et al., 2004). Despite the growing research in the field and a wide range of applications developed in the last decades, BCIs, and especially non-invasive BCIs, suffer from a number of limitations, that prevent them from being integrated in current Assistive Technologies (AT) (Millán et al., 2010). The interest towards non-invasive BCIs, mainly relying on electroencephalographic (EEG) signals, and supported by the need of a portable and acceptable technology for the patients, brought to the development of different adaptive signal processing approaches.

One of the limitations of EEG-based BCIs based on voluntary control, e.g. motor imagery (MI), is related to the non-stationarity of data, which leads to a decrease in performance from training to testing phase. In order to overcome this problem, many approaches have been proposed based on adaptive classification: assuming that the labels of incoming trials are known, it was proven that proper updates in classifier parameters can improve the performance of the static classifier (Shenoy et al., 2006). In a real BCI application, though, user intention, corresponding to the class label, is usually unknown. One interesting approach to cope with this lack of knowledge is to exploit the same neural channel both for extraction of an active control signal (the output of the BCI classifier) and for retrieving information on user's awareness of a misinterpreted intention. The latter can be achieved by detection of a passive EEG feature, the so called Error-related Potential (ErrP), which is evoked in

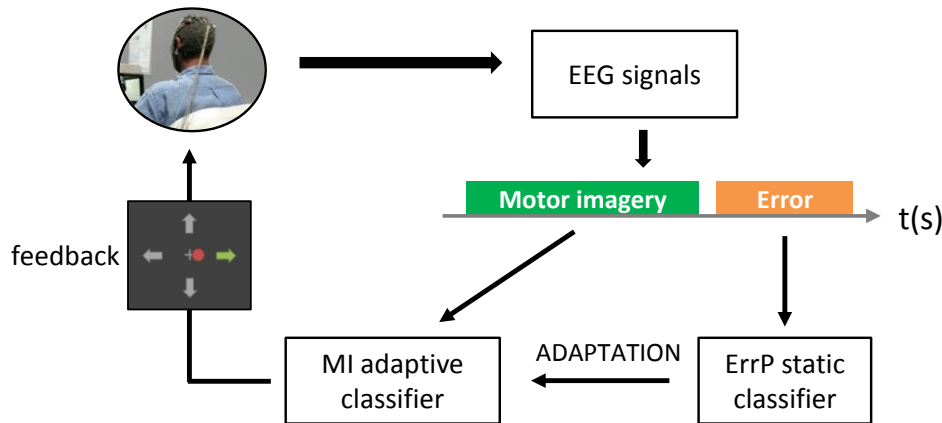


FIGURE 8.1: Scheme of adaptive classifier functioning. EEG signals are used both to extract an active control signal (from a motor imagery task), and a passive information (ErrP) on user's evaluation of the MI classifier's output (after feedback is provided). The output of static ErrP classifier is then used to update the MI adaptive classifier's parameters, and to improve its performance over time.

user's fronto-central activity, and has been proven to be detectable on a single-trial basis with a quite high (about 80%) accuracy (Chavarriaga et al., 2014). Since ErrP it is an evoked potential, contrary to sensorimotor rhythms exploited to detect motor imagery, features allowing its detection are quite stationary over time. This characteristic makes it suitable to be exploited in a reinforcement learning framework. Here, ErrP is used to provide a passive signal, stable over time, to improve the performance of an adaptive classifier, used for the detection of an active EEG pattern, e.g. the EEG pattern underlying motor imagery. This concept was implemented by Llera et al., 2011, on magneto-encephalographic (MEG) data recorded during a two-class covert attention paradigm. Their approach is shown in Fig. 8.1. ErrP decoding was used to identify misclassification and provide labels for the new incoming data. Results from offline analysis showed that this technique can significantly improve the performance of the BCI classifier.

In the present work, the method proposed by Llera et al., 2011 was applied to EEG data recorded during a four-classes motor imagery task. During the experiment, a classification feedback was also simulated by means of a virtual cursor movement shown after each motor imagery phase, in order to collect a realistic dataset for both motor imagery and ErrP detection. Only data related to left and right hand motor imagery were considered in this preliminary study, in a binary classifier implementation. In the described setting, ErrP detection greatly depends on how feedback is designed. Previous studies supported the evidence that using a tactile feedback channel to close the control loop between user and the assistive interface/device, can greatly improve MI-based BCIs performance (Chatterjee et al., 2007, Gomez-Rodriguez et al., 2011, Jeunet et al., 2015). Furthermore, vibrotactile feedback is simple to implement, keeps user attention free, and can be easily integrated in non-invasive systems (Kaczmarek et al., 1991).

The main contribution of the present study consists in evaluating the effect of tactile feedback on both adaptive motor imagery classification and ErrP detection. To this aim, a 'within' experimental design was chosen. Each subject repeated the experiment in two different conditions, i) with visual and ii) with visuo-tactile stimulation during motor imagery and feedback phases (see Fig. 8.1).

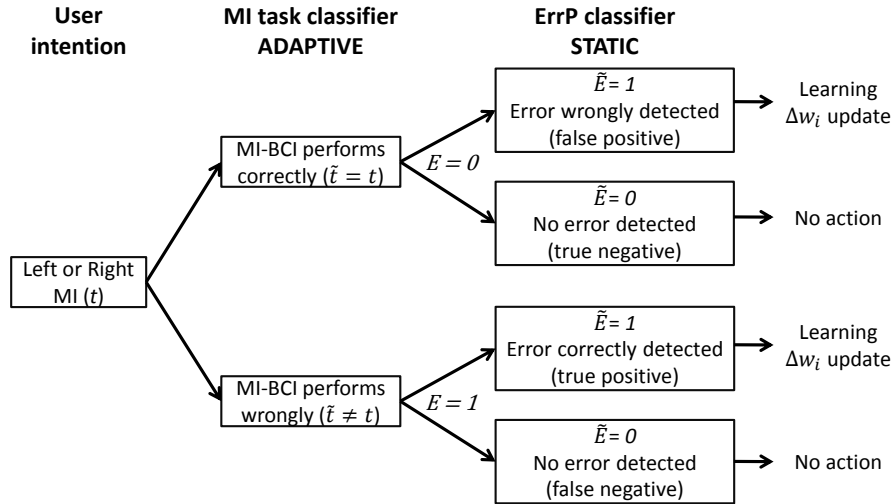


FIGURE 8.2: Block diagram of adaptive classifier algorithm presented in Llera et al., 2011, and used in the present work.

8.2 Methods

8.2.1 Adaptive classification

The adaptive classifier implemented in this study was introduced by Llera et al., 2011, and proved to be effective in improving the binary classification of left and right hand motor imagery on MEG data. The working principle of this adaptive algorithm is reported in Fig. 8.2. The learning, namely the updating of MI classifier's parameters, only happens when an error is detected after the motor imagery task classification. Ideally, if the static ErrP classifier had a perfect behavior, the learning would happen only when true errors, i.e. true positives (TP), are detected at the output of task classification. In practice, the performance of the adapting rule is affected by false positives (FP), i.e. correct trials wrongly detected as erroneous, and false negative (FN), i.e. erroneous trials wrongly classified as correct.

Specifically, labeling as $t \in \{0,1\}$ the true target class, i.e. left or right, corresponding to subject's intention, the output of the MI task classifier can be denoted as \tilde{t} . In the same vein, the subject's awareness of an interface error is denoted as $E \in \{0,1\}$, while \tilde{E} represents the output of the static ErrP classifier. When the BCI (task classifier) performs correctly ($\tilde{t} = t$), the detection of an error $\tilde{E} = 1$ corresponds to a false positive, and causes the MI classifier to learn from incorrectly labeled data. When instead the MI task classifier performs wrongly, a correct ErrP classification ($\tilde{E} = 1$), i.e. a true positive, results in a correct update, while a wrong ErrP classification ($\tilde{E} = 0$), i.e. a false negative, prevents the algorithm to perform a correct update. The FP rate (α_p) affects the adaptive MI classifier's performance in a worse way than FN rate (α_n). In fact, while in the latter case trials useful for updating are discarded, FPs cause an erroneous update to occur.

From the computational point of view, a logistic regression model is used to compute \tilde{t} , in terms of the probability:

$$p(t = 1|x, w) = \sigma(x, w) = \frac{1}{1 + e^{-\sum_{i=0}^n w_i x_i}} \quad (8.1)$$

where $x = (x_1, \dots, x_n)$ is a vector of features values extracted from user's EEG activity, which is relevant to discriminate between the two considered classes. The vector $w \in \mathbb{R}^{n+1}$ is the vector of weights, with $x_0 = 1$ accounting for the bias term. The output of the MI task classifier is defined by the function:

$$\tilde{t} = \chi \left((t = 1 | x, w) > \frac{1}{2} \right) \quad (8.2)$$

where χ returns 1 if the argument is true, and 0 otherwise. The prediction error is quantified by the log-likelihood function:

$$G(x, w, t) = -(t \ln \sigma(x, w) + (1 - t) \ln(1 - \sigma(x, w))) \quad (8.3)$$

The learning rule for the classifier parameters w consists in an update of w in the gradient direction (Eq.8.3):

$$\Delta w_i = \frac{\partial G(x, w, t)}{\partial w_i} = \eta(t - \sigma(x, w))x_i \quad (8.4)$$

where η is the learning rate. In a real system, the subject's real intention t is unknown. Updates Δw_i occur only when the static ErrP classifier detects an error ($\tilde{E} = 1$), in which case it can be assumed that the observed output \tilde{t} is incorrect, and $t = 1 - \tilde{t}$. Therefore, the learning rule for the adaptive MI classifier can be written as:

$$\Delta w_i = \eta \tilde{E} (1 - \tilde{t} - \sigma(x, w))x_i \quad (8.5)$$

8.2.2 Experimental protocol

The experimental protocol was designed in order to simulate errors made by a BCI in recognizing subject's intents in a bi-dimensional control task. Subjects did not actually control the interface, rather, they performed a 4-classes motor imagery task, with the goal of moving a virtual cursor in one of the four directions (up, right, down, left). The presence of ErrP generated by a wrong cursor movement was tested simulating an error made by the interface in recognition of subject's intent.

The experimental paradigm was implemented following the classic scheme for collection of motor imagery data (Schlögl et al., 2005), and it is illustrated in Fig. 8.3. Each trial encompassed a fixation cross appearing in a black screen (1.5 s), followed by a green arrow pointing one among four directions, indicating to the subject which motor imagery task to perform. A red dot superposed to the fixation cross was also shown, simulating a virtual cursor. Arrow pointing up, right, down and left indicated both hands, right hand, feet, and left hand motor imagery respectively. The MI task lasted for 4 s, and was followed by a break of 1 s (black screen), after which a feedback, simulating the result of MI classification, was presented. This consisted in a movement of the red cursor in either the direction pointed by the arrow (correct trials) or one of the other three directions (erroneous trial). Experiment was repeated by each subject in two conditions:

- **Visual feedback (V):** the task was performed with visual feedback shown in Fig. 8.3;

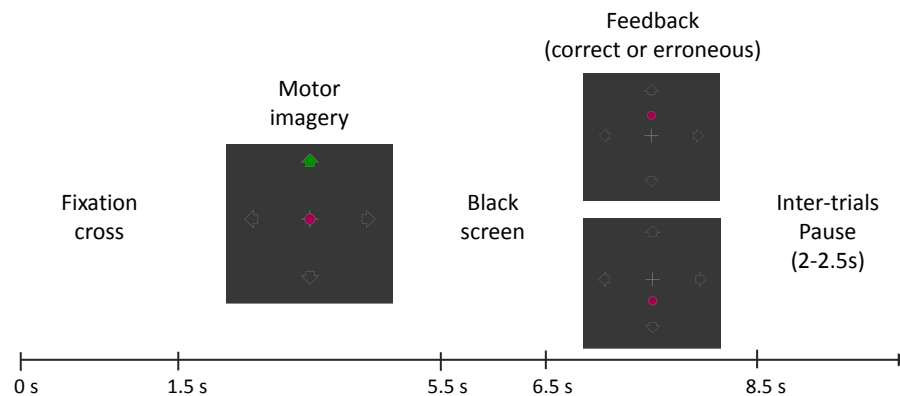


FIGURE 8.3: Experimental protocol. After 1.5 s from cue onset, a green arrow indicating which motor imagery task to performs appears for 4 s. After 1 s break a feedback, simulating MI classification output, is presented. It consists in the movement of a virtual cursor in either the correct direction or one randomly chosen among the other ones (erroneous).

- **Visuo-tactile feedback (VT):** during motor imagery and feedback phases the subject was provided with a vibrotactile stimulus by means of vibrating bands placed on wrists and ankles. Vibrations on both wrists, right wrist, both ankles and left wrist were provided for up, right, down, and left directions respectively. Tactile stimulus was provided for the entire duration of the motor imagery task (4 s), and for 1 s starting from the feedback presentation, according to the cursor movement.

Each experiment encompassed 8 sessions (half in V and half in VT condition, according to a 'within' experimental design) of 90 trials, uniformly distributed over the four classes. The chance of receiving an erroneous feedback was set to 40%. This value, higher than the one used in classic error detection experimental paradigms (Ferrez et al., 2008b), was chosen in order to guarantee the collection of enough trials for a robust ErrP classification, while keeping the duration of the entire experiment acceptable for the subject. A 'within' design for comparing V and VT conditions was chosen starting from the observation that performance for both motor imagery and ErrP detection varies greatly among subjects. For this reason, the improvement achievable with a tactile feedback should be assessed following a subject-specific approach.

Six healthy subjects (27.7 ± 4.6 y.o., all males) participated in the study. Each subject performed the experiment in two consecutive days, recording two V and two VT sessions each day, in random order. Before the experiment started, all subjects agreed with experiment's guidelines, and signed an informed consent document¹. All anonymized experimental data will be made available online². Only trials related to left hand and right hand motor imagery were considered in the present study, leading to around 45 trials x 8 sessions (4 with V and 4 with VT feedback), for each subject.

8.2.3 Experimental setup

The experimental setup consisted of 20 active gel electrodes (g.LADYbird from g.tec³) located at F1, Fz, F2, FC3, FC1, FCz, FC2, FC4, C5, C3, C1, Cz, C2, C4, C6, CP3, CP1,

¹IIT ADVR TEEP01 protocol, approved by the Ethical Committee of Liguria on June 14th, 2016.

²<http://teep-sla.eu>

³<http://www.gtec.at>

TABLE 8.1: Classification accuracy for V condition with static ErrP classifier

	Accuracy	FN ratio (α_n)	FP ratio (α_p)
S01	0.65	0.26	0.47
S02	0.58	0.39	0.46
S03	0.84	0.16	0.15
S04	0.67	0.31	0.37
S05	0.71	0.22	0.42
S06	0.73	0.25	0.30
Mean	0.70	0.26	0.36

TABLE 8.2: Classification accuracy for VT condition with static ErrP classifier

	Accuracy	FN ratio (α_n)	FP ratio (α_p)
S01	0.68	0.29	0.36
S02	0.68	0.27	0.39
S03	0.84	0.09	0.24
S04	0.78	0.15	0.32
S05	0.61	0.38	0.41
S06	0.72	0.23	0.34
Mean	0.72	0.24	0.34

CPz, CP2 and CP4 according to the standard 10/20 international system. Electrodes locations were chosen in order to cover the motor cortex area where changes related to movement imagination are known to happen, and in the frontal area for error potential detection. Experiments were started only after impedance of all electrodes was stably under 5 k Ω . EEG signals were acquired using a g.USBamp biosignal amplifier. Ground and reference were respectively placed on the forehead (AFz) and left ear lobe. Hardware filters were set to perform a bandpass between 0.1 and 100 Hz, with notch filter at 50 Hz. Signals were sampled at 512 Hz.

The graphical protocol was developed in Matlab, while data acquisition occurred through a Simulink model that handled the g.USBamp amplifier. A set of four custom-made silicone rubber (ACC Silicone M230) cuffs with embedded vibration motors (Precision Microdrives 304-116) were cast in order to provide tactile stimuli. Control of the vibratory motors occurred through serial communication, implemented over a direct USB connection.

8.2.4 ErrP classification

For ErrP classification, EEG data were spatially filtered by means of common-average re-referencing (CAR), then band-pass filtered between 1 and 10 Hz with a 4th order Butterworth filter, since EEG error correlates are known to be slow potentials. Time windows of length 1 s were extracted from recorded data, starting from feedback presentation (6.5 s from the trial's beginning in Fig. 8.3). Both time and frequency features were extracted and used for ErrP classification. Time features were obtained by sub-sampling signals to 64 Hz. Frequency analysis was performed selecting non-overlapping 0.5 Hz-wide power spectrum bands between 1 and 10 Hz, on the same time window mentioned above, after applying the Fast Fourier Transform. Features were ranked by means of z-score, and only features with score below the threshold of 0.25 were selected. A Support Vector Machine (SVM) with second order polynomial kernel was used for classification, using a leave-one-out cross validation procedure.

TABLE 8.3: Classification accuracy for V condition with static MI classifier

	TW1	TW2	TW3	TW4	TW5	TW6	TW7
S01	0.49	0.45	0.54	0.53	0.45	0.54	0.49
S02	0.59	0.59	0.60	0.57	0.59	0.59	0.57
S03	0.52	0.57	0.53	0.50	0.45	0.52	0.50
S04	0.49	0.53	0.57	0.51	0.58	0.51	0.46
S05	0.50	0.57	0.53	0.52	0.57	0.59	0.63
S06	0.55	0.60	0.67	0.46	0.48	0.52	0.51
Mean	0.52	0.55	0.57	0.52	0.52	0.54	0.53

TABLE 8.4: Classification accuracy for VT condition with static MI classifier

	TW1	TW2	TW3	TW4	TW5	TW6	TW7
S01	0.74	0.76	0.77	0.74	0.76	0.75	0.74
S02	0.55	0.60	0.56	0.54	0.50	0.61	0.56
S03	0.53	0.56	0.56	0.58	0.59	0.55	0.61
S04	0.94	0.79	0.87	0.96	0.94	0.95	0.96
S05	0.67	0.73	0.70	0.59	0.61	0.71	0.66
S06	0.68	0.69	0.55	0.50	0.49	0.48	0.60
Mean	0.68	0.69	0.67	0.65	0.65	0.67	0.69
$\Delta\text{Mean}[\%]$	30	25	16	26	25	24	30

These classification results, in terms of false negative (α_n) and false positive rate (α_n) were then used for the adaptive MI classification, to simulate the output of the static ErrP classifier and the updating algorithm's functioning in realistic conditions for each subject.

8.2.5 Motor imagery task classification

For the MI task classification, data were filtered between 8 and 30 Hz with a zero-phase FIR filter of order 20, and spatially filtered by means of small Laplacian (McFarland et al., 1997). Seven partially overlapping (overlap 0.5 s) time windows (TW) of 1 s length were extracted starting from each trial in the interval 1.5-5.5 s, corresponding to the motor imagery task. Log band-power features were then computed in each TW , considering the five 4 Hz frequency bands: 8-12 Hz, 12-16 Hz, 16-20 Hz, 20-24 Hz, 24-28 Hz. Data were divided in a training set, including data from the first session (about 20 trials per class), and testing set, including data from the remaining three sessions. Only the first 20 most significant features, i.e. with the lowest z-score computed on the training set, were considered for subsequent analysis. For static MI classification, the logistic regression model presented in Eq. 8.1 was exploited. The value of static MI classification accuracy was used as ground-truth to evaluate the adaptive classifier performance. This latter was implemented using the same logistic regression model, starting from the weights values of the static MI classifier, tuned on the training set, and applying the learning rule in Eq. 8.5 to update classifier's weights after each new testing example.

TABLE 8.5: ANOVA results on classification accuracy change between V and VT condition for each subject. Statistical significance threshold was chosen as $p < 0.01$.

Subject	F(1,6)	p
S01	250	4.06e-06
S02	3.399	0.115
S03	7.096	0.0373
S04	137	2.33e-05
S05	21.82	0.00343
S06	0.623	0.46

8.3 Results and Discussion

ErrP classification

In Table 8.1 and 8.2 results related to static ErrP classification accuracy are reported, for V and VT conditions respectively. A mean accuracy of 0.7 is obtained in both cases, regardless from the presence of tactile feedback. This result differ from what obtained in previous experiments (see chapter 5), suggesting an improvement in ErrP detection when tactile feedback was used in addition to the visual one. Such an observation could be motivated by different factors. The first one is the fact that in the present experiment, differently from the previous one, the task is bi-dimensional, so three different actions can be considered as an error after each trial. A decrement in the positive effect of tactile feedback on ErrP detection was observed also during the robot learning experiment, where the task was not binary as well (see chapter 6). Another reason for the ineffectiveness of tactile feedback on ErrP classification could be the high error ratio (40%), that in general could lead to worse detection accuracy. The α_n and α_p are slightly higher than in Llera et al., 2011, probably due to the lower ErrP classification performance. Furthermore, the α_p is greater than α_n for almost all subjects. This is an undesirable condition, since the adaptive algorithm executes a wrong update when a false positive is detected. For this reason, a probable decrease in the adaptive MI classifier performance, compared to the ideal condition (100% ErrP detection accuracy) is expected, from this source.

8.3.1 Motor imagery task classification

Static classification

Tables 8.3 and 8.4 show results related to static MI classification, in terms of accuracy for each subject and time window, for V and VT feedback conditions. When only visual feedback is provided, the mean accuracy among all subjects and TW is barely above chance level, with top results (0.55 and 0.57) between 0.5 and 1.5 s after stimulus onset. Adding tactile stimulation during motor imagery increases the classification accuracy of a value between 16% and 30% on average. The best results on single subjects' data passes from 0.63 in the V condition to 0.94 in VT.

To statistically evaluate the difference between V and VT considering all subjects, a within-subjects experimental design of 2×7 was considered, with 2 levels of feedback variable (V/VT) and 7 levels of repeated measures variable (the 7 windows). No significant effect emerged through ANOVA for the feedback ($F_{(1,5)}=4.333$, with $p=0.0919$), for the repeated measures ($F_{(6,30)}=1.097$, with $p=0.387$), and for their interaction ($F_{(6,30)}=0.658$, with $p=0.684$). Since single accuracy values vary greatly for

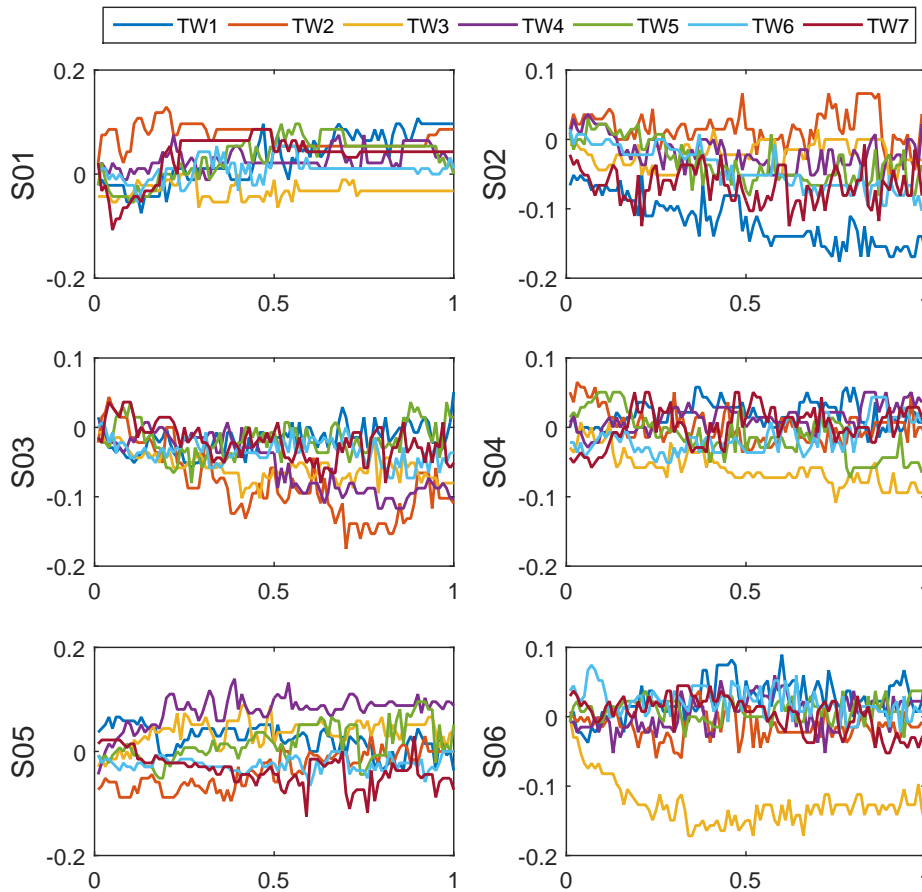


FIGURE 8.4: Variation in classification accuracy from static to adaptive MI task classifier, as function of the learning rate and considering 100% ErrP detection accuracy, for all time windows, in V feedback condition.

different subject, this evaluation could not be appropriate, when dealing with a very low number of subjects, as in this case.

A one-way repeated measures experimental design was then considered, with 2 levels of feedback variable (V/VT) in order to find its effects on the accuracy for each subject. Significant effects emerged through ANOVA for the subjects S01, S03, S04, S05 (as shown in the table 8.5). The assumptions (just the normality, calculated through the Shapiro-Wilk test) of the test were checked ($p=0.117$ for subject S01, $p=0.535$ for S03, $p=0.374$ for S04, $p=0.139$ for S05).

The evident improvement observable in MI classification, in presence of tactile feedback, leads to another consideration about the absence of the same result on ErrP classification. The use of the identical kind of feedback (only differing in its duration) could not be appropriate in order to enhance simultaneously the detection of an active and a passive feature. More than excluding the beneficial effect of a tactile stimulation on ErrP detection, this observation suggests that a different feedback design could be necessary to draw more solid conclusions to this regard.

8.3.2 Adaptive classification

To evaluate the MI adaptive classifier, a first analysis considering an ErrP detection of 100% was carried on, in order to assess the optimal learning rate value for each subject. Results are reported in Fig. 8.4 and 8.5. Each panel shows the absolute

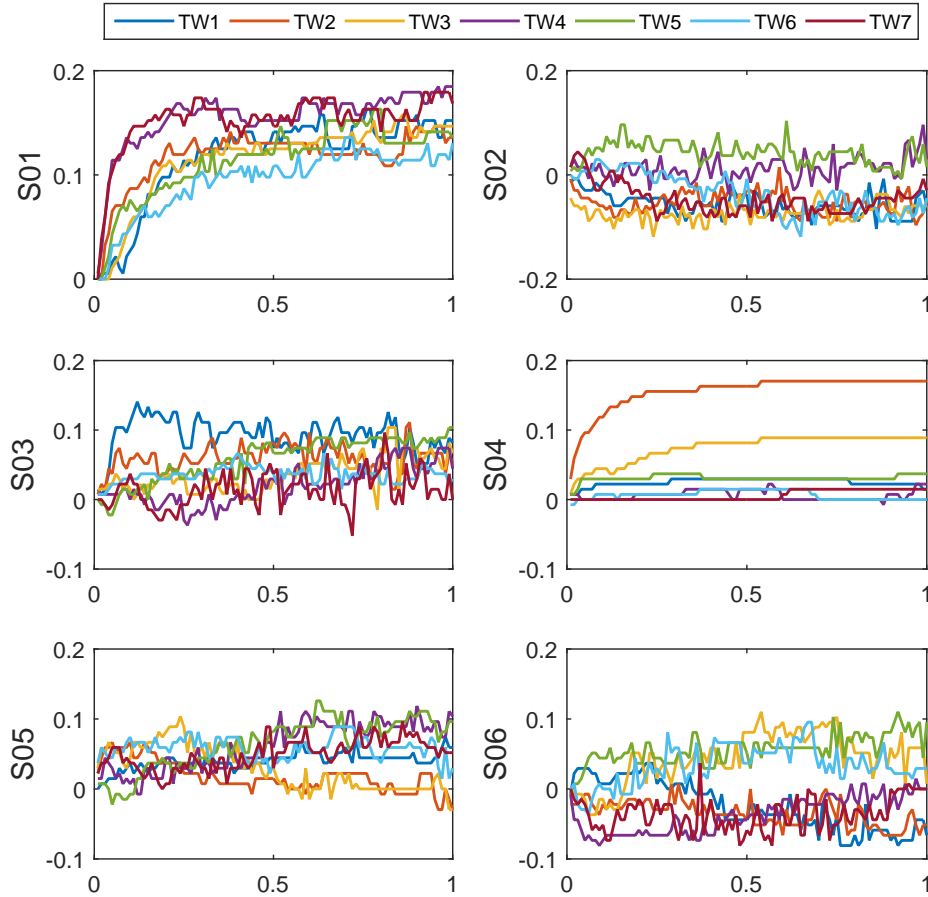


FIGURE 8.5: Variation in classification accuracy from static to adaptive MI task classifier, as function of the learning rate and considering 100% ErrP detection accuracy, for all time windows, in VT feedback condition.

classification accuracy improvement, compared to the static condition (tables 8.3 and 8.4), considering different TW, for learning rate values ranging from 0.01 to 1. As visible in Fig. 8.4, results for the V condition vary greatly based on the considered TW, and in general classification accuracy changes do not show a stable behavior, especially for high η values. A good behavior of the learning algorithm is shown for example by features in TW2 for subject S01, and η between 0.1 and 0.2; by features in TW2, TW4 and TW5 for subject S02, η between 0.01 and 0.15; by features in TW3 and TW4 for subject S05 after $\eta = 0.2$, and so on.

Results for VT condition show a much more regular and efficient behavior of the adaptive algorithm (see Fig.8.5). Subjects S01 and S04 in particular (who also showed the bigger improvement in static MI classification in presence of tactile feedback, see Tables 8.3 and 8.4), show the most desirable behavior for the learning algorithm. For all time windows, there is an improvement in classification accuracy up to 15%, and the algorithm converge to a stable behavior for $\eta > 0.25$. For subject S04, the improvement is only achieved for TW2 and TW3, since for the other ones the starting accuracy was already close to 1 (Table 8.4). These results suggest that the addition of tactile feedback, beside the beneficial effect on motor imagery detection, also facilitates the good functioning of adaptive techniques. In fact, the better behavior of the adaptive MI classifier on VT condition than V condition, could be explained by a more stationary character of the features over the sessions. For this reason, adding new samples of the two classes distributions, i.e. the updating rule,

TABLE 8.6: Change in classification accuracy from static to adaptive classifier considering the optimal TW and relative η for each subject, in V and VT conditions, in case of ideal 100% ErrP accuracy, and for real values of α_n and α_p (Tables 8.1 and 8.2)

	ErrP 100%		ErrP real	
	V	VT	V	VT
S01	9%	17%	3%	-5%
S02	3%	10%	3%	4%
S03	4%	10%	1%	12%
S04	7%	15%	5%	10%
S05	14%	8%	6%	1%
S06	7%	5%	4%	3%

improves the classifier performance.

To quantify the performance improvements achievable in a real setting, the classification accuracy improvement was computed considering false positive and false negative ratios reported in Table 8.1 for each subject. Classification was computed on features in the TW with the best adaptive behavior, and suitable η (values chosen between 0.04 and 0.45) according to the previous results, for each subject and for both conditions V and VT. Table 8.6 reports changes in classification performance (ErrP real), and the comparison with values achievable in an ideal setting. i.e. 100% of ErrP detection accuracy (ErrP 100%). The adaptive algorithm allows for a MI classification performance improvement ranging from few percentage points to 17% in the ideal case. These values decrease when taking into account the false positive and false negative rate. In particular, performance of subjects with very high α_p , such as subject S05 ($\alpha_p=0.42,0.41$ in V and VT conditions respectively) presents a big decrease of accuracy improvements achievable with the adaptive algorithm, as expected. The algorithm performance is overall higher for VT condition even in the realistic case. It could be further improved by setting the static ErrP classifier as more conservative, i.e. reducing α_p .

8.4 Conclusions

This work presented the evaluation of an adaptive motor imagery classification algorithm based on ErrP detection, on a novel EEG dataset recorded in two different feedback conditions, either visual, or visuo-tactile. The impact of tactile feedback was evaluated on both MI and ErrP detection. While results on ErrP classification did not show any relevant effect of the tactile feedback, MI classification accuracy presented a significant improvement for most of the subjects, in a simulated cursor control task. This confirmed literature results on benefits coming from the integration of haptic biofeedback in motor imagery-based rehabilitation and neuroprosthetic control tasks.

Furthermore, results from adaptive classifier suggested that tactile feedback not only improves the static classification performance of motor imagery features, but also helps in generating features more stationary over time, thus allowing a better performance of an adaptive classification algorithm based on the principle of parameters re-tuning, as the one implemented in this work.

Conclusions

This PhD research was motivated by the belief that non-invasive BCI technology is approaching the level of maturity required to bring it to real-life assistive applications. In particular, I share the view that with the available hardware and software technology, the path towards out-of-the-lab effective EEG-based BCI implementations passes through the integration with currently available assistive technologies. In this perspective, it appears essential to keep the BCI system concept simple, by extracting few meaningful and reliable control signals, and to rely on hybrid and adaptive solutions in order to achieve usable and comfortable assistive products. Adaptation at the level of EEG signal processing, in particular feature extraction and classification, can cope with the difficulties arising from the non-stationarity of EEG signals and the need of detecting meaningful features, stable over time. Such design can facilitate the development of systems with automatic calibration and re-calibration, able to adapt to each particular user, and to reduce the cognitive effort necessary for the control. A second level of adaptation, which also greatly facilitates the interaction, can be achieved by exploiting hybrid techniques at different levels. These range from the combined use of different biosignals to the integration of multiple mental processes and imaging techniques. In fact, a hybrid approach allows to increase the system reliability by switching between different control modalities, and taking into account the reliability of each input channel for an effective and responsive control.

In this view, the present work proposed a concept of hybrid and adaptive Brain-Machine Interface, where passive and active signals are combined together to provide co-adaptation between the user and the assistive device. Such concept was elaborated throughout its different components, and novel co-adaptive control strategies were proposed considering as control input either active signals, passive processes or their combination.

Contributions of this research include:

- The presentation of the EyeBCI system. An hybrid eye-tracking and BCI solution was proposed in which the BCI channel is exploited to provide adaptation to eye-tracking technology, by actively varying dwell time. This solution is based on the combination of two active control signals, and adaptation is achieved by means of user volitional control. It resulted in an overall improvement of system's performance and user experience compared to eye-tracking or BCI approaches alone.
- The implementation of the SoftBMI system. This solution was again based on the combination of two active control signals. In this case, the BCI channel was exploited to provide an additional degree of freedom for the control, when combined with the eye-tracking technology. This allowed for an effective control of a robotic arm-hand system in 3D space, to realize pick and place tasks, with volitional control of the system's stiffness during interaction. The exploitation of the BCI channel to control a dynamic aspect of a robotic system was new and introduced the possibility of achieving both kinematic and

dynamic control by exploiting the residual functional capabilities available in severely impaired patients.

- Research results regarding the use of a passive EEG process, namely the error-related potential, to provide a signal for adaptation of the assistive interface/device to the human. This concept relies on the advances in robotic systems' autonomy, and points towards the development of intelligent devices, able to learn a task co-evolving with the person's will. Error-related EEG potentials provide a (passive) information on user's evaluation of the system behavior, that can be exploited for the system's learning. In this context, a first contribution of this research regards a study on the effect of tactile feedback on ErrP single-trial detection. Results suggested that the addition of a supplementary sensory channel in the BMI system helps in providing a more reliable classification. This is important for systems that base their learning on ErrP signals. A second contribution consisted in the implementation of an online framework for ErrP-based robot learning. Results confirmed that robot learning is accelerated when including an information on human evaluation of robot behavior into the learning loop. Furthermore, a novel use of this concept was shown as the possibility of simultaneously learn two different tasks (target reaching and target identification). This allowed to achieve a further degree of learning (target identification) compared to a scenario of robot learning without any information available from the user. Both studies are related to the control achievable by only exploiting a passive signal from user's brain activity. Publicly available EEG datasets are included in the contributions from these works.
- The use of a subject-adaptive feature selection method based on mutual information was proposed to retrieve an optimal set of features for motor imagery tasks discrimination. This study was connected to the design of adaptation at the level of signal processing, and in particular feature extraction, to obtain an EEG-based reliable active signal for the control. This work presented the novel application in the BCI context of a method based on mutual information and conditional mutual information to select features more relevant to the task and less redundant to each other. Results showed the method usefulness in identifying optimal features, even in a low quality dataset with few suboptimal channels available. This stresses the importance of adaptive signal processing especially when coping with limitations coming from the use of portable and low-cost systems, that nonetheless constitute the future pathway towards the implementation of real-life applications.
- A last contribution concerned the adaptation designed at the level of the classification stage of the EEG signal processing pipeline. The method was already proposed for motor imagery online adaptive classification, and it is based on error-related potential detection after classification feedback. In this case, the passive signal is used to allow for adaptation of the active signal decoder. Contributions were here related to the evaluation of tactile feedback impact on both active and passive signals detection, and its effect on the adaptive algorithm performance. Results showed that tactile feedback can remarkably improve motor imagery static and adaptive classification, while no relevant effect was observed on ErrP detection. A publicly available dataset was also made available from this work.

All studies here presented were tested on healthy population. The future perspective of this research certainly requires real-time testing on a clinical setting involving individual with severe motor disabilities. This will allow to understand if the observed results can be extended in case of severe paralysis, which is the condition of the final intended user of this investigation. In view of an integration of the proposed control strategies within real assistive products, performance and usability ISO metrics such as accuracy (to quantify effectiveness) and information transfer rate (to evaluate efficiency) need to be assessed during systematic studies involving a sufficiently large sample of both unimpaired and impaired people. The second aspect that has to be taken into account to push forward the present research concerns the definition and development of the low-cost hardware components, in particular the EEG sensing system, that allow for an affordable overall cost of the proposed assistive technology. Finally, the iterative process leading through progressive prototypes up to the final product should follow a user-centered design. Patients will be involved into the evaluation process by means of questionnaires to assess their user experience when testing each prototype for a prolonged period of time, in terms of subjective workload, e.g. through the National Aeronautics and Space Administration Task Load Index (NASA TLX), and user satisfaction, e.g. using the Quebec User Evaluation of Satisfaction with assistive Technology (QUEST 2.0) and the Assistive Technology Device Predisposition Assessment (ATD PA) Device Form.

In conclusion, the research presented in this PhD work aimed at advancing the state of the art of assistive Brain-Machine Interfaces, by following the design of adaptive control strategies to facilitate the co-evolution and interaction between the human and the assistive technology. Contributions are relevant to the field of research towards the development of effective assistive solutions to provide additional degrees of independence to people with severe motor disabilities, or a viable solution to restore communication and control capabilities in patients with total paralysis.

Bibliography

- Abbott, William Welby and Aldo Ahmed Faisal (2012). "Ultra-low-cost 3D gaze estimation: an intuitive high information throughput compliment to direct brain-machine interfaces". In: *Journal of neural engineering* 9.4, p. 046016.
- Ajoudani, Arash (2016). *Transferring Human Impedance Regulation Skills to Robots*. Springer.
- Ajoudani, Arash, Nikolaos G Tsagarakis, and Antonio Bicchi (2012). "Tele-impedance: Teleoperation with impedance regulation using a body-machine interface". In: *The International Journal of Robotics Research*, p. 0278364912464668.
- Albu-Schäffer, A. et al. (2003). "Cartesian impedance control of redundant robots: recent results with the DLR-light-weight-arms". In: *IEEE Intl. Conf. on Robotics and Automation (ICRA)*. Vol. 3, pp. 3704–3709.
- Artusi, Xavier et al. (2011). "Performance of a simulated adaptive BCI based on experimental classification of movement-related and error potentials". In: *IEEE Journal on Emerging and Selected Topics in Circuits and Systems* 1.4, pp. 480–488.
- Barachant, Alexandre and Stephane Bonnet (2011). "Channel selection procedure using Riemannian distance for BCI applications". In: *Neural Engineering (NER), 2011 5th International IEEE/EMBS Conference on*. IEEE, pp. 348–351.
- Barresi, Giacinto et al. (2015). "Brain-Controlled AR Feedback Design for User's Training in Surgical HRI". In: *Systems, Man, and Cybernetics (SMC), 2015 IEEE International Conference on*. IEEE, pp. 1116–1121.
- Barresi, Giacinto et al. (2016). "Focus-sensitive dwell time in EyeBCI: Pilot study". In: *Computer Science and Electronic Engineering (CEECE), 2016 8th*. IEEE, pp. 54–59.
- Bashashati, Ali et al. (2007). "A survey of signal processing algorithms in brain-computer interfaces based on electrical brain signals". In: *Journal of Neural engineering* 4.2, R32.
- Bates, R et al. (2005). "Survey of de-facto standards in eye tracking". In: *COGAIN conf. on comm. by gaze inter.*
- Bauer, Gerhard, Franz Gerstenbrand, and Erik Rimpl (1979). "Varieties of the locked-in syndrome". In: *Journal of neurology* 221.2, pp. 77–91.
- Beukelman, David and Pat Mirenda (2005). "Augmentative and alternative communication". In:
- Birbaumer, Niels et al. (1999). "A spelling device for the paralysed". In: *Nature* 398.6725, pp. 297–298.
- Blankertz, Benjamin, Gabriel Curio, and Klaus-Robert Muller (2002). "Classifying single trial EEG: Towards brain computer interfacing". In: *Advances in neural information processing systems* 1, pp. 157–164.
- Blankertz, Benjamin et al. (2007). "The non-invasive Berlin brain-computer interface: fast acquisition of effective performance in untrained subjects". In: *NeuroImage* 37.2, pp. 539–550.
- Borasio, Gian Domenico and Robert G Miller (2001). "Clinical characteristics and management of ALS". In: *Seminars in neurology*. Vol. 21. 02. Copyright© 2001 by Thieme Medical Publishers, Inc., 333 Seventh Avenue, New York, NY 10001, USA. Tel.:+ 1 (212) 584-4662, pp. 155–166.

- Breitwieser, Christian et al. (2012). "Stability and distribution of steady-state somatosensory evoked potentials elicited by vibro-tactile stimulation". In: *Medical & biological engineering & computing* 50.4, pp. 347–357.
- Carter, Cameron S et al. (1998). "Anterior cingulate cortex, error detection, and the online monitoring of performance". In: *Science* 280.5364, pp. 747–749.
- Catalano, Manuel G et al. (2014). "Adaptive synergies for the design and control of the Pisa/IIT SoftHand". In: *The International Journal of Robotics Research* 33.5, pp. 768–782.
- Chatterjee, Aniruddha et al. (2007). "A brain-computer interface with vibrotactile biofeedback for haptic information". In: *Journal of NeuroEngineering and Rehabilitation* 4.1, p. 40.
- Chaudhary, Ujwal, Niels Birbaumer, and Ander Ramos-Murguialday (2016). "Brain-computer interfaces for communication and rehabilitation". In: *Nature Reviews Neurology* 12.9, pp. 513–525.
- Chavarriaga, Ricardo and José del R Millán (2010). "Learning from EEG error-related potentials in noninvasive brain-computer interfaces". In: *IEEE transactions on neural systems and rehabilitation engineering* 18.4, pp. 381–388.
- Chavarriaga, Ricardo et al. (2012). "Anticipation-and error-related EEG signals during realistic human-machine interaction: A study on visual and tactile feedback". In: *Engineering in Medicine and Biology Society (EMBC), 2012 Annual International Conference of the IEEE. Ieee*, pp. 6723–6726.
- Chavarriaga, Ricardo, Aleksander Sobolewski, and José del R Millán (2014). "Errare machinale est: The use of error-related potentials in brain-machine interfaces." In: *Frontiers in Neuroscience* 8.
- Chawla, Nitesh V et al. (2002). "SMOTE: synthetic minority over-sampling technique". In: *Journal of artificial intelligence research* 16, pp. 321–357.
- Chen, Shih-Ching et al. (2004). "Infrared-based communication augmentation system for people with multiple disabilities". In: *Disability and Rehabilitation* 26.18, pp. 1105–1109.
- Choi, Inchul et al. (2017). "A systematic review of hybrid brain-computer interfaces: Taxonomy and usability perspectives". In: *PloS one* 12.4, e0176674.
- Chou, Samuel M and Forbes H Norris (1993). "Issues & Opinions: Amyotrophic lateral sclerosis: Lower motor neuron disease spreading to upper motor neurons". In: *Muscle & nerve* 16.8, pp. 864–869.
- Cipresso, Pietro et al. (2011). "The combined use of brain computer interface and eye-tracking technology for cognitive assessment in amyotrophic lateral sclerosis". In: *Pervasive Computing Technologies for Healthcare (PervasiveHealth), 2011 5th International Conference on. IEEE*, pp. 320–324.
- Danoczy, M et al. (2008). *Brain2robot: a grasping robot arm controlled by gaze and asynchronous EEG BCI*. na.
- Di Mattia, Philip A, Francis Xavier Curran, and James Gips (2001). *An eye control teaching device for students without language expressive capacity: EagleEyes*. Vol. 53. Edwin Mellen Press.
- Doble, Jennifer E et al. (2003). "Impairment, Activity, Participation, Life Satisfaction, and Survival in Persons With Locked-In Syndrome for Over a Decade: Follow-Up on a Previously Reported Cohort". In: *The Journal of head trauma rehabilitation* 18.5, pp. 435–444.
- Dobrea, Monica-Claudia and Dan Marius Dobrea (2009). "The selection of proper discriminative cognitive tasks—A necessary prerequisite in high-quality BCI applications". In: *Applied Sciences in Biomedical and Communication Technologies, 2009. ISABEL 2009. 2nd International Symposium on. IEEE*, pp. 1–6.

- Donoghue, John P (2002). "Connecting cortex to machines: recent advances in brain interfaces." In: *Nature neuroscience* 5.11.
- Duchowski, Andrew T (2002). "A breadth-first survey of eye-tracking applications". In: *Behavior Research Methods, Instruments, & Computers* 34.4, pp. 455–470.
- Duvinage, Matthieu et al. (2013). "Performance of the Emotiv Epoc headset for P300-based applications". In: *Biomedical engineering online* 12.1, p. 56.
- Dziemian, Sabine, William W Abbott, and A Aldo Faisal (2016). "Gaze-based teleprosthetic enables intuitive continuous control of complex robot arm use: Writing & drawing". In: *Biomedical Robotics and Biomechatronics (BioRob), 2016 6th IEEE International Conference on*. IEEE, pp. 1277–1282.
- Ehrlich, Stefan and Gordon Cheng (2016). "A neuro-based method for detecting context-dependent erroneous robot action". In: *Humanoid Robots (Humanoids), 2016 IEEE-RAS 16th International Conference on*. IEEE, pp. 477–482.
- Enzinger, Christian et al. (2008). "Brain motor system function in a patient with complete spinal cord injury following extensive brain–computer interface training". In: *Experimental brain research* 190.2, pp. 215–223.
- Evans, D Gareth, Roger Drew, and Paul Blenkhorn (2000). "Controlling mouse pointer position using an infrared head-operated joystick". In: *IEEE Transactions on rehabilitation engineering* 8.1, pp. 107–117.
- Falkenstein, Michael et al. (2000). "ERP components on reaction errors and their functional significance: a tutorial". In: *Biological psychology* 51.2, pp. 87–107.
- Ferrez, P W and J d R Millán (2005). "You Are Wrong!—Automatic Detection of Interaction Errors from Brain Waves". In: *Proceedings of the 19th international joint conference on Artificial intelligence*. EPFL-CONF-83269.
- Ferrez, P W and José del R Millán (2008a). "Simultaneous real-time detection of motor imagery and error-related potentials for improved BCI accuracy". In: *Proceedings of the 4th international brain-computer interface workshop and training course*. CNBI-CONF-2008-004, pp. 197–202.
- Ferrez, Pierre W and José del R Millán (2008b). "Error-related EEG potentials generated during simulated brain–computer interaction". In: *IEEE transactions on biomedical engineering* 55.3, pp. 923–929.
- Gallegos-Ayala, Guillermo et al. (2014). "Brain communication in a completely locked-in patient using bedside near-infrared spectroscopy". In: *Neurology* 82.21, pp. 1930–1932.
- Ganguly, Karunesh et al. (2011). "Reversible large-scale modification of cortical networks during neuroprosthetic control". In: *Nature neuroscience* 14.5, pp. 662–667.
- Golub, Matthew D et al. (2016). "Brain–computer interfaces for dissecting cognitive processes underlying sensorimotor control". In: *Current opinion in neurobiology* 37, pp. 53–58.
- Gomez-Rodriguez, Manuel et al. (2011). "Closing the sensorimotor loop: haptic feedback facilitates decoding of motor imagery". In: *Journal of neural engineering* 8.3, p. 036005.
- Gribble, Paul L et al. (2003). "Role of cocontraction in arm movement accuracy". In: *Journal of neurophysiology* 89.5, pp. 2396–2405.
- Gryfe, P et al. (1996). "Freedom through a single switch: coping and communicating with artificial ventilation". In: *Journal of the neurological sciences* 139, pp. 132–133.
- Henshaw, James, Wei Liu, and Daniela Romano (2014). "Problem Solving Using Hybrid Brain-Computer Interface Methods: a Review". In: *Cognitive Infocommunications (CogInfoCom), 2014 5th IEEE Conference on*. IEEE, pp. 215–219.
- Hochberg, Leigh R et al. (2006). "Neuronal ensemble control of prosthetic devices by a human with tetraplegia". In: *Nature* 442.7099, pp. 164–171.

- Hochberg, Leigh R et al. (2012). "Reach and grasp by people with tetraplegia using a neurally controlled robotic arm". In: *Nature* 485.7398, pp. 372–375.
- Holroyd, Clay B and Michael GH Coles (2002). "The neural basis of human error processing: reinforcement learning, dopamine, and the error-related negativity." In: *Psychological review* 109.4, p. 679.
- Huang, Cheng-Ning, Chun-Han Chen, and Hung-Yuan Chung (2006). "Application of facial electromyography in computer mouse access for people with disabilities". In: *Disability and Rehabilitation* 28.4, pp. 231–237.
- Hurtado-Rincón, J et al. (2014). "Motor imagery classification using feature relevance analysis: An emotiv-based bci system". In: *Image, Signal Processing and Artificial Vision (STSIVA), 2014 XIX Symposium on*. IEEE, pp. 1–5.
- Iturrate, Inaki, Luis Montesano, and Javier Minguez (2010a). "Robot reinforcement learning using EEG-based reward signals". In: *Robotics and Automation (ICRA), 2010 IEEE International Conference on*. IEEE, pp. 4822–4829.
- (2010b). "Single trial recognition of error-related potentials during observation of robot operation". In: *Engineering in Medicine and Biology Society (EMBC), 2010 Annual International Conference of the IEEE*. IEEE, pp. 4181–4184.
- Iturrate, Inaki et al. (2012). "Latency correction of error potentials between different experiments reduces calibration time for single-trial classification". In: *Engineering in Medicine and Biology Society (EMBC), 2012 Annual International Conference of the IEEE*. IEEE, pp. 3288–3291.
- Iturrate, Iñaki, Jason Omedes, and Luis Montesano (2013). "Shared control of a robot using EEG-based feedback signals". In: *Proceedings of the 2nd Workshop on Machine Learning for Interactive Systems: Bridging the Gap Between Perception, Action and Communication*. ACM, pp. 45–50.
- Iturrate, Iñaki et al. (2015). "Teaching brain-machine interfaces as an alternative paradigm to neuroprosthetics control". In: *Scientific reports* 5.
- Jacob, Robert JK (1991). "The use of eye movements in human-computer interaction techniques: what you look at is what you get". In: *ACM Transactions on Information Systems (TOIS)* 9.2, pp. 152–169.
- Jaeschke, Roman, Joel Singer, and Gordon H Guyatt (1990). "A comparison of seven-point and visual analogue scales: data from a randomized trial". In: *Controlled clinical trials* 11.1, pp. 43–51.
- Jain, Siddarth et al. (2015). "Assistive robotic manipulation through shared autonomy and a body-machine interface". In: *Rehabilitation Robotics (ICORR), 2015 IEEE International Conference on*. IEEE, pp. 526–531.
- Jeunet, Camille et al. (2015). "Continuous tactile feedback for motor-imagery based brain-computer interaction in a multitasking context". In: *Human-Computer Interaction*. Springer, pp. 488–505.
- Jiang, Hairong et al. (2013a). "3D joystick for robotic arm control by individuals with high level spinal cord injuries". In: *Rehabilitation Robotics (ICORR), 2013 IEEE International Conference on*. IEEE, pp. 1–5.
- Jiang, Hairong, Juan P Wachs, and Bradley S Duerstock (2013b). "Integrated vision-based robotic arm interface for operators with upper limb mobility impairments". In: *Rehabilitation Robotics (ICORR), 2013 IEEE International Conference on*. IEEE, pp. 1–6.
- Kaczmarek, Kurt A et al. (1991). "Electrotactile and vibrotactile displays for sensory substitution systems". In: *IEEE Transactions on Biomedical Engineering* 38.1, pp. 1–16.
- Kamiya, Joseph (1969). "Operant control of the EEG alpha rhythm and some of its reported effects on consciousness". In: *Alerted states of consciousness* 489.

- Kennedy, Philip R et al. (2000). "Direct control of a computer from the human central nervous system". In: *IEEE Transactions on rehabilitation engineering* 8.2, pp. 198–202.
- Kim, Dae-Jin et al. (2012). "How autonomy impacts performance and satisfaction: Results from a study with spinal cord injured subjects using an assistive robot". In: *IEEE Transactions on Systems, Man, and Cybernetics-Part A: Systems and Humans* 42.1, pp. 2–14.
- Kim, Hyun K et al. (2006). "Continuous shared control for stabilizing reaching and grasping with brain-machine interfaces". In: *IEEE Transactions on Biomedical Engineering* 53.6, pp. 1164–1173.
- King, Christine E et al. (2015). "The feasibility of a brain-computer interface functional electrical stimulation system for the restoration of overground walking after paraplegia". In: *Journal of NeuroEngineering and Rehabilitation* 12.1, p. 80.
- Kos' Myna, Nataliya and Franck Tarpin-Bernard (2013). "Evaluation and comparison of a multimodal combination of BCI paradigms and Eye-tracking in a gaming context". In: *IEEE Transactions on Computational Intelligence and AI in Games (T-CIAIG)*, pp. 150–154.
- Kübler, Andrea et al. (2001). "Brain-computer communication: self-regulation of slow cortical potentials for verbal communication". In: *Archives of physical medicine and rehabilitation* 82.11, pp. 1533–1539.
- Lancioni, Giulio E et al. (2005). "A new microswitch to enable a boy with minimal motor behavior to control environmental stimulation with eye blinks". In: *Behavioral Interventions* 20.2, pp. 147–153.
- Lancioni, Giulio E et al. (2006). "Children with multiple disabilities and minimal motor behavior using chin movements to operate microswitches to obtain environmental stimulation". In: *Research in Developmental Disabilities* 27.3, pp. 290–298.
- Laureys, Steven et al. (2005). "The locked-in syndrome: what is it like to be conscious but paralyzed and voiceless?" In: *Progress in brain research* 150, pp. 495–611.
- Leeb, Robert, Hesam Sgha, Ricardo Chavarriaga, et al. (2010). "Multimodal fusion of muscle and brain signals for a hybrid-BCI". In: *Engineering in Medicine and Biology Society (EMBC), 2010 Annual International Conference of the IEEE*. IEEE, pp. 4343–4346.
- Lehne, Moritz et al. (2009). "Error-related EEG patterns during tactile human-machine interaction". In: *Affective Computing and Intelligent Interaction and Workshops, 2009. ACII 2009. 3rd International Conference on*. IEEE, pp. 1–9.
- Li, Yuanqing et al. (2013). "A hybrid BCI system combining P300 and SSVEP and its application to wheelchair control". In: *IEEE Transactions on Biomedical Engineering* 60.11, pp. 3156–3166.
- Lightbody, Gaye et al. (2010). "A user centred approach for developing brain-computer interfaces". In: *Pervasive Computing Technologies for Healthcare (PervasiveHealth), 2010 4th International Conference on-NO PERMISSIONS*. IEEE, pp. 1–8.
- Llera, A, Vicenç Gómez, and Hilbert J Kappen (2012). "Adaptive classification on brain-computer interfaces using reinforcement signals". In: *Neural Computation* 24.11, pp. 2900–2923.
- Llera, Alberto et al. (2011). "On the use of interaction error potentials for adaptive brain computer interfaces". In: *Neural Networks* 24.10, pp. 1120–1127.
- Lotte, Fabien et al. (2007). "A review of classification algorithms for EEG-based brain-computer interfaces". In: *Journal of neural engineering* 4.2, R1.

- Lotte, Fabien, Laurent Bougrain, and Maureen Clerc (2015). "Electroencephalography (EEG)-Based Brain-Computer Interfaces". In: *Wiley Encyclopedia of Electrical and Electronics Engineering*.
- Majaranta, Päivi and Kari-Jouko Rähkä (2002). "Twenty years of eye typing: systems and design issues". In: *Proceedings of the 2002 symposium on Eye tracking research & applications*. ACM, pp. 15–22.
- Margaux, Perrin et al. (2012). "Objective and subjective evaluation of online error correction during P300-based spelling". In: *Advances in Human-Computer Interaction 2012*, p. 4.
- Martinez-Leon, Juan-Antonio, Jose-Manuel Cano-Izquierdo, and Julio Ibarrola (2016). "Are low cost Brain Computer Interface headsets ready for motor imagery applications?" In: *Expert Systems with Applications* 49, pp. 136–144.
- McFarland, Dennis J et al. (1997). "Spatial filter selection for EEG-based communication". In: *Electroencephalography and clinical Neurophysiology* 103.3, pp. 386–394.
- Meng, Jianjun et al. (2016). "Noninvasive Electroencephalogram Based Control of a Robotic Arm for Reach and Grasp Tasks". In: *Scientific Reports* 6.
- Milan, Jose del R and Jose M Carmenta (2010). "Invasive or noninvasive: Understanding brain-machine interface technology [conversations in bme]". In: *IEEE Engineering in Medicine and Biology Magazine* 29.1, pp. 16–22.
- Millán, J d R et al. (2010). "Combining brain-computer interfaces and assistive technologies: state-of-the-art and challenges". In: *Frontiers in neuroscience* 4.
- Millán, J del R et al. (2009). "Asynchronous non-invasive brain-actuated control of an intelligent wheelchair". In: *Engineering in Medicine and Biology Society, 2009. EMBC 2009. Annual International Conference of the IEEE*. IEEE, pp. 3361–3364.
- Millan, Jd R et al. (2004). "Noninvasive brain-actuated control of a mobile robot by human EEG". In: *IEEE Transactions on biomedical Engineering* 51.6, pp. 1026–1033.
- Millán, José del R (2002). *Brain-computer interfaces*. Tech. rep. The MIT Press.
- Mladenov, T, Kunsu Kim, and Saeid Nooshabadi (2012). "Accurate motor imagery based dry electrode brain-computer interface system for consumer applications". In: *Consumer Electronics (ISCE), 2012 IEEE 16th International Symposium on*. IEEE, pp. 1–4.
- Moghimi, Saba et al. (2013). "A review of EEG-based brain-computer interfaces as access pathways for individuals with severe disabilities". In: *Assistive Technology* 25.2, pp. 99–110.
- Müller-Putz, Gernot et al. (2015). "Towards noninvasive hybrid brain-computer interfaces: framework, practice, clinical application, and beyond". In: *Proceedings of the IEEE* 103.6, pp. 926–943.
- Müller-Putz, Gernot R et al. (2005a). "EEG-based neuroprosthesis control: a step towards clinical practice". In: *Neuroscience letters* 382.1, pp. 169–174.
- Müller-Putz, Gernot R et al. (2005b). "Steady-state visual evoked potential (SSVEP)-based communication: impact of harmonic frequency components". In: *Journal of neural engineering* 2.4, p. 123.
- Murguialday, A Ramos et al. (2011). "Transition from the locked in to the completely locked-in state: a physiological analysis". In: *Clinical Neurophysiology* 122.5, pp. 925–933.
- Neuper, Christa, Michael Wörtz, and Gert Pfurtscheller (2006). "ERD/ERS patterns reflecting sensorimotor activation and deactivation". In: *Progress in brain research* 159, pp. 211–222.
- Nguyen, Jordan S, Steven W Su, and Hung T Nguyen (2013). "Experimental study on a smart wheelchair system using a combination of stereoscopic and spherical

- vision". In: *Engineering in Medicine and Biology Society (EMBC), 2013 35th Annual International Conference of the IEEE*. IEEE, pp. 4597–4600.
- Nijboer, Femke et al. (2008). "An auditory brain-computer interface (BCI)". In: *Journal of neuroscience methods* 167.1, pp. 43–50.
- Omedes, Jason et al. (2013). "Using frequency-domain features for the generalization of EEG error-related potentials among different tasks". In: *Engineering in Medicine and Biology Society (EMBC), 2013 35th Annual International Conference of the IEEE*. IEEE, pp. 5263–5266.
- Ouyang, Wenjia, Kelly Cashion, and Vijayan K Asari (2013). "Electroencephalograph based brain machine interface for controlling a robotic arm". In: *Applied Imagery Pattern Recognition Workshop (AIPR): Sensing for Control and Augmentation, 2013 IEEE*. IEEE, pp. 1–7.
- Palankar, Mayur et al. (2009). "Control of a 9-DoF wheelchair-mounted robotic arm system using a P300 brain computer interface: Initial experiments". In: *Robotics and Biomimetics, 2008. ROBIO 2008. IEEE International Conference on*. IEEE, pp. 348–353.
- Perring, Stephen et al. (2003). "A novel accelerometer tilt switch device for switch actuation in the patient with profound disability". In: *Archives of physical medicine and rehabilitation* 84.6, pp. 921–923.
- Petit, Damien et al. (2014). "Navigation assistance for a bci-controlled humanoid robot". In: *Cyber Technology in Automation, Control, and Intelligent Systems (CYBER), 2014 IEEE 4th Annual International Conference on*. IEEE, pp. 246–251.
- Pfurtscheller, Gert et al. (2000). "Brain oscillations control hand orthosis in a tetraplegic". In: *Neuroscience letters* 292.3, pp. 211–214.
- Pfurtscheller, Gert et al. (2003). "'Thought'-control of functional electrical stimulation to restore hand grasp in a patient with tetraplegia". In: *Neuroscience letters* 351.1, pp. 33–36.
- Polich, John (2007). "Updating P300: an integrative theory of P3a and P3b". In: *Clinical neurophysiology* 118.10, pp. 2128–2148.
- Poole, Alex and Linden J Ball (2006). "Eye tracking in HCI and usability research". In: *Encyclopedia of human computer interaction* 1, pp. 211–219.
- Ramadan, Rabie A and Athanasios V Vasilakos (2017). "Brain computer interface: control signals review". In: *Neurocomputing* 223, pp. 26–44.
- Ranky, GN and S Adamovich (2010). "Analysis of a commercial EEG device for the control of a robot arm". In: *Bioengineering Conference, Proceedings of the 2010 IEEE 36th Annual Northeast*. IEEE, pp. 1–2.
- Salazar-Gomez, Andres F et al. (2017). "Correcting robot mistakes in real time using eeg signals". In: *ICRA. IEEE*.
- Schiatti, Lucia et al. (2016). "Mutual information-based feature selection for low-cost BCIs based on motor imagery". In: *Engineering in Medicine and Biology Society (EMBC), 2016 IEEE 38th Annual International Conference of the*. IEEE, pp. 2772–2775.
- Schiatti, Lucia et al. (2017). "Soft brain-machine interfaces for assistive robotics: A novel control approach". In: *Rehabilitation Robotics (ICORR), 2017 International Conference on*. IEEE, pp. 863–869.
- Schie, Hein T van et al. (2004). "Modulation of activity in medial frontal and motor cortices during error observation". In: *Nature neuroscience* 7.5, pp. 549–554.
- Schlögl, Alois et al. (2005). "Characterization of four-class motor imagery EEG data for the BCI-competition 2005". In: *Journal of neural engineering* 2.4, p. L14.
- Schwartz, Andrew B (2004). "Cortical neural prosthetics". In: *Annu. Rev. Neurosci.* 27, pp. 487–507.

- Sellers, Eric W, Theresa M Vaughan, and Jonathan R Wolpaw (2010). "A brain-computer interface for long-term independent home use". In: *Amyotrophic lateral sclerosis* 11.5, pp. 449–455.
- Shenoy, Pradeep et al. (2006). "Towards adaptive classification for BCI". In: *Journal of neural engineering* 3.1, R13.
- Spataro, R et al. (2014). "The eye-tracking computer device for communication in amyotrophic lateral sclerosis". In: *Acta Neurologica Scandinavica* 130.1, pp. 40–45.
- Stytsenko, Kirill, Evaldas Jablonskis, and Cosima Prahm (2011). "Evaluation of consumer EEG device Emotiv EPOC". In: *MEI: CogSci Conference 2011, Ljubljana*.
- Surakka, Veikko, Marko Illi, and Poika Isokoski (2004). "Gazing and frowning as a new human-computer interaction technique". In: *ACM Transactions on Applied Perception (TAP)* 1.1, pp. 40–56.
- Sutton, Richard S and Andrew G Barto (1998). *Reinforcement learning: An introduction*. Vol. 1. 1. MIT press Cambridge.
- Szafir, Daniel and Bilge Mutlu (2012). "Pay attention!: designing adaptive agents that monitor and improve user engagement". In: *Proceedings of the SIGCHI Conference on Human Factors in Computing Systems*. ACM, pp. 11–20.
- Tahboub, Karim A (2001). "A semi-autonomous reactive control architecture". In: *Journal of Intelligent & Robotic Systems* 32.4, pp. 445–459.
- Tai, Kelly, Stefanie Blain, and Tom Chau (2008). "A review of emerging access technologies for individuals with severe motor impairments". In: *Assistive Technology* 20.4, pp. 204–221.
- Tessadori, J. et al. (2017). "Does tactile feedback enhance single-trial detection of error-related eeg potentials?" In: *2017 IEEE International Conference on Systems, Man, and Cybernetics (SMC)*, pp. 1417–1422. DOI: [10.1109/SMC.2017.8122812](https://doi.org/10.1109/SMC.2017.8122812).
- Thorns, Johannes et al. (2010). "Movement initiation and inhibition are impaired in amyotrophic lateral sclerosis". In: *Experimental neurology* 224.2, pp. 389–394.
- Tonin, Luca et al. (2010). "The role of shared-control in BCI-based telepresence". In: *Systems Man and Cybernetics (SMC), 2010 IEEE International Conference on*. IEEE, pp. 1462–1466.
- Tsimpiris, Alkiviadis, Ioannis Vlachos, and Dimitris Kugiumtzis (2012). "Nearest neighbor estimate of conditional mutual information in feature selection". In: *Expert Systems with Applications* 39.16, pp. 12697–12708.
- Tsui, Katherine M et al. (2008). "Survey of domain-specific performance measures in assistive robotic technology". In: *Proceedings of the 8th Workshop on Performance Metrics for Intelligent Systems*. ACM, pp. 116–123.
- Tudor, Mario, Lorainne Tudor, and Katarina Ivana Tudor (2005). "Hans Berger (1873–1941)–the history of electroencephalography". In: *Acta medica Croatica: casopis Hrvatske akademije medicinskih znanosti* 59.4, pp. 307–313.
- Vanhooydonck, Dirk et al. (2003). "Shared control for intelligent wheelchairs: an implicit estimation of the user intention". In: *Proceedings of the 1st international workshop on advances in service robotics (ASER'03)*, pp. 176–182.
- Vidal, Jacques J (1973). "Toward direct brain-computer communication". In: *Annual review of Biophysics and Bioengineering* 2.1, pp. 157–180.
- Vidaurre, Carmen et al. (2009). "Time domain parameters as a feature for EEG-based brain-computer interfaces". In: *Neural Networks* 22.9, pp. 1313–1319.
- Vidaurre, Carmen and Benjamin Blankertz (2010). "Towards a cure for BCI illiteracy". In: *Brain topography* 23.2, pp. 194–198.
- Vilimek, Roman and Thorsten O Zander (2009). "BC (eye): Combining eye-gaze input with brain-computer interaction". In: *Universal Access in Human-Computer*

- Interaction. Intelligent and Ubiquitous Interaction Environments*. Springer, pp. 593–602.
- Vogel, Jörn et al. (2015). “An assistive decision-and-control architecture for force-sensitive hand–arm systems driven by human–machine interfaces”. In: *The International Journal of Robotics Research* 34.6, pp. 763–780.
- Wang, Haofei et al. (2015). “Hybrid gaze/EEG brain computer interface for robot arm control on a pick and place task”. In: *Engineering in Medicine and Biology Society (EMBC), 2015 37th Annual International Conference of the IEEE*. IEEE, pp. 1476–1479.
- Wolpaw, Jonathan R et al. (1998). “EEG-based communication: improved accuracy by response verification”. In: *IEEE transactions on Rehabilitation Engineering* 6.3, pp. 326–333.
- Wolpaw, Jonathan R et al. (2002). “Brain–computer interfaces for communication and control”. In: *Clinical neurophysiology* 113.6, pp. 767–791.
- Wolpaw, Jonathan R and Dennis J McFarland (2004). “Control of a two-dimensional movement signal by a noninvasive brain-computer interface in humans”. In: *Proceedings of the National Academy of Sciences of the United States of America* 101.51, pp. 17849–17854.
- Zhu, Danhua et al. (2010). “A survey of stimulation methods used in SSVEP-based BCIs”. In: *Computational intelligence and neuroscience* 2010, p. 1.